NUMERICAL INVESTIGATION OF THE EFFECTIVENESS OF FRP AND TRM IN REPAIRING CORROSION DAMAGED REINFORCED CONCRETE BEAMS

by

P.K.M. Moniruzzaman

B.Sc., Bangladesh University of Engineering & Technology, Bangladesh, 2009

A THESIS SUBMITTED IN PARTIAL FULFILLMENT
OF THE REQUIREMENTS FOR THE DEGREE OF

MASTER OF APPLIED SCIENCE

in

THE COLLEGE OF GRADUATE STUDIES
(Civil Engineering)

THE UNIVERSITY OF BRITISH COLUMBIA
(Okanagan)

April 2013

ABSTRACT

In steel reinforced concrete (RC) structures, corrosion reduces the reinforcement cross-sectional area and causes cracking and/or spalling of the concrete cover. This will reduce the strength of the structure and may cause collapse. A certain degree of structural strength can be preserved and/or increased by using strengthening techniques. Fibre reinforced polymer (FRP) composite material has gotten approval in the rehabilitation engineering community for possessing superior mechanical properties in terms of resistance to corrosion, high strength to weight ratio and ease of installation. On the other hand, an efficient, sustainable and durable material, namely, textile reinforced mortar (TRM), has been introduced recently as a retrofitting material that maintains the positive characteristics of FRP while eliminating its drawbacks. Thus, to use this system in practical conditions it is necessary to evaluate its effectiveness and compare it with the FRP system.

The current numerical study investigated the structural performance of corrosion damaged reinforced concrete beams repaired with externally bonded FRP and TRM systems. The studied parameters were the reinforcement ratio, the corrosion level and the existence and type of the strengthening system. Results showed that failure mode was initiated by steel yielding for all studied beams. The study found that the TRM/FRP system should be applied such that the strengthened beams would not be over-reinforced to prevent compression failure. In addition, for the given material properties, the TRM strengthened beams showed better performance with respect to stiffness compared to their FRP strengthened counterparts, while the FRP strengthened beams were better in terms of loading capacity, displacement and ductility behaviours except for

beams having high tensile steel reinforcement ratio. In such case, the TRM strengthened beams showed almost equal effectiveness as the FRP ones. Given the scope of this study, it is suggested that the full strength of the FRP and TRM systems could be achieved if the unstrengthen beam have tensile steel reinforcement ratio less than 24% and 73% of its balanced reinforcement ratio, respectively.

TABLE OF CONTENTS

LIST OF TABLES

LIST OF FIGURES

ACKNOWLEDGEMENTS

I am extremely grateful to almighty Allah for giving me the strength and ability to bring my thesis into reality. I also greatly appreciate the benign support and able mentoring of my supervisor, Dr. Ahmad Rteil in completing my research. He gave me valuable insight and motivation for this work. His knowledge, counseling and care were always there through my graduate studies at UBC.

I would like to thank my committee members: Dr. Abbas S. Milani, Dr. Adil Al-Mayah and Dr. Solomon Tesfamariam.

UBC has provided an excellent educational and work environment through her systematic and efficient management systems which were essential for my research. I would like to thank Natural Sciences and Engineering Research Council of Canada (NSERC) for their financial support.

Lastly, I would like to express my deepest appreciation to Shirsho, Sharsha, Shosso, Afrah, Arfah and my friends who were always there for me through their insistent support, enthusiasm and encouragement.

DEDICATION

My parents and sisters

Anywhere they stay I get bazillion of love from them.

CHAPTER 1: INTRODUCTION

1.1 Problem Statement

The strength and life span of steel reinforced concrete (RC) structures can be severely reduced by environmental attack on either concrete or steel reinforcement or both. In the past, a structure that had become unsuitable to serve its purpose or that had decayed was replaced. That situation has changed recently due to the deterioration of infrastructure and the high expense of replacement (ACI 546R, 2001; Mailvaganam, 2004).

Despite the recommendations and precautions provided by the current codes of practice, the witness of the vulnerability of RC structures to corrosion damage can be attested by some structural collapse in recent years such as the Silver Bridge in Ohio (1967), the Berlin Congress Hall in Germany (1980), a parking garage in Minnesota (1984), the Rainbow Bridge in China (2004), resulting in enormous casualties and damages in each case (Isecke, 1982; Borgand et al., 1990; LeRose, 2001; CEP, 2012; Roberts, 2012). Hence, the employment of rational rehabilitation techniques is vital when the corrosion of the steel reinforcement in concrete passes off (El-Maaddawy et al., 2005; Mailvaganam, 2004).

The rehabilitation cost is in the order of billions of dollars (ACI 546R, 2001; Tullmin, 2007; Gjorv, 2009). The required repair cost of corrosion damaged structures in Canada is estimated to be approximately $3 billion per year (Tullmin, 2007). The United States and Australia spend almost 1% and 2%, respectively, of their gross domestic product (GDP) to address the corrosion of reinforcement in RC structures (Whitmore and Ball, 2004; Tullmin, 2007). This has put the construction industry under increasing pressure to use new and innovative materials and techniques with proven superiority in terms of their durability, performance and cost.

To rehabilitate RC structures, several techniques and materials were used such as applying an external steel plate as additional reinforcement. However, potential of corrosion damage has turned this system into limited application. Couple decades ago, fibre reinforced polymer (FRP) emerged as an innovative and cost efficient technology to repair and strengthen the corrosion damaged load bearing structural members (ACI 440.1R, 2006; Mobasher and Raji, 2007). FRP materials offer some favourable properties such as high strength-to-weight ratio, minimal change of geometry, corrosion resistance, ease and speed of application (Bournas et al., 2007). Despite these advantages, FRP retrofitting technique has few disadvantages, in particular, they are difficult to apply on wet surfaces, hard to assess post-earthquake behaviour underneath the FRP jackets, loose the strength at high temperatures and are expensive. These drawbacks are mainly attributed to the bonding agent i.e. the organic resins (typically epoxy) used to bind the fibres together and to the concrete substrate (Papanicolaou et al., 2010). On the other hand, recent research has shown that appropriately designed textiles bonded by inorganic binders (cement mortar) have great potential to repair and strengthen RC structures. These features are found in the textile reinforced mortar (TRM) system. TRM is a new high-performance textile composite material consisting of continuous fibres impregnated in a fine grained cementitious matrix (Brameshuber, 2006; Papanicolaou et al., 2007; Bournas and Triantafillou, 2008).

Many studies have been conducted to investigate the effect of different fibre orientation, type and geometry of FRP as a repairing material for corrosion damaged beams (Bonacci and Maalej, 2000; Soudki and Sherwood, 2000; El-Maaddawy et al. 2007; Kutarba et al., 2007; Al-

Hammoud et al., 2011). However, to date, very limited information is available on the viability of using the FRP laminates to repair corrosion damaged RC beams having different reinforcement ratios. Moreover, the flexural performance of the TRM strengthened corroded beams has not been studied yet. To use this system in practice, the investigation of the effectiveness of the TRM system and how it behaves compare to the FRP system is undeniable and demanding. Therefore, the aim of this research is to numerically investigate the effectiveness of a TRM system to repair damaged beams at different corrosion level and having different tensile reinforcement ratio and compare its performance to an FRP repairing system.

1.2 Thesis Overview

The present research work numerically investigates the performance of reinforced concrete beams, 100 x 150 x 1200 mm each, damaged by corrosion and/or strengthened with externally bonded FRP or TRM system.

Background information on the subject of corrosion of steel in concrete and the two strengthening techniques, namely, FRP and TRM composite systems is provided in Chapter 2. A review of the available literature on the flexural performance of corroded and FRP strengthened corroded beams is also presented in this chapter. Research needs along with the specific objectives of the current study wrap up the chapter.

The methods adopted in the finite element simulation phase of the present study along with a description of the specimen geometry, the loading and boundary conditions, the meshing and analysis techniques and the different materials' constitutive laws are reported in Chapter 3. The validation of the FE models is presented in the same chapter.

Chapter 4 presents the results and observations of the analysis. The overall load-deflection behaviour and failure modes for all specimens are presented and discussed in that chapter. An evaluation of the flexural performance in terms of loading capacity, displacement, ductility and stiffness of corroded and FRP and TRM strengthened beams having different tensile reinforcement ratio are also included. Moreover, a comparative effectiveness between the FRP and TRM composite systems is presented in the same chapter. Based on the strain analysis a discussion and comments relevant to the results are presented.

Chapter 5 documents the general conclusions of the research along with recommendations for future research and developments on the structural performance of corroded and FRP/TRM strengthened beams.

CHAPTER 2: LITERATURE REVIEW AND RESEARCH OBJECTIVES

2.1 Corrosion

In general, corrosion is defined as the gradual destruction of a material when it reacts with its environment (Ahmad, 2006).

In metals, corrosion can be considered as the process of extractive metallurgy in reverse. Extractive metallurgy is the process of processing, refining and/or alloying ore into a usable metal form (Fig. 2.1). This process involves a large amount of energy addition to the metal, creating a condition of high potential energy in the metal making it thermodynamically unstable under normal conditions. Therefore, corrosion can be thought of as the process where the metal reacts with its environment to return to its original form, i.e. release the energy and be thermodynamically stable (Ahmad, 2006). Chemically, this process involves a metal losing electron(s) in order to achieve this stability.

$$M \rightarrow M^{+} + e^{-} \tag{2.1}$$

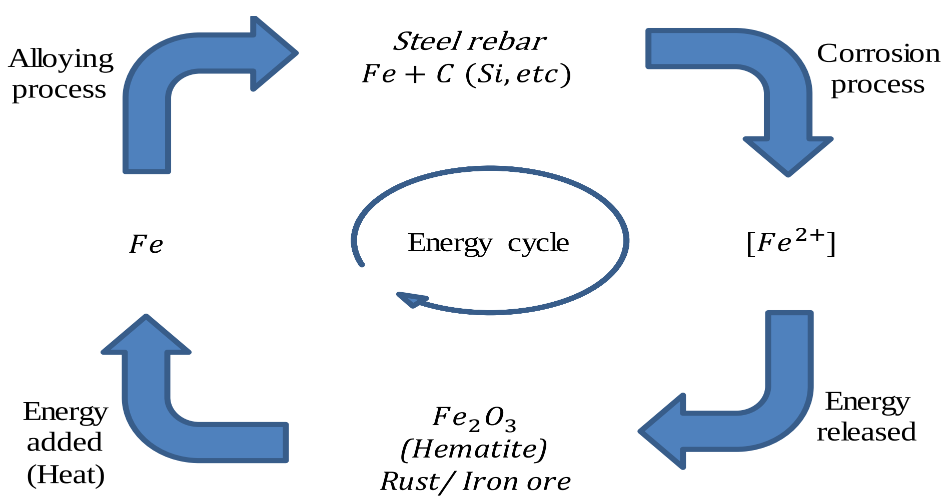

Figure 2.1: Corrosion: extractive metallurgy in reverse

2.1.1 Corrosion Process in Reinforced Concrete

According to ACI 222R (2001), the corrosion is an electrochemical process. For making this process, four key elements must be present (ACI 222R, 2001; El-Maaddawy, 2004; PCA, 2013):

- An anode, where iron ions (Fe^{2+}) are removed from the steel (iron oxidation or anodic reaction)

$$F_e \rightarrow {F_e}^{2+} + 2e^- \tag{2.2}$$

- A cathode, where hydroxyl ions (OH^-) are generated (oxygen reduction or cathodic reaction)

$${}^{1}\!/_{2}\, O_2 + H_2O + 2e^- \rightarrow 2(OH)^- \tag{2.3}$$

- An electrolyte (aqueous medium), for ions to flow from the cathode to the anode and

- An electrical conductor, for the flow of charges (electrons) and complete the corrosion cell.

In reinforced concrete, the rebar may have many separate zones at different energy levels which act as an anode and a cathode (PCA, 2013). In addition, a concrete act as the electrolyte and the metallic connection is allowed by chair supports, wire ties, or the rebar itself (Fig. 2.2).

Concrete contains lots of microscopic pores with high concentrations of soluble sodium, potassium and calcium oxides. When water is added, those oxides generate hydroxides, which lead to very alkaline condition of pH 12-13 (Broomfield, 1997). The alkaline condition allows the creation of a ‘passive’ layer on the steel surface that would protect the steel from corroding. Passivation of the steel may be spiflicated by either the presence of high chloride concentration or by carbonation attack. Once the passive film is interrupted corrosion will start (ACI 222R, 2001).

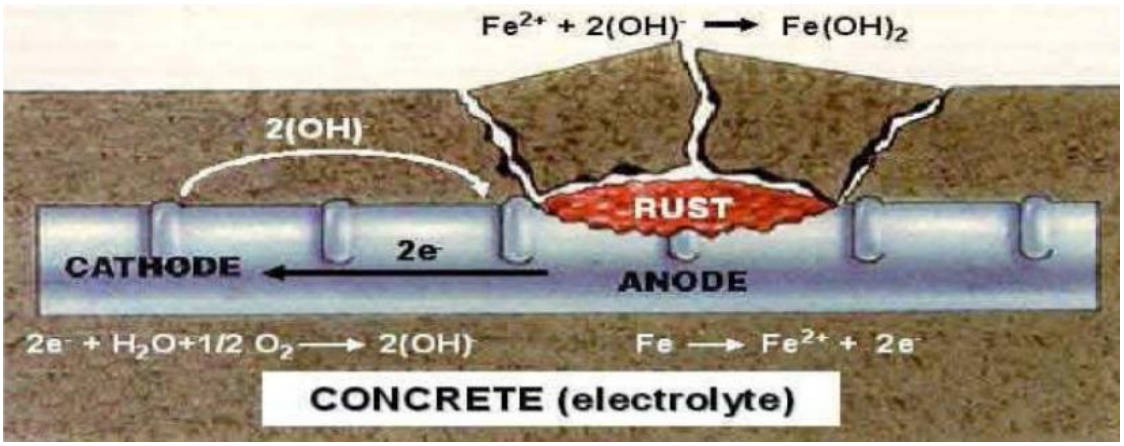

Figure 2.2: Corrosion environment in concrete (Broomfield, 1997)

2.1.1.1 Carbonation Induced Corrosion

Carbonation of concrete occurs when CO_2, (from the atmosphere) penetrates the concrete to react with calcium hydroxide ($Ca(OH)_2$) to produce calcium carbonate ($CaCO_3$) in the presence of moisture (ACI 222R, 2001).

$$CO_2 + Ca(OH)_2 \overset{H_2O}{\rightarrow} CaCO_3 + H_2O \tag{2.4}$$

The formation of calcium carbonate will reduce the pH of the concrete to as low as 9. When the pH around the steel rebars is reduced to such level, the passive film will no longer be stable and corrosion of steel rebars will start (Broomfield, 1997; ACI 222R, 2001; Ahmad, 2006).

2.1.1.2 Chloride Induced Corrosion

The chlorides in the concrete could be present from internal sources (i.e. in one or more of the concrete ingredients) or they could penetrate from external sources (usually seawater and deicing chemicals). The role of chlorides in depassivation has been much argued in terms of how much chloride is needed to depassivate steel and the mechanism by which it does that (Broomfield, 1997; ACI 222R, 2001). The consensus is that once the concentration of chlorides in the concrete at the steel level exceeds a certain limit (referred to as the chloride corrosion threshold), the corrosion starts (ACI 222R, 2001). As for how they depassivate the steel reinforcement several theories exists (Broomfield, 1997; ACI 222R, 2001; Ahmad, 2006):

- Chlorides may make the passive layer permeable to ions allowing the anodic reaction to occur even when the passive film is present;
- Chloride ions may interrupt the passive film;
- Chlorides may decrease the pH level of the concrete, making the passive film unstable;
- Chloride ions may penetrate the passive film; react with iron in the steel. The product then is broken to release the chloride ion, which will react with more iron to form more chloride ions, i.e. chloride acts as a catalyst.

2.1.2 Corrosion Effects on Concrete Structures

Following the oxidation-reduction reactions (anodic and cathodic reactions) a variety of secondary reactions occur to form the expansive products of the corrosion.

If the supply of oxygen is limited, one or both of the following reactions take place to form ferrous oxides and/or hydroxides as follows (West, 1999):

$$Fe^{2+} + 2(OH)^{-} \rightarrow FeO + H_2O \tag{2.5}$$

$$Fe^{2+} + 2(OH)^{-} \rightarrow Fe(OH)_2 \tag{2.6}$$

Whereas if oxygen is available, ferric oxides and/or hydroxides generate according to the following reactions (West, 1999):

$$2Fe(OH)_2 + {}^1/_2\, O_2 \rightarrow Fe_2O_3.H_2O + H_2O \tag{2.7}$$

$$3Fe(OH)_2 + {}^1/_2\, O_2 \rightarrow Fe_3O_4 + 3H_2O \tag{2.8}$$

$$2Fe(OH)_2 + {}^1/_2\, O_2 + H_2O \rightarrow 2Fe(OH)_3 \tag{2.9}$$

$$3FeO + {}^1/_2\, O_2 \rightarrow Fe_3O_4 \tag{2.10}$$

$$2FeO + {}^1/_2\, O_2 + H_2O \rightarrow 2Fe(OH)_3 \tag{2.11}$$

$$2FeO + {}^1/_2\, O_2 + H_2O \rightarrow Fe_2O_3.H_2O \tag{2.12}$$

All these products are characterized by being expansive and hence they occupy more volume than the parent steel occupies (Fig 2.3).

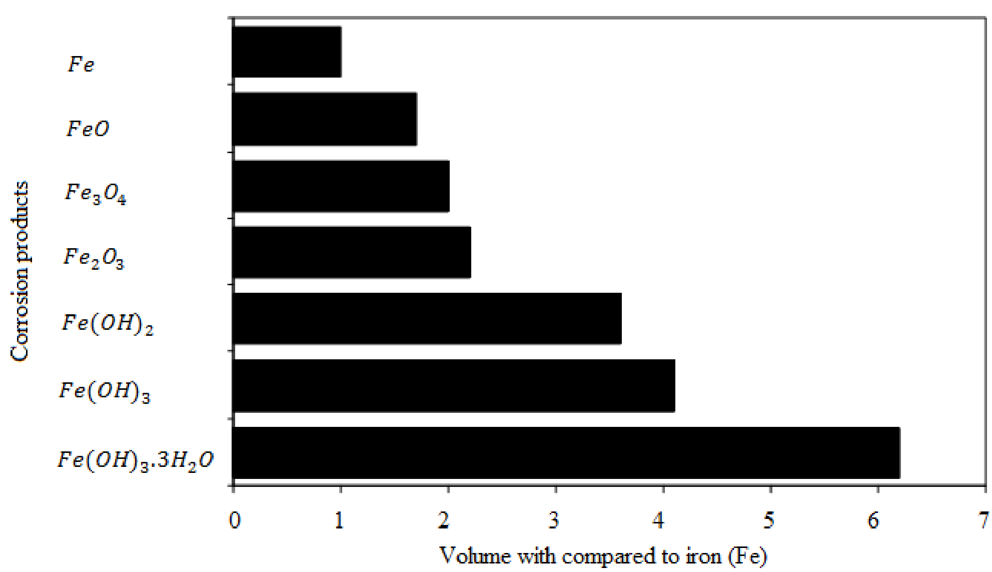

Figure 2.3: Volume of corrosion products with compared to iron (ACI 222R, 2001)

The effect of the steel corrosion in concrete can be summarized in Fig. 2.4. It shows that oxidation of iron results in reduction of steel area (Fig. 2.2). In addition, the corrosion products can occupy 8 times as much volume as steel (Liu and Weyers, 1998; ACI 222R, 2001); thus, subjecting the concrete to high tensile stresses that causes the concrete cover to crack and spall.

This will impair the bond between the steel and the concrete. The reduction of steel area and the decrease in bond strength between steel and concrete reduce the structural capacity of the structure at service (large deflection, cracks) and at ultimate (strength, collapse) limit states. Research has shown that as the corrosion increase by 12%, the yield and the ultimate load decreased in the range of 8% to 33% (Uomoto et al., 1984; Al-Sulaimani et al., 1990; Rodriquez et al., 1997, Soudki et al., 2000; Al-Hammoud et al., 2011).

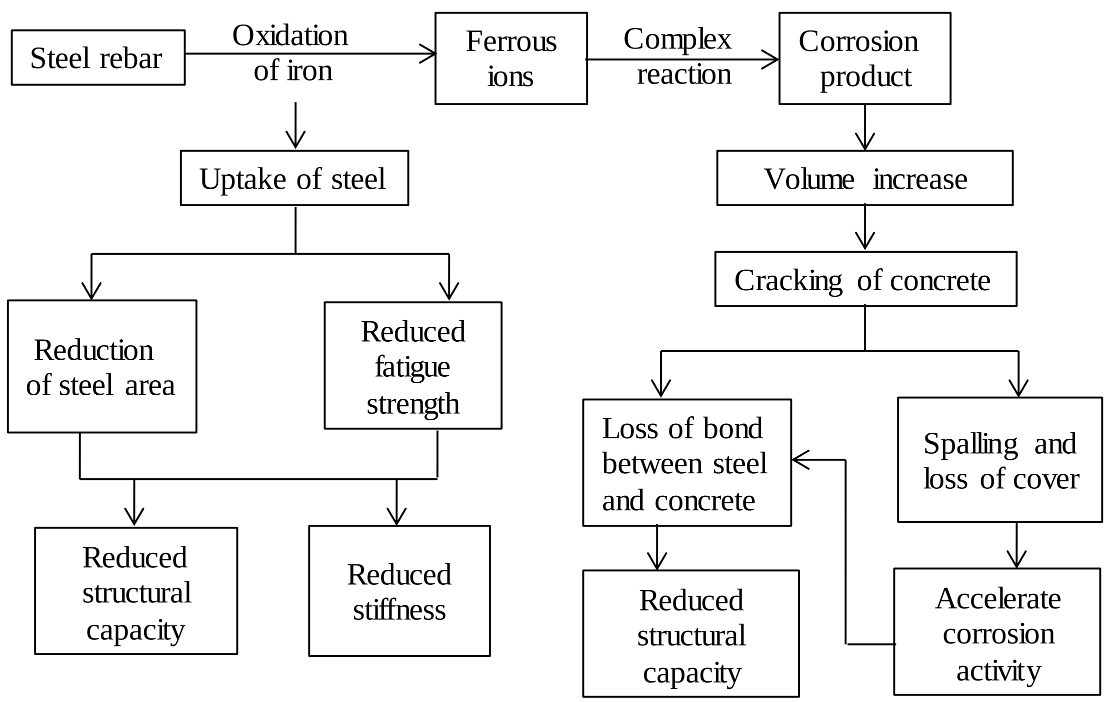

Figure 2.4: Effects of corrosion on reinforced concrete

2.1.3 Studies of the Effect of Corrosion on the Flexural Strength

The study conducted by Uomoto et al. (1984) was one of the earliest experimental attempts to examine the effect of the corrosion levels on the load carrying capacity of corroded reinforced concrete beams. Test specimens were 100 x 100 x 700 mm or 100 x 100 x 400 mm, reinforced with 19 mm diameter steel rebars and having concrete cover of 20 mm or 10 mm. Test results showed that allowing corrosion to increase to 5% and 10% mass loss, the load carrying capacity of the corroded beams was dropped by 5% and 33%, respectively, compared to the uncorroded beams. Moreover, the corroded beams failure mode was shear bond failure while that of the uncorroded beams was a flexural failure.

The previous study extended by Uomoto and Misra in 1988 through testing larger beams. The beams dimension were 100 x 200 x 2100 mm, reinforced with two steel reinforcing bars with diameter of 16 mm. Test results showed that the load carrying capacity reduced by 4, 8 and 17% of that of the uncorroded specimen with mass losses of 1, 1.2 and 2.4% in the steel reinforcement, respectively.

Okada et al. (1988) carried out an experimental study on repaired and unrepaired corrosion damaged concrete beams. The beams were reinforced with two 10 mm diameter steel bars, had cross section of 100 x 200 mm and different shear span/effective depth ratios, 2.29, 2.86, or 3.43. Although the degree of corrosion were not reported but the result showed that at the end of 13 to 20 weeks corrosion process, the yield and ultimate strengths were reduced by about 8% and 9% of that of the uncorroded beams, respectively.

The flexural capacity of corroded beams was investigated by Al-Sulaimani et al. (1990). The beams were 150 x 150 x 1000 mm having shear span/effective depth ratio of 2.5, reinforced with a single 12 mm diameter steel bar and 6 mm diameter stirrups spaced at 50 mm. The results pointed that the ultimate strength of the beam was not changed with steel mass loss up to 1.5%, however, the ultimate load was reduced by 12% at 6% steel mass loss.

Tachibana et al. (1990) worked with simply supported beams to study the effect of corrosion on the load carrying capacity. The beams were 150 x 200 x 1500 mm, reinforced with two 16 mm diameter steel bars. The researchers reported that a 5% loss in steel area caused 12% reduction in the load carrying capacity. Like Uomoto et al. (1984), the mode of failure shifted from flexural to shear bond failure.

The flexural strength of corroded slabs was reported by Almusallam et al. (1996). The dimensions of the slabs tested were 63.5 x 305 x 711 mm having five 6 mm diameter steel bars. The reported test results indicated that the ultimate strength was reduced by about 25% and 60% of that of the control specimen at 5% and 25% corrosion levels, respectively. Like Uomoto et al. (1984) and Tachibana et al. (1990), the failure mode was changed from flexural to bond-shear failure.

Cabrera (1996) investigated the flexural strength of reinforced concrete beams (125 x 160 x 1000 mm) reinforced with two 12 mm diameter steel bars. Results showed that compared to the uncorroded beam, 9.2% steel mass loss caused a reduction of 21.4% in the load carrying capacity and increase of 1.5 times in the midspan deflection.

An extensive work was done by Rodriquez et al. (1997) to evaluate the flexural capacity of corroded beams. The beams were 150 x 200 x 2300 mm having different amount of tensile, compression and shear steel reinforcements. Results showed that 22% steel mass loss reduced the ultimate strength by 43% and increased the mid span deflection by 75% compared to the uncorroded beams. Moreover, beams with steel reinforcement ratio of 1.51% failed by crushing of the concrete with a significant drop-off in ductility, whereas, beams with tensile steel ratio of 0.52% failed by yielding of the steel in a ductile manner.

Potisuk et al. (2011) conducted a numerical study to investigate the structural response of the corroded reinforced concrete beams. The beams were 254 x 610 x 3048 mm reinforced with two 22 mm diameter steel bars in compression, five 25 mm diameter steel bars in tension and 13 mm diameter stirrups spaced at 152 mm and 254 mm in the shear span and constant moment region, respectively. The corrosion damaged parameters were considered as- spalling of concrete covers, localized stirrup cross sectional loss due to pitting, uniform stirrup cross-sectional loss and debonding of stirrups. Test results showed that the ultimate load was reduced by 11% as compared to the undamaged beam model in response to the concrete cover spalling due to corrosion. Besides, as compared to the undamaged beam, the ultimate strength was reduced by 7% and 31% for the 50% and 100% uniform loss of the stirrup cross-sectional area, respectively.

To date, the results obtained from studies carried out to investigate the effect of the corrosion showed a considerable decrease in the load carrying capacity and an increase in deflection. However, few studies were reported on the effect of corrosion on beams with different reinforcement ratio.

2.2 Composites as Strengthening Materials

One or two alternatives may be necessary for repairing reinforcing steel: replacement of damaged rebar; or supplementing partially damaged bar. Which alternative to employ is an engineering decision based on the function of the reinforcement and the expected structural capacity for the reinforced member (ACI 222R, 2001; ACI 546R, 2001). The methods of replacing reinforcement are described in ACI 546R (2001) and ACI 318 (2005). Whereas ACI 546R (2001) suggested to provide supplemental reinforcing when the original reinforcing steel inadequate, the reinforcement has lost cross sectional area, or the existing member is to be strengthened. The current study focuses on the reinforced concrete beams which have to be strengthened due to steel mass loss of up to 15%.

The wide acceptance of the use of externally bonded fibre reinforced polymer (FRP) system in strengthening and retrofitting of reinforced structural elements in flexure and shear has been established in the rehabilitation engineering community and reported extensively (David and Djelal, 1998; ACI 544.3R, 1998; ACI 544.4R, 1999; Teng et al., 2001; Mailvaganam, 2004; Esfahani et al., 2007; Mobasher and Raji, 2007; ACI 506.1R, 2008; Gjorv, 2009; Al-Hammoud et al., 2011; Rami et al., 2012). In addition, FRP laminates have been used to repair corroded reinforced concrete elements (ACI 546R, 2001; Soudki et al., 2003; El-Maaddawy, 2004; Bousias et al., 2005; Kutarba et al., 2007).

On the other hand, textile reinforced mortar (TRM) has been introduced recently as a retrofitting material that maintains FRP positive characteristics while eliminates its drawbacks (Wang and Backer, 1990; Holler et al., 2004; Brameshuber, 2006; Ortlepp et al., 2006; Papanicolaou et al., 2007; Bournas and Triantafillou, 2008; Hartig et al., 2008; Hegger and Voss, 2008; Amir et al., 2010; Jun and Mechtcherine, 2010; Colombo et al., 2011; Alhaddad et al., 2012; Ambrisi and Focacci, 2012; Basalo et al., 2012; Hashemi and Al-Mahaidi, 2012; Schladitz et al., 2012; SiLarbi et al., 2012; Ambrisi and Focacci, 2013; Contamine et al., 2013). In the following sections FRP and TRM will be discussed in details.

2.3 Fibre reinforced polymer (FRP)

Fibre reinforced polymer (FRP) are composite materials that typically consist of strong fibres impregnated in a resin matrix. The fibres- carbon, glass or aramid- provide strength and stiffness to the composite and generally carry most of the applied loads. The matrix- typically epoxies, polyesters and vinyl esters- acts to bond and protect the fibres and to provide for transfer of forces from fibre to fibre through shear stresses (Zeweben et al., 1989; Mobasher and Raji, 2007; ACI 506.1R, 2008; Basalo et al., 2012).

2.3.1 Properties of FRP

The properties of the currently available FRP systems vary significantly depending on their formulation, constituents and manufacturing method. They are highly directional dependant. The properties of the FRP composite materials are usually obtained by experimental testing of the FRP material and products. Experimental procedures are given in CSA S806 (2002) and S807 (2010), ACI 440.1R (2006) and different ASTM standards. From the typical stress-strain curves shown in the Fig. 2.5, it is noted that all FRP systems exhibit linear tensile stress-strain behaviour (in the direction of the fibres), have no yielding, lower rupture strain than steel and except for some carbon FRP systems, they have lower modulus of elasticity compared to steel.

Table 2.1 represents typical properties of unidirectional FRP bars, strips and laminates. In general glass FRP (GFRP) has longer elongation capacity but lesser tensile strength and modulus of elasticity than that of the carbon FRP (CFRP) (ACI 506.1R, 2008). Average tensile strength of CFRP bars, strips and laminates lie in the range of 2000-2300 MPa, 1200-2800 MPa and 3500-3800 MPa, respectively (ACI 440.1R, 2006; ACI 506.1R, 2008). Usually the thickness of the FRP strips and laminates range between 0.17-2.9 mm and the density of the FRP bars btween 1.5-2.2 g/cm^3.

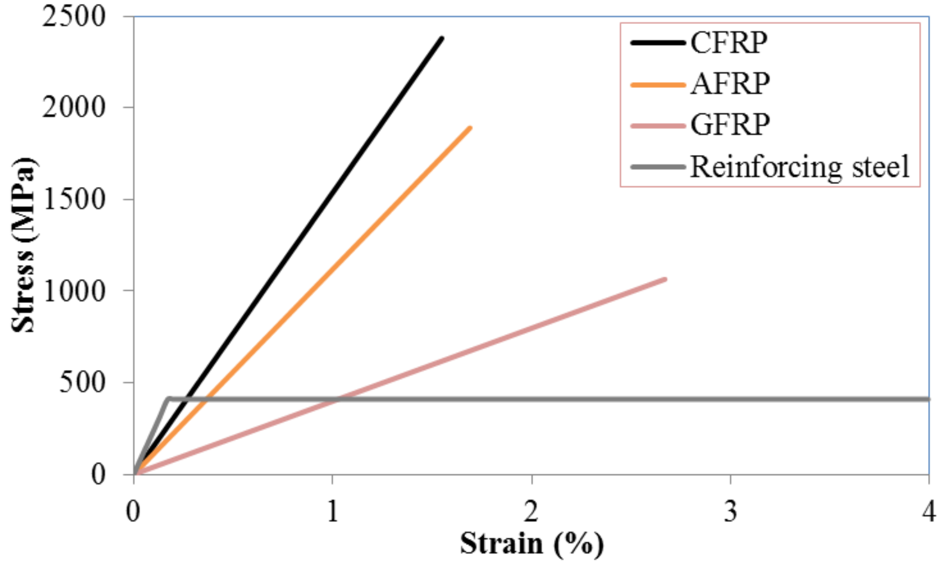

Figure 2.5: Stress-strain curve of FRP and steel (ACI 440.1R, 2006; ACI 506.1R, 2008)

Table 2.1: Typical properties of comercially available FRP materials (ACI 440.1R, 2006; ACI 506.1R, 2008)

Properties	FRP bars		FRP strips		FRP laminates	
	GFRP	CFRP	GFRP	CFRP	GFRP	CFRP
Fibre volume (%)	50-60	50-60	65-70	60-70	-	-
Fibre architechture (direction)	Uni	Uni	Uni	Uni	Uni	Uni
Nominal thickness (mm)	-	-	1.4-1.9	1.2-2.9	0.35	0.17-0.33
Width (mm)	-	-	50-100	16-100	1200	600
Density (g/cm^3)	2-2.2	1.5-1.7	-	-	-	-
Tensile strength, longitudinal (MPa)	500-700	2000-2300	700-900	1200-2800	1500-3300	3500-3800
Tensile strain, longitudinal (%)	2.2-2.4	0.8-1.4	2-2.2	1.7-1.8	2.1-2.45	0.90-1.7
Tensile modulus, longitudinal (MPa)	40-50	120-150	40-50	131-300	70-80	230-370

2.3.2 Forms and Use of FRP

In the last 20 years, composite materials have developed into economically and structurally viable construction material for buildings and bridges (David and Djelal, 1998; ACI 546, 2001; Mobasher and Raji, 2007). Today, FRP are used in structural engineering in a variety of forms:

structural profiles, reinforcing bars and tendons for internal reinforcement or strengthening (internally- near surface mounted or externally- external prestressing) and laminates and plates for external strengthening (Wang et al., 2004; ACI 440.1R, 2006; ACI 506.1R, 2008).

The use of FRP materials in structural engineering can be categorized in three main areas:

- Reinforcement material for new concrete construction: The FRP material can be used in new construction as: internal rebars, prestressing tendons and stay-in-place formwork (ACI 544.4R, 1999; ACI 440.1R, 2006; ACI 506.1R, 2008). The FRP rebars are made as either sand coated, helically wound spiral outer surface, indented, braided, or with ribs (ACI 440.1R, 2006; ACI 506.1R, 2008).

- Strengthening material for existing structures: FRP strengthening has been used in concrete, steel, masonry and timber structures to increase their existing flexural, shear, or confinement strength (ACI 440.1R, 2006; ACI 506.1R, 2008). Materials used are either prestressing tendons, pre-manufactured rigid FRP strips adhesively bonded to the surface of the structure, or hand layup that consists of in situ forming of FRP composite on the surface of the structural member using flexible, dry FRP laminate and liquid polymer resins (Bonacci and Maalej, 2001; Esfahani et al., 2007).

- Structural members (prefabricated) for new construction: Pultrusion is an automated and continuous process used to produce an FRP part from the raw materials. The FRP part could take any shape and manufactured in different dimensions (ACI 440.1R, 2006; ACI 506.1R, 2008).

2.3.3 *Effect of FRP on the Flexural Strength of Corroded Concrete Structures*

The feasibility of using composite fabrics to strengthen corrosion damaged beams was first established by Dimas et al. (1996). They evaluated the strength and effectiveness of fibre composite sheets to strengthen a 6.4 m long corroded concrete beam. The beam was strengthened with three longitudinal layers of glass fabric along the tension side. In addition, three transverse layers were added to increase the shear capacity. Results showed that the load carrying capacity of the retrofitted beam enhanced by a factor of nearly two and the stiffness was significantly higher than that of the control (unretrofitted) beam.

The effectiveness of the FRP strengthening on the corrosion-damaged beams was reported by Lee et al. (1997). The beams were 200 x 250 x 2400 mm, reinforced with three 13 mm diameter tension and compression steel bars and 6 mm diameter stirrups spaced at 50 mm. The corroded specimens were strengthened by FRP laminates; however, the percentage of corrosion was not reported. Compared to the unstrengthened beam, the ultimate strength of the corroded specimen dropped by about 15% while after strengthening with FRP laminates it was enhanced by about 42%.

Soudki and Sherwood (2000) carried out a study on the flexural behaviour of the FRP strengthened corrosion damaged reinforced concrete beams. The beams were 100 x 150 x 1200 mm, reinforced with two 6 mm diameter steel bars at compression, two 10 mm diameter steel bars at tension and 6 mm diameter stirrups spaced at 75 mm. The beams were strengthened by FRP laminates along the tension face. In addition, one transverse laminate was attached to the full height of the beam as another strengthening scheme. Compared to the unstrengthened beam, the flexural strength of the corroded beams was reduced by about 5%, 8.5% and 15%, while those of the strengthened-corroded beams increased by about 20%, 13% and 8%, at corrosion levels of about 5%, 10% and 15% steel mass loss, respectively.

The effectiveness of the FRP strengthening on the corrosion-damaged beams was studied by Bonacci and Maalej (2000). The beams were 270 x 400 x 4350 mm, reinforced with two 9.5 mm diameter steel bars at compression, three 20 mm diameter steel bars at tension and 9.5 mm diameter stirrups spaced at 135 mm. The three test variables were- 1) the strengthening scheme (one longitudinal layer with sporadic transverse strips or two longitudinal FRP layers), 2) the state of concrete damage (undamaged or damaged) and 3) the loading condition during the application of the FRP laminates (unloaded or loaded). The results showed that the ultimate load carrying capacity of a strengthened-uncorroded beam was about 35% higher than that of the unstrengthened-uncorroded (control) beam. On the other hand, relative to the values of the control beam, the ultimate load carrying capacity was reduced by 9% and 17%, whereas, the deflection capacity increased by 33% and 42% at 5% and 10% steel mass loss due to corrosion, respectively. The load carrying capacity of a beam strengthened by two longitudinal FRP layers was only 2% higher compared to the specimen strengthened by one longitudinal layer with sporadic transverse strips, while the deflection capacity of the same specimen was about 32% lower.

Soudki et al. (2000) and Masoud and Soudki (2002) carried out a study on the behaviour of corroded RC beams repaired with FRP laminates. The beams were 152 x 254 x 3200 mm, reinforced with two 8 mm diameter bars in compression, two 16 mm diameter steel bars in tension and 8 mm diameter stirrups spaced at 80 mm and 333 mm in the shear span and constant moment region, respectively. The three test variables were- 1) the repair scheme (flexural strengthening with U-wrapping or U-wrapping only), 2) the loading procedure (monotonic or fatigue) and 3) the degree of corrosion (0, 5.5%, 9% and 12.5%). Test results showed that the ultimate capacity was reduced by only 2.8% at 12.5% steel mass loss due to corrosion. In addition, specimens with U-wrapping strengthening scheme showed no change in the yield load and a negligible improvement (up to 3%) in the ultimate strength compared to those of the corroded-unstrengthened specimens. Whereas, the yield and ultimate loads of the beams with flexural strengthening with U-wrapping enhanced, on average, by about 21% and 28%, respectively, compared to those of the corroded-unstrengthened specimens.

El-Maaddawy and Soudki (2005) and El-Maaddawy et al. (2005 and 2007) investigated experimentally and analytically the performance of corrosion-damaged reinforced concrete beams repaired with FRP laminates. The beams were 152 x 254 x 3200 mm, reinforced with two 8 mm diameter steel bars in compression, two 16 mm diameter steel bars in tension and 8 mm diameter stirrups spaced at 80 mm and 333 mm in the shear span and constant moment region, respectively. The test variable was the time of corrosion exposure, the loading condition during the corrosion exposure (corrosion without load or corrosion under a sustained load) and the FRP repair scheme (flexural strengthening with an intermittent wrapping or flexural strengthening with a continuous wrapping). Test results showed that the time between corrosion initiation and corrosion cracking was decreased by about 44% when the beams were allowed to corrode under a sustained load. Reductions of about 6%, 11%, 20% and 29% in the ultimate load were recorded for 8.88%, 14.20%, 22.25% and 31.65% steel mass losses due to corrosion, respectively. The deflection capacity of the corroded-unrepaired beams was increased on average by about 12% at about 15% corrosion than that of the virgin beam. Moreover, the yield and ultimate loads of the

FRP strengthened beams were on average about 32% and 70% higher, respectively, while the deflection capacity was on average 41% lower than that of the control beam.

Wang et al. (2004) carried out both experimental and analytical studies on the behaviour of corroded RC beams repaired with FRP patching. The beams were 200 x 350 x 3500 mm, reinforced with two 12 mm diameter bars in compression, two 20 mm diameter steel bars in tension and 10 mm diameter stirrups spaced at 100 mm. The three test variables were- 1) the state of corrosion of the steel (7% steel mass loss), 2) the type of concrete (22 MPa and 8 MPa) and 3) the arrangement and number of the FRP laminates. The reported test results showed that all of the studied parameters affect the strength as well as the failure mechanisms of the retrofitted RC beams. The equally spaced U-anchorage FRP strips together with the longitudinal strips can improve the load carrying capacity by 16% of both cracked and corroded RC beams compared to the control beam. Besides, the load carrying capacity increased by 11% for the higher concrete strength compared to the lower concrete strength.

Kutarba et al. (2007) evaluated the post-repair performance of corrosion damaged reinforced concrete beams repaired with FRP systems. The beams were 205 x 300 x 2920 mm, reinforced with two 10 mm diameter steel bars in compression, two 20 mm diameter steel bars in tension and without proving any stirrups. The test variable was three repair schemes i.e. I) the specimen strengthened with separate FRP laminates for flexure and shear, II) the same as scheme I except that the shear laminates were used as anchors for the flexural laminate and III) a single FRP laminate used as a full wrap. Test results showed that due to corrosion, unstrengthened beams lost between 8% and 15% of their load carrying capacity compared to the control beam. After repairing corrosion cracks, beams strengthened with FRP increased the load carrying capacity on average by 30% over the control beam. On the other hand, unrepaired beams strengthened by scheme III had an increase in load capacity by 18% over the virgin beam.

Gadve et al. (2009) studied the progression of steel corrosion in a concrete cylinder after it has been treated with FRP. The diameter and height of the cylinder was 102 and 229 mm, respectively. The test variable was the timing of FRP application (pre-corroded and corroding stage) and the type of FRP laminates (carbon and glass). The experiment showed that FRP wrappings dramatically slowed down the rate of corrosion. In addition, due to high electric resistance and thickness, glass FRP laminates had impeded the rate of corrosion more than the carbon laminates.

Al-Hammoud et al. (2011) conducted an experimental study on the flexural behaviour of corroded RC beams repaired with FRP laminates under fatigue loading. The beams were 152 x 254 x 2000 mm, reinforced with two 8 mm diameter steel bars in compression, two 16 mm diameter steel bars in tension and 8 mm diameter stirrups spaced at 100 mm and 250 mm in the shear span and constant moment region, respectively. The four test variables were- 1) the severity of corrosion (from 0 to 15% average mass loss of steel), 2) the load range, 3) the time of the FRP repair and 4) the number of the FRP laminates. Test results reported that the fatigue strength decreased by 30% at 50,000 cycles and by 18% at 750,000 cycles at high corrosion level (15%) compared to uncorroded beams. FRP increased the flexural fatigue capacity of the corroded beams by 28% at 50,000 cycles and 20% at 750,000 cycles at high corrosion level. In addition, at high corrosion level, the beams repaired with a double FRP laminates increased the flexural capacity of the corroded beams by 42% at 50,000 cycles and 17% at 750,000 cycles compared to an unrepaired beam having 15% mass loss in the steel reinforcement.

From the above presentation of the available literature, it can be concluded that the post-repair flexural performance of the FRP strengthened beams having different reinforcement ratios was not investigated.

2.4 Textile Reinforced Mortar (TRM)

Textile reinforced mortar (TRM) is a new high-performance composite material consisting of continuous fibres embedded in a fine-grained cementitious matrix (Fig. 2.6). The textiles fibres are made from a variety of materials such as alkali-resistant glass, carbon or aramid (Hegger and Voss, 2005; Triantafillou et al., 2005; Bournas et al., 2009; Alhaddad et al., 2012). The textiles are used in the form of a mesh made of long woven, knitted, or unwoven fibre roving in at least two (usually orthogonal) directions (Papanicolaou et al., 2007; Bournas et al., 2009). The quantity and the spacing on the roving can be independently controlled, thus affecting the mechanical properties and the degree of penetration of the mortar. The cementitious matrix used is usually made from cement mortar with maximum aggregate size less than 4 mm (Brameshuber, 2006; Bournas and Triantafillou, 2008). Similar to the FRP system, the TRM system is characterized with several advantages compared to other rehabilitation materials used, such as: high strength, lightweight (high strength-weight ratio) and non-corrosive characteristics (Triantafillou et al., 2005; Brameshuber, 2006; Bournas and Triantafillou, 2008; Hartig et al., 2008; Hegger and Voss, 2008). In addition, due to the use of the inorganic cement-based adhesive, TRM is inexpensive, has higher fire resistance (high durability), is easily applied on wet surfaces, is more compatible with the concrete substrate surface (better bond) and is environmentally friendly (mortar recyclability) (Brameshuber, 2006; Ortlepp et al., 2006; Papanicolaou et al., 2007; Bournas and Triantafillou, 2008; Hartig et al., 2008; Hegger and Voss, 2008; Amir et al., 2010; Jun and Mechtcherine, 2010; Colombo et al., 2011; Alhaddad et al., 2012; Ambrisi and Focacci, 2012; Basalo et al., 2012; Hashemi and Al-Mahaidi, 2012; Schladitz et al., 2012; SiLarbi et al., 2012; Ambrisi and Focacci, 2013; Contamine et al., 2013). These properties make TRM systems an efficient, sustainable and durable material for the rehabilitation and repair of structures.

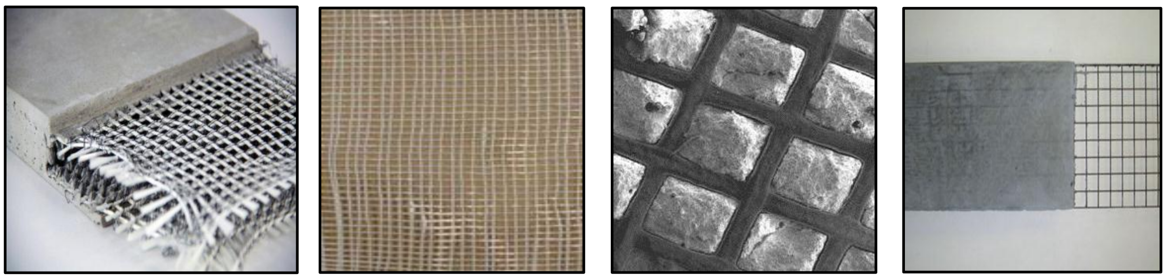

a) b) c) d)

Figure 2.6: TRM composite systems: a) TRM system b) fabric meshes, c) textiles impregnated into mortar and d) apply on concrete substrate (Bournas et al., 2006)

2.4.1 Properties of TRM

The performance of TRM is affected by the geometrical characteristics and bulk properties of the textile fabrics and fine grained concrete properties (Brameshuber, 2006; Hegger and Voss, 2008). Fabrics can be formed by different methods, such as knitting, weaving, non-woven and breading.

A woven is defined as a fabric manufactured by casting two rectangular crossing thread systems, warp and weft (Brameshuber, 2006). The kind and crossing of warp and weft (weaving pattern) influences the fabric properties and design. There are three basic weaving pattern- plain, twill and stain weave (Fig. 2.7). Plain weave can be formed by successively passing each filling yarn over and under each warp yarn, alternating each row (Fig. 2.7a). Twill weave can be indicated by diagonal lines that are produced by a series of floats staggered in the warp direction (Fig. 2.7b). Stain weave has a considerably greater number of yarns in the set of threads, either warp or filling, that forms the face smooth, lustrous surface (Fig. 2.7c).

On the other hand, knitting is a method of constructing fabric by interlocking series of loops of one or more yarns. The two major classes of knitting are warp knitting and weft knitting. Warp knitting is a type of knitting in which the yarns generally run lengthwise in the fabric while weft knitting is a common type of knitting, in which one continuous thread runs crosswise in the fabric making all of the loops in one course (Fig. 2.7d). In the short weft knitted fabric the warp yarns are knitted into stiches and bind together a set of yarns, which are laid-in intermittently in both the weft and the warp directions (Fig. 2.7e).

Types, distribution and geometry of the fibres are considered as variables of a textile fabric (Brameshuber, 2006; Papanicolaou and Papantoniou, 2010; Yin and Xu, 2011; Hinzen et al., 2012). High performance fibres made of aramid, glass and carbon can be made up as filament or twisted yarns (Fig 2.8). Filament yarns are a bundle of elementary fibres where one yarn consists of several hundreds up to thousands of single filament (Table 2.2). The fitness of the yarn, indicated as tex (gram per 1 kilometre). Tex values depend on the average filament diameter, the number of filaments and the fibre density (Brameshuber, 2006).

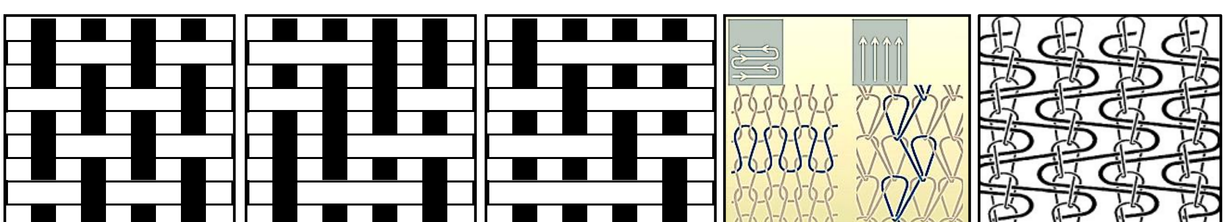

a) b) c) d) e)

Figure 2.7: Fabric geometry: a) plain weave, b) twill weave, c) stain weave, d) weft and warp knit, e) short weft warp knit (Brameshuber, 2006)

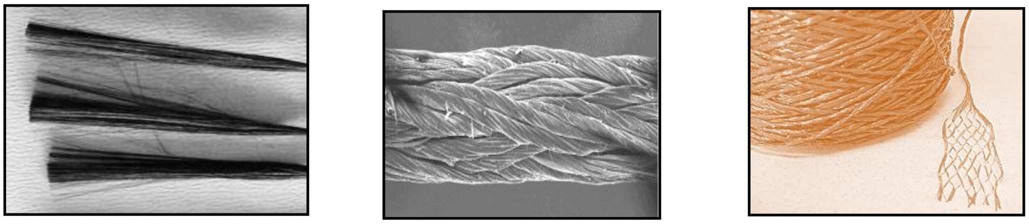

a) b) c)

Figure 2.8: Yarn types: a) filament yarn, b) bundled yarn, c) foil fibrillated tape (Brameshuber, 2006)

Table 2.2 lists typical properties of commercially available glass, aramid and carbon textile rovings. Tensile stress lies in the range of 700-1200 MPa, 1200-1450 MPa and 1500-2600 MPa for the glass, aramid and carbon textile rovings, respectively. It also shows that carbon fibres are thinner and lighter than the aramid or glass fibres.

Table 2.2: Typical properties of comercially available textile rovings (Brameshuber, 2006).

Properties	Glass	Aramid	Carbon
Fibres diameter (μm)	13.5-27	10.0-12.0	7-10.0
Number of filaments	800-2000	1000-2000	3000-24000
Tex (g/km)	310-2500	167-2520	198-1600
Tensile stress (MPa)	700-1200	1200-1450	1500-2600
Tensile strain (%)	1.2-2.2	1.7-1.8	0.8-1.7
Tensile modulus (MPa)	70-80	70-120	220-300

The stress-strain behaviour of a typical TRM system is shown in Fig. 2.9. The stiffness of the uncracked composite material fits approximately to the modulus of the fine concrete at the initial stage of loading (Brameshuber, 2006; Hegger and Voss, 2008). Then, the state of first cracking is observed when the concrete tensile strength is exceeded. The textile reinforcement, interaction between concrete and textile and the tension failure strain of the matrix control the cracking distance and the crack width (Hegger and Voss, 2008). Since the used materials have no or little plastic capacity, the TRM composite fails in a brittle manner when the tensile failure strain of the textile is reached (Brameshuber, 2006; Bournas and Triantafillou, 2008).

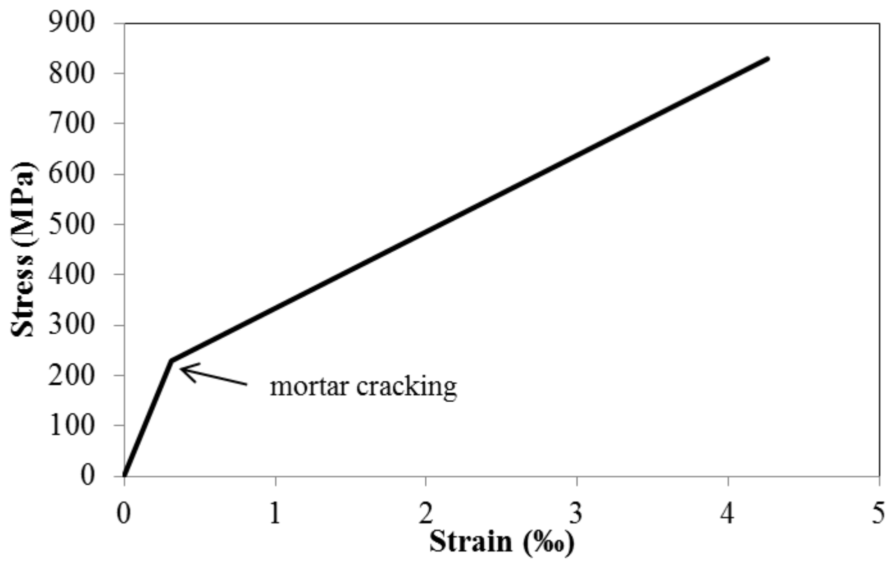

Figure 2.9: The tensile stress-strain curve for a typical TRM system

2.4.2 Uses of TRM

TRM can be applied in various fields such as in integrated formworks, facades, structural building members, as well as in the strengthening of existing structures. The type of matrices and textiles e.g. carbon, aramid, alkali resistant glass, or polyacetal determine the cost of raw materials of this system (Brameshuber, 2006). However, to apply TRM effectively in practical conditions, engineers should have full understanding of the behaviour of TRM rehabilitated RC structures or long-term performance of such structures which is obscure until now (Brameshuber, 2006; Amir et al. 2010; Ambrisi et al., 2012).

2.4.2.1 Reinforcement for new structure

TRM can be applied in a new structure as stay-in-place formwork. By applying TRM system, thin wall thickness (around 10 mm) is possible to achieve instead of thick concrete covers needed for ordinary RC structures to protect against corrosion (Brameshuber, 2006). In addition, fine grain concrete matrices guarantee an even and sharp edged high quality surface, so that TRM could be used for architectural applications. Although the knowledge about the load bearing behaviour of TRM is still limited, applications such as cladding panels (Hegger and Voss, 2005) and an integrated framework system (Papanicolaou et al., 2010) have already been implemented. TRM offers today a wide spectrum of applications either as an alternative to customary building materials or on account of his favourable characteristics for entirely new ranges of application. Hegger and Voss (2005) and Brameshuber (2006) have listed some applications of the TRM systems that have been executed such as diamond shaped framework, exterior cladding panels and wastewater treatment plant in RWTH Achen University, Germany; parapet sheet and balcony floor system in Dresden University, Germany; and footbridge in Oschatz, Germany.

2.4.2.2 Strengthening for existing structure

To date, very limited studies have been reported in the literature on the use of TRM system as a repair and strengthening material.

The preliminary results of the few studies have shown that TRM was able to increase the flexural and shear strength of reinforced concrete beams and enhanced the seismic performance of reinforced concrete columns (Triantafillou et al., 2005; Brameshuber, 2006; Bournas and Triantafillou, 2007; Amir et al., 2010; Yin and Xu, 2011; Alhaddad et al., 2012; Schladitz et al., 2012). Ortlepp et al. (2006), Bruckner et al. (2008) and Hashemi and Mahaidi (2010 and 2012) reported that the efficiency of the TRM depends on the anchoring of the TRM system in the compression zone and FRP textile is the better alternative compared to fabric.

The first study using TRM as a flexural strengthening system was on an 1800 mm one-way slab (Hegger and Voss, 2005; Triantafillou et al., 2005; Brameshuber, 2006; Bruckner et al., 2006). The main variables were the number of the textile layers used, the kind of anchorage and the percentage of steel reinforcement. The results showed an increase in the slabs' stiffness at service loads and 50%-85% increase in the slabs' capacity at ultimate load. The rotation capacity of the slabs at ultimate load was higher than that required by Eurocode 2. A bond length of 60 mm was used to anchor the TRM system and resulted in no bond failure between the strengthening layer and the concrete substrate.

In addition, studies on using TRM for shear strengthening of rectangular and T-beams reported an increase in the shear strength between 45% and 70% depending on the number of layers of textile used in the TRM system (Triantafillou et al., 2005; Bruckner et al., 2006; Ortlepp et al., 2006; Bruckner et al., 2008; Basalo et al., 2012; Contamine et al., 2013).

The first investigations of the torsional strengthening with TRM were carried out by Ortlepp and Curbach (2002). The results showed that the strengthened masts fail by a nearby 60% higher ultimate load than the unstrengthened masts.

Bournas and Triantafillou (2007, 2008, 2009 and 2011) studied the confinement effect of TRM systems on columns under static and seismic loads. Textile reinforced mortar systems increased the compressive strength and deformability of small specimens (100 mm long) under static loads. The gain was dependant on the number of layers of textile used and the tensile strength of the mortar. When compared with FRP, the TRM system was slightly less effective (about 10%). However, cyclic load tests on full-scale columns showed that TRM and FRP systems were equally effective in increasing the deformation capacity and the energy dissipation of the poorly detailed column specimens.

The seismic performance of the reinforced concrete beam-column joints upgraded by FRP and TRM systems was experimentally and numerically investigated by Alhaddad et al. (2012). The test results showed that the ultimate load carrying capacity of the TRM strengthened specimen was 13% less than the FRP strengthened specimen's.

The seismic behaviour of a TRM confined RC building was compared with that of a building confined with FRP jackets having equal stiffness and strength has been numerically investigated by Moniruzzman and Rteil (2012). The study concluded that TRM system is as effective as the FRP system in terms of load carrying capacity, inter-storey drift and energy dissipation capacity.

A few studies have been conducted on the use of TRM to strengthen masonry structures (Papanicolaou et al., 2007 and 2008). The results of these studies showed that TRM is comparable to FRP laminates, FRP near surface mounted (NSM) and steel wire mesh strengthening systems in increasing the strength and deformability of masonry structures.

Hashemi and Mahaidi (2012) investigated the heat endurance capacity of TRM retrofitted RC beams under constant service load. The retrofitted RC beam bonded with cement-based adhesive showed a significant improvement (41%) in flexural performance at high temperature compared to the specimens bonded with epoxy. The failure temperature was 844^0C which is near to the failure temperature of reinforced concrete beams. Thus, the results showed that the desired high temperature resistance was achieved by TRM system.

Ambrisi et al. (2012 and 2013) proposed a typical TRM bond-slip relationship by experimentally and analytically investigating the bond behaviour between TRM (made out of a poliparafenilenbenzobisoxazole (PBO) net embedded in a cement based matrix) and concrete substrate.

The studies reported in the literature have led to the following main conclusions:

- Rehabilitating reinforced concrete structures with TRM systems is a promising solution and can be as effective as the FRP systems and
- The behaviour of TRM strengthening systems is different from that of other strengthening systems, especially FRP due to different material properties and behaviour.

While the studies supported the use of TRM as a strengthening and repair material for reinforced concrete structures, it did not provide a full understanding of the behaviour of TRM rehabilitated RC structures. None of the research found was related to the application of TRM system to corrosion damaged beams.

2.5 Research Needs

The literature review presented in this chapter highlighted in detail the level to which flexural behaviour of corroded unstrengthened and FRP strengthened beams have been investigated. However, up to the author’s best knowledge, the performance of the TRM strengthened corroded beams was not reported in the literature. Thus, for inception of TRM in repairing corrosion damaged reinforced concrete beams, in lieu of FRP, a comparative evaluation is necessary.

To date, the results obtained from studies carried out to investigate the effect of the corrosion on the load carrying capacity of reinforced concrete beams did not encounter the case where both tensile reinforcement and corrosion level are varied.

Finally, little effort has been devoted to the development of finite element models to investigate the non-linear flexural response of corroded or FRP/TRM strengthened reinforced concrete beams. An accurate non-linear finite element model that can predict the load-deflection response of corroded and strengthened beams in both pre-yield and post-yield stages up to failure is needed which could serve as a numerical platform to the expensive and time consuming experimental testing.

2.6 Objectives of the Current Investigation

The purpose of this investigation is to examine the flexural performance of the beams damaged by corrosion and strengthened with FRP and TRM composite systems by finite element simulation. The specific objectives of the current numerical research work are as follows:

- To develop an accurate non-linear finite element model for the uncorroded and corroded beams,
- To develop an accurate non-linear finite element model for the FRP/TRM strengthened uncorroded and corroded beams,
- To study the effect of different corrosion levels and the steel reinforcement ratios on the structural performance in terms of load carrying capacity, displacement and ductility, stiffness and failure modes of the reinforced concrete beams,

- To investigate the viability of using FRP/TRM composite systems to repair uncorroded and corroded reinforced concrete beams having different reinforcement ratios at various levels of damage and
- To compare the behaviour of TRM composite system with the FRP system in terms of structural performance including load carrying capacity, displacement and ductility, stiffness and failure mode.

CHAPTER 3: FINITE ELEMENT MODELLING AND MODEL VERIFICATION

3.1 General

This chapter describes the procedure followed to develop and validate the finite element (FE) model used in this study. A total of eight three-dimensional (3D) nonlinear finite element (FE) models were developed using the simulation environment, ABAQUS (2013). The model considered different material constitutive laws for concrete in compression (crushing) and tension (cracking), steel yielding and material properties for the FRP and the TRM composite systems. The FE model was validated by comparing the obtained load–midspan deflection response, ultimate load carrying capacity and failure mode with the experimental results reported by Soudki and Sherwood (2000).

3.2 Geometry of the Developed FE Model

In order to validate the FE model, the current numerical study chose the experimental study conducted by Soudki and Sherwood (2000) which considered two test variables, corrosion level and the existence of FRP. The tested RC beams, reported by Soudki and Sherwood (2000), were 1200 mm long, 150 mm deep and 100 mm wide (Fig. 3.1). The clear span of the tested RC beams was 1050 mm. The main flexural steel reinforcement were two 10M (10 mm) Grade 400 rebars located at a depth of 130 mm from the compression fibers of the beam. In addition, two 6 mm diameter smooth bars were included in the compression zone at a depth of 20 mm from the aforementioned location. To prevent shear failure, shear reinforcement consisting of 6 mm diameter Grade 400 smooth bars spaced at 75 mm centre to centre were provided. The FRP strengthening system was applied on the soffit of the control (unstrengthened) beam. The length and width of the strengthening system were 950 mm and 60 mm respectively which were placed symmetrically under the control beam. The corrosion was applied to the tensile reinforcement in the constant moment region only (Fig. 3.1).

Due to the symmetry of the geometry, loading, boundary conditions and material properties, a quarter FE model was built and simulated in the finite element software, ABAQUS (2013). Fig. 3.2 shows the two planes of symmetry in the longitudinal and transverse directions for all tested beam specimens. The advantage of building quarter models for the tested beam specimens is the reduction in the total number of elements which resulted in tremendous savings of computational time (Ebead and Marzouk, 2005; Obaidat, 2011; Hawileh et al., 2013). Fig. 3.3 shows the boundary conditions and the loading set-up of the modelled quarter beam. The symmetrical boundary conditions were developed by inserting vertical restrains (rollers) at each node located in the two planes of symmetry in the transverse and longitudinal directions.

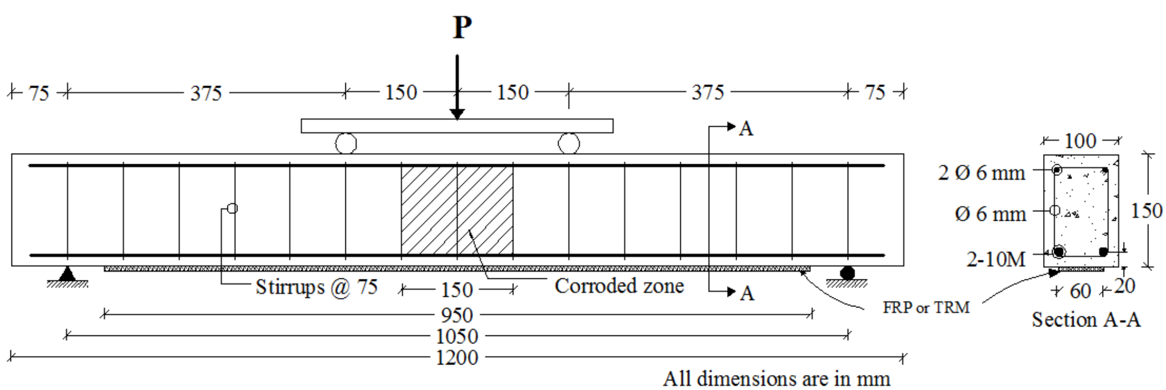

Figure 3.1: Tested beam details and location of point loading (Soudki and Sherwood, 2000)

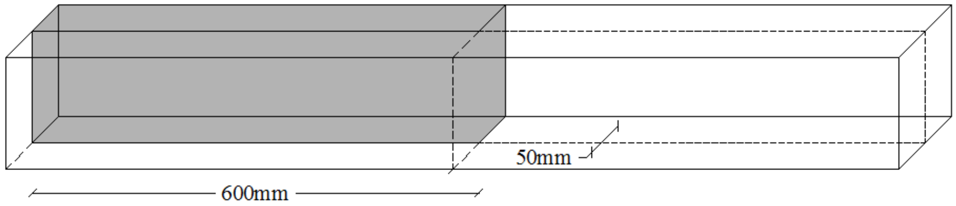

Figure 3.2: The modelled one quarter beam section

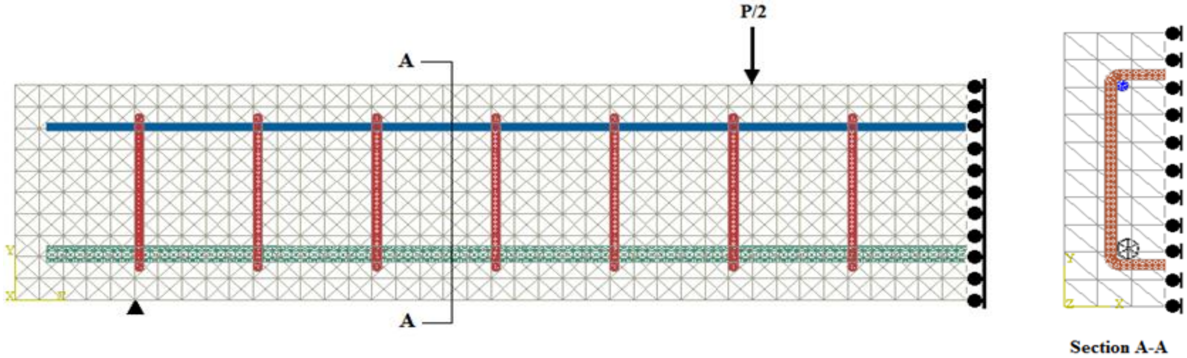

Figure 3.3: Loading and boundary conditions of a typical finite element meshed beam

3.3 Material Properties and Constitutive Models

3.3.1 Concrete

To predict the behaviour of concrete two concrete models are available in ABAQUS (2013): smeared crack and damage plasticity models. The concrete damage plasticity (CDP) model was selected for this study due to the following reasons (Obaidat, 2011; Chaudhari and Chakrabarti, 2012; ABAQUS, 2013):

- It has higher potential for convergence compared to the smeared crack model;
- It can consider different yield strength in tension and compression;
- It counts true post yield (plastic) response like softening behaviour in tension as opposed to initial hardening followed by softening in compression;
- Different degradation of the elastic stiffness in tension and compression can be considered in this model.

The concrete damage plasticity model assumes two failure modes as tensile cracking and compressive crushing. ABAQUS (2013) allows to model crack propagation by using stiffness degradation. The degradation of the elastic stiffness is characterized by two damage variables, d_c and d_t, which are assumed to be functions of the plastic strains. They can take values ranging from zero, for the undamaged material, to one, for the fully damaged material. Linear relationship between the damage variables and the stress in the concrete was assumed in this study. More details about the concrete damage plasticity model are provided in Appendix A. Poisson's ratio for concrete was assumed to be 0.15.

The concrete model in compression is elastic until the initial yield is reached. The initial yield defines the elastic limit at which the linear elastic constitutive relationships are valid (line OA in Fig. 3.4). The failure stress (point B in Fig. 3.4) corresponds to the onset of micro-cracking in the concrete material. Beyond the failure stress the formation of micro-cracks is represented with a softening stress–strain response (segment BC in Fig. 3.4). For defining the stress-strain curve of concrete, this study used Collins and Mitchell (1997) model (Fig. 3.4):

$$\frac{f_c}{{f_c}'} = \frac{n\left(\frac{\epsilon_c}{\epsilon_0}\right)}{n-1+\left(\frac{\epsilon_c}{\epsilon_0}\right)^{nk}} \tag{3.1}$$

where, ${f_c}'$ is the concrete compressive strength; n = curve fitting factor $= 0.8 + \frac{f_c'}{17}$; ϵ_0 = concrete strain at ${f_c}' = \frac{f_c}{E_c}\frac{n}{n-1}$; k = stress decay factor = $0.67 + \frac{{f_c}'}{62} > 1$; E_c = modulus of elasticity = $\left(3300\sqrt{{f_c}'} + 6900\right)\left(\frac{\gamma_c}{2300}\right)$ for concrete density $1500 \le \gamma_c \le 2500$ Kg/m^3.

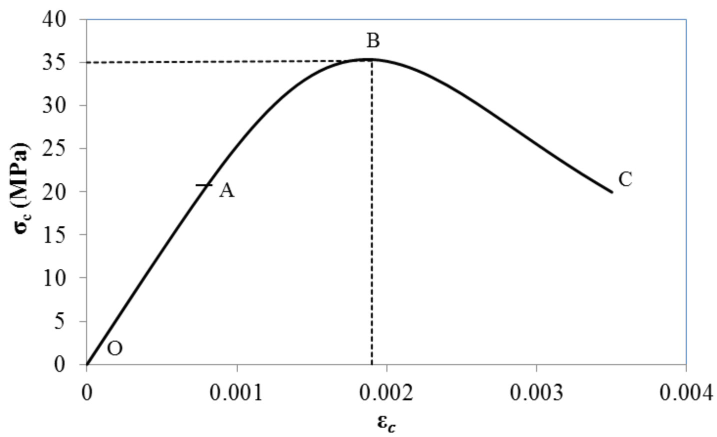

Figure 3.4: Stress–strain relationship for concrete under uniaxial compression

Concrete behaviour in tension is linear elastic until the cracking stress is reached (Fig. 3.5). Cracks develop in reinforced concrete when the tension stress in the concrete exceeds its tensile capacity. Therefore, at the crack location, the tension force is resisted only by the steel. In between the cracks, interfacial shear stresses between the reinforcement and the concrete transmit some of the tension force back to the concrete. This result is increased stiffness between the cracks, a phenomenon known as tension stiffening (Ebead and Marzouk, 2005; ABAQUS, 2013).

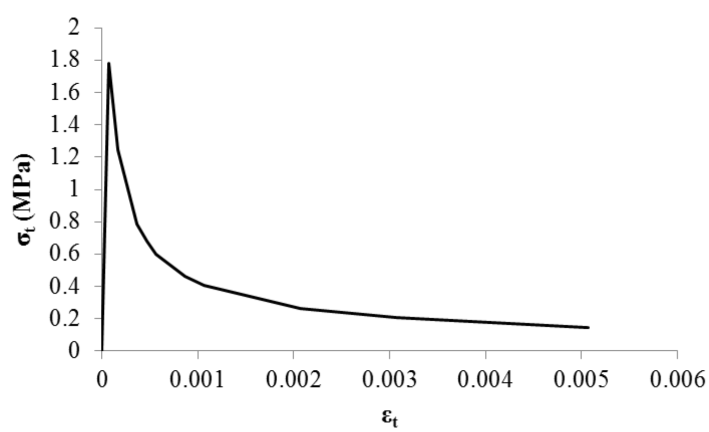

Figure 3.5: Stress–strain relationship for concrete under uniaxial tension

The concrete damage plasticity constitutive model addresses the tensile behaviour of concrete by considering several characteristics like cracking, fracture energy, shear modulus degradation and tension stiffening. In the case of reinforced or strengthened concrete, the calculations are made based on the assumption of a smeared crack approach (Lodygowski and Jankowiak, 2005; Yu and Huang, 2008; Lin and Scanlon, 2010; Kmiecik and Kamiński, 2011; Obaidat, 2011; ABAQUS, 2013). In this study, the tensile behaviour of concrete was described through the tensile stress-strain relationship. By this way, the smeared crack approach was adopted in the finite element simulation. The expressions given by Marzouk and Chen (1995), were used to define tension stiffening model for concrete as follows (Fig. 3.5):

For $\varepsilon_t \geq \varepsilon_{to}$

$$\sigma_t = \sigma_t{}^u \left[\frac{\varepsilon_t / \varepsilon_{to}}{\alpha\left(\varepsilon_t / \varepsilon_{to} - 1\right)^{\beta} + \left(\varepsilon_t / \varepsilon_{to}\right)} \right] \tag{3.2}$$

where, $\alpha = C_3 \sigma_t{}^u$, ε_t is the concrete tensile strain and ε_{to} is the concrete tensile strain at maximum stress ($\sigma_t{}^u$).

In order to determine the constants C_3 and β, several attempts were implemented in the finite element model by altering the values of C_3 (in the range of 0.2 to 0.4) and β (in the range of 1.1 to 2.0) until an agreement of the FE results with the available experimental results with respect to the ultimate load carrying capacity was achieved. Table 3.1 shows the results of this analysis.

Table 3.1: Values of C_3 and β

Strengthening system	Corrosion	C_3	β
None	0	0.25	2.00
	5	0.30	1.87
	10	0.35	1.90
	15	0.40	2.00
FRP	0	0.40	1.10
	5	0.20	1.70
	10	0.30	1.85
	15	0.40	1.70

It should be noted that in this study, for the TRM strengthened specimens, the values of C_3 and β derived for the FRP were used. This is because of considering both systems were equal in terms of stiffness and strength.

3.3.2 Steel Reinforcement

Steel is a linear-elastic material up to the initial yield stress. At ultimate tensile strain, it begins to narrow and strength is reduced. Subsequently, it fractures and the load carrying capacity is lost (ASTM A615, 1995). An elastic-plastic constitutive model, either with or without strain hardening, is normally assumed for general structural engineering applications to define ductile reinforcing steel (Fig. 3.6). However, an elastic-perfectly plastic relationship generally gives acceptable results for the prediction of RC members' behaviour (Neale et al., 2005; Obaidat, 2011).

Therefore, in this study the constitutive model used to simulate the steel reinforcement was the classical elastic-perfectly plastic model. The elastic modulus (E_s) was taken as 200 GPa, yield stress (f_y) as 445 MPa and Possion's ratio as 0.3. The corrosion was considered in the constant moment area only, while the anchorage zone (shear span) in all specimens was unaffected. Given that the available anchorage length is enough to develop the yield stress in the steel reinforcement, then according to Cairns and Zhao (1993), the flexural behavior of the beam would not be affected. Accordingly, the interaction between steel reinforcement and concrete was assumed as a perfect bond (Fig. 3.7).

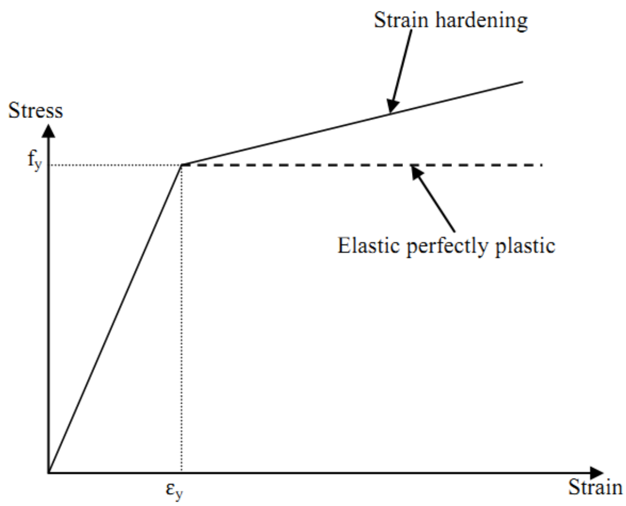

Figure 3.6: Idealized stress-strain relationship for reinforcing steel

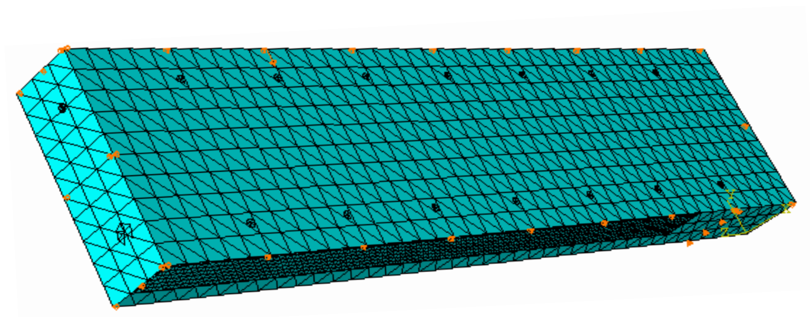

Figure 3.7: Beams with reinforcements

3.3.2.1 Corroded reinforcement

The current study used a mass loss due to pit corrosion and, therefore, in terms of equivalent volume loss ($A_{initial} - A_{res} = 5\%, 10\%, and\ 15\%\ of\ A_{initial}$). Consider a reinforcing bar with initial diameter, d_b. As a result of corrosion, the bar diameter is reduced. The residual cross sectional area of the tensile reinforcement attacked by corrosion can be evaluated as follows (Fig. 3.8):

$$A_{res} = \frac{\pi.(d_b)_r{}^2}{4} = \frac{\pi.(d_b - \lambda x)^2}{4} \tag{3.3}$$

where $(d_b)_r$ is the residual bar diameter, λ is a coefficient depending on the type of attack and x is the corrosion penetration.

When uniform corrosion occurs, λ is equal to 2. In the case of pit corrosion, the value of λ is in the range between 4 to 10 (Gonzalez et al., 1995; GEOCISA, 2004). Table 3.2 summarizes the values of λ and x used in this study following the recommendation by Gonzalez et al. (1995).

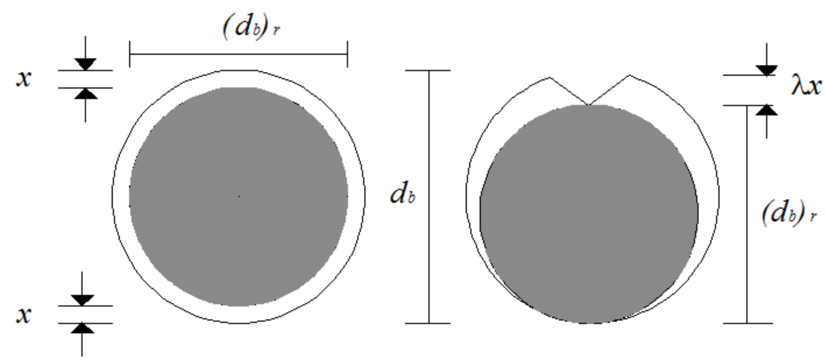

a) Uniform corrosion b) Pit corrosion

Figure 3.8: Corrosion in reinforcement

Table 3.2: Corroded and uncorroded reinforcement parameters

Corrosion level (%)	α	Reinforcement ratio (%)	x (mm)
5	6	0.77	0.439
		1.54	0.621
		2.31	0.760
10	8	0.77	0.465
		1.54	0.659
		2.31	0.806
15	10	0.77	0.456
		1.54	0.645
		2.31	0.789

3.3.3 Fibre Reinforced Polymer

An isotropic linear elastic relationship up to failure was used in this study to model the stress-strain behaviour of the FRP system. While the FRP properties are not isotropic, in this study it was assumed isotropic since the direction of the fibres is parallel to that of the principal stresses (Neale et al., 2005). The properties of the FRP system used were similar to the one reported by Soudki and Sherwood (2000). It had an elasticity modulus of 73 GPa, an ultimate strength of 960 MPa and an ultimate elongation of 1.33%. Poisson's ratio was assumed to be 0.22 in this study. A perfect bond between the FRP laminates and concrete was considered (Fig. 3.7).

3.3.4 Textile Reinforced Mortar

In order to have both strengthening systems (the FRP and the TRM) equivalent in stiffness and strength [$(EA)_{FRP} = (EA)_{TRM}$], the layers in the TRM strengthened beams were considered twice as many compared with their FRP counterparts (Bournas and Triantafillou, 2009; Alhaddad et al., 2012). Due to functioning in together, the bulk properties of the textile sheets were utilized in the modelling and not the properties of individual textile fibres. Moreover, the mortar contribution was ignored because its effect on tensile strength is insignificant.

To simulate the TRM behaviour, its properties were adopted from Alhaddad et al. (2012) which referred to a manufacturer's reported data sheet. Two commercial textiles with equal quantity of carbon rovings in two orthogonal directions were used. Each fiber roving was 3.93 mm wide and the clear spacing between rovings was 10.67 mm. The weight of the carbon fibers in the textiles was 348 g/m^2, while the nominal thickness of each layer based on the equivalent smeared distribution of fibers was 0.49 mm (Alhaddad et al., 2012). The material was assumed to fail if the maximum strain reached a limiting value of 0.0095. To keep harmony with FRP system, a perfect bond was assumed between TRM composite system and concrete substrate. The TRM validation was performed in a previous study by the author (Moniruzzaman and Rteil, 2012).

A summary of the material properties used in the modelling of specimens are shown in Table 3.3.

Table 3.3: Material properties of specimens

Material	Property	Value
Concrete	Average concrete strength, f_c'	35 MPa
	Elastic modulus of concrete, E_c	26 GPa
Steel	Average yield strength of steel, f_y	445 MPa
	Elastic modulus of steel, E_s	200 GPa
FRP sheets	Elastic modulus	73 GPa
	Fracture strain	1.33%
	Ultimate tensile strength	960 MPa
	Thickness per layer	1.1 mm
TRM sheets	Elastic modulus per one textile	82.33 GPa
	Fracture strain	0.95%
	Ultimate tensile strength per one textile	777 MPa
	Thickness per one textile	0.49 mm
	Width per one textile	3.93

3.4 Nonlinear Analysis

To model specimens having internal steel bars as reinforcement, 4-node linear tetrahedral elements (C3D4) were used for the concrete, reinforcement steel, FRP and TRM (Fig. 3.9). In C3D4 element, each node has three translational degrees of freedom in the x, y and z directions (ABAQUS, 2013). This element type was used because the beam has a complex geometry since there are steel bars inside the concrete. Moreover, this element exhibits the damage variables, d_c and d_t in the output result.

A fine top-down meshing technique with element deletion was adopted to obtain results with sufficient accuracy. In this regard, a mesh convergence study was performed by simulating the same beam with a finer mesh. The mesh was said to be converged when further mesh refinement produced a negligible change in the results. Moreover, the fine mesh ensured very low internal and artificial energy (less than 2%). To connect FRP/TRM and concrete a tied contact was used. In this approach, each of the nodes on the FRP or TRM material has the same displacement as the point on the concrete (ABAQUS, 2013). This allowed for the modelling of normal and shear stresses along the entire tied surfaces. On the other hand, steel reinforcements were considered as embedded elements in the concrete host region. Static nonlinear analysis was followed by adopting Quasi-Newton solution techniques. The analysis was nonlinear in terms of geometry, materials and boundary conditions.

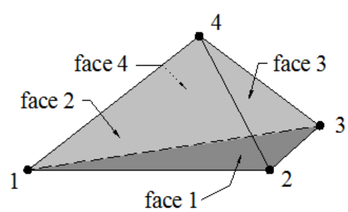

Figure 3.9: 4-node linear tetrahedron (C3D4) element

3.5 Model Validation

The current numerical analysis was involved with the material nonlinearity and associated large deformations that made the convergence of the solution initially hard to achieve using the program default values. In order to validate the model i.e. to ensure the analysis will follow the load-deflection curve and to improve the convergence, very small time increments were used in the ABAQUS/Standard. In addition, in order to ensure that the residual force is almost equal to the load increment when considering non-linear analysis, a damping factor based on the dissipated energy fraction of 2.0×10^{-5} was used (Lodygowski and Jankowiak, 2005; Obaidat, 2011). The model was verified by comparing its failure modes, load carrying capacity and displacement behaviour to the experimental results.

3.5.1 Failure Mode

Figs. 3.10 and 3.11 represent the failure modes of the simulated beams. Failure occurred as follows:

- For the unstrengthened beam specimens, yielding of the steel reinforcement in tension followed by concrete crushing;
- For the strengthened beam specimens with FRP laminates, yielding of steel reinforcement in tension, concrete failing in compression before FRP laminates rapture.

These failure modes are in agreement with those observed in the experimental study.

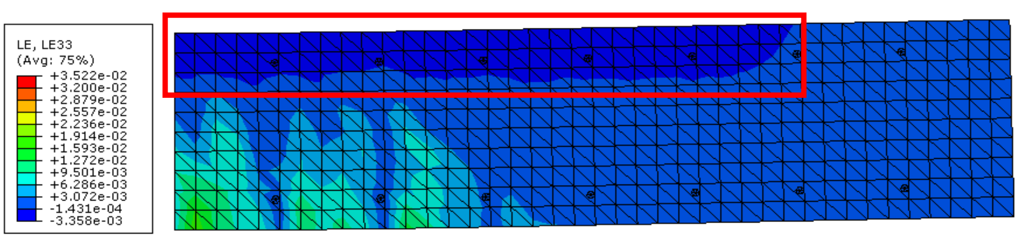

a) Unstrengthened beam (red box shows concrete crushing zone)

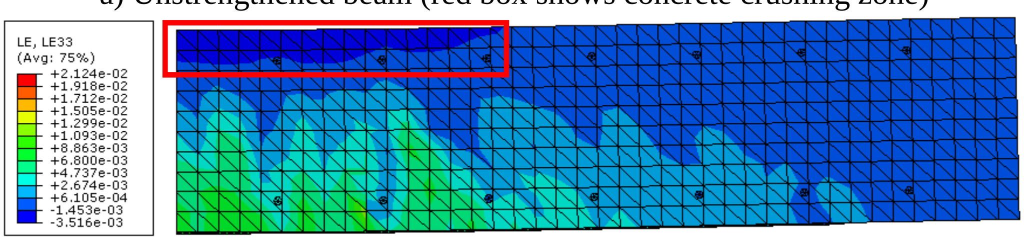

b) Strengthened beam (red box shows concrete crushing zone)

Figure 3.10: Axial strain distribution of unstrengthened and strengthened corrosion damaged beams (at 15%)

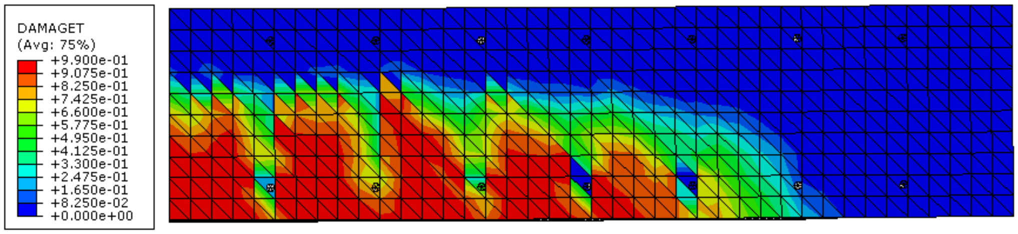

Figure 3.11: Flexural crack pattern of the strengthened 15% corrosion damaged beam

3.5.2 Load-Deflection Behaviour

Fig. 3.12 compares the load–midspan deflection behaviour obtained by FE analysis and observed by the experimental tests for the low (0%) and the severe (15%) corrosion damaged beams. The structural performance of the FRP strengthened specimens was improved with the exception of ductility, as shown in Fig. 3.12.

The comparison between the FE model and the experimental values of the load and the corresponding displacement at yield and failure of the corroded and uncorroded beams, are shown in Tables 3.4 and 3.5. From the comparison presented in Tables 3.4 and 3.5 and in Fig. 3.12 it can be seen that the FE predictions of strengthened and unstrengthened beams in terms of ultimate loads were very close to the experimental results with on average prediction/ experiment ratio of 1.03 and a standard deviation (SD) of less than 3% (Table 3.4). This close alignment was observed in case of the ultimate displacements of the strengthened beams as well (Table 3.5). However, values from the FE simulation for the ultimate deflection of the control beams were about 17% off from the experimental values. On the other hand, the variations between the FE and the experimental yield loads of the control and strengthened beams were on average 19% and 0%, respectively (Table 3.4). The displacements at the yield load of the control and the FRP beams were on average 12% and 20% lower than the experiment, respectively (Table 3.5).

The FE and the experimental results in terms of the yield and ultimate loads and their corresponding displacements were in general in good agreement (Fig. 3.12, Table 3.4 and 3.5). The variation seen between the experiment and the FE model could be attributed to the assumptions made especially concrete crushing at 3500 micro-strain (με) and to the fact that variations are expected in the experimental results. Hence, it can be concluded that the good agreement between the FE models and the experimental values indicates that the FE and the constitutive models used for the concrete and the reinforcement can capture the general behaviour well.

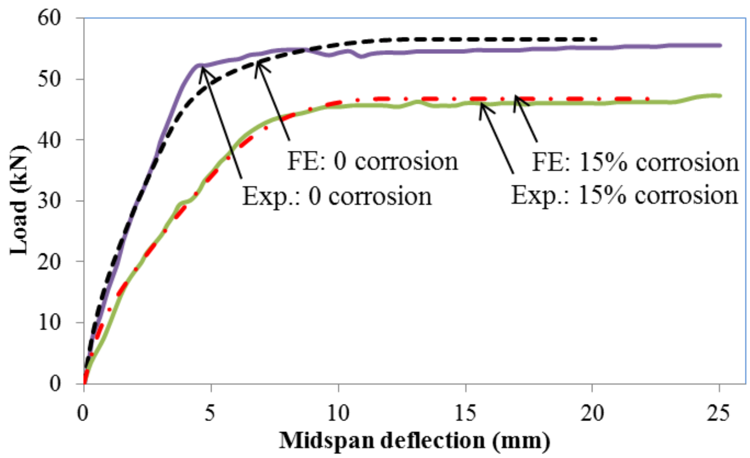

a) Control beams

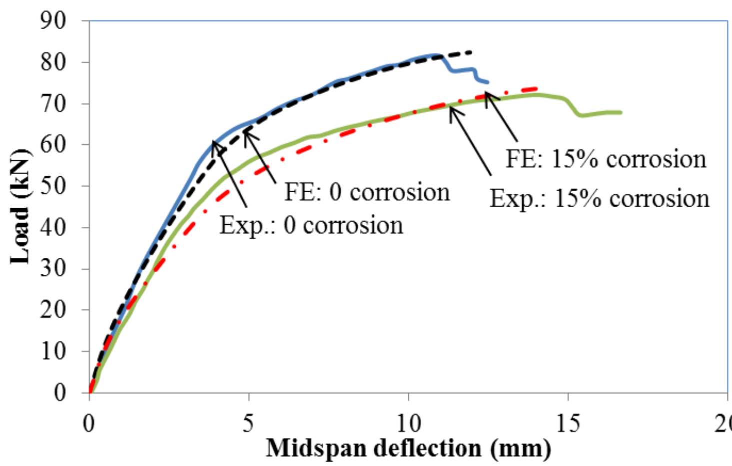

b) FRP strengthened beams

Figure 3.12: Load–deflection curves of obtained by experiments and FE analysis

Table 3.4: Model validation: load carrying capacity

Group	Corrosion	Yield load (kN)		FE/ Exp.	Avg.	SD (%)	Ultimate load (kN)		FE/ Exp.	Avg.	SD (%)
		Exp.	FE				Exp.	FE			
Control	0	51.70	45.16	0.87	0.81	8.0	55.8	56.5	1.01	1.03	2.9
	5	49.00	42.55	0.87			51.9	54.8	1.06		
	10	47.30	37.51	0.79			50	53.1	1.06		
	15	44.10	30.99	0.70			47.3	47.5	1.00		
FRP	0	62.90	63.88	1.02	1.00	1.9	81.8	82.2	1.00	1.02	2.6
	5	62.00	61.44	0.99			78.7	78.2	0.99		
	10	58.40	59.65	1.02			75.5	79.5	1.05		
	15	56.00	54.92	0.98			72.2	73.7	1.02		

Table 3.5: Model validation: displacement

Group	Corrosion	Yield deflection (mm)		FE/ Exp.	Avg.	SD (%)	Ult. deflection (mm)		FE/ Exp.	Avg.	SD (%)
		Exp.	FE				Exp.	FE			
Control	0	5.80	4.94	0.85	0.88	6.1	25.0	20.15	0.81	0.83	1.9
	5	5.90	4.80	0.81			25.0	20.37	0.81		
	10	5.00	4.71	0.94			25.0	20.73	0.83		
	15	4.73	4.37	0.92			25.0	21.21	0.85		
FRP	0	4.80	3.75	0.78	0.80	6.5	12.15	11.26	0.93	1.03	15.5
	5	4.70	3.87	0.82			9.89	11.92	1.21		
	10	5.50	4.07	0.74			11.20	12.66	1.13		
	15	5.20	4.54	0.87			16.64	14.29	0.86		

CHAPTER 4: RESULTS AND DISSCUSSION

4.1 General

The previous chapter described the eight finite element (FE) models which were validated with experimental results conducted by Soudki and Sherwood (2000). This chapter examines the effects of reinforcement ratio and the strengthening technique on corrosion damaged beams in terms of failure modes, load carrying capacity, displacement, stiffness and ductility behaviours.

4.2 Parametric Study

A parametric study was carried out by developing 28 models to investigate the effect of steel reinforcement ratios, corrosion levels and the type of the strengthening techniques used. It should be noted that the FE models used in the parametric study had the same material constitutive laws and assumptions described in the previous chapter. According to CSA A23.3 (2004) the balanced reinforcement ratio for the beam used in this study, ρ_b is 3.0% and the minimum reinforcement ratio, ρ_{min} is 0.3%. Soudki and Sherwood (2000) used a reinforcement ratio ρ_{used} of 1.54% in their experimental study. The parametric study considered $\pm$ 50% variation of ρ_{used} i.e. ρ_l was 0.77% and ρ_h was 2.31% which were 26% and 77% of ρ_b, respectively. Also, two repair materials- the FRP and the TRM systems were applied to strengthen the corrosion damaged beams. Thus, the study consisted of three main groups- control (unstrengthened), FRP and TRM strengthened beams having 12 specimens in each group. These specimens were further divided into 4 groups based on their corrosion level (0%, 5%, 10% and 15% mass loss), each having 3 beams. The corrosion was applied in the constant moment region only (Fig. 3.1). Table 4.1 shows the matrix of the parametric study. The beam specimens were designated using a 3-part system, X-Y-Z where X indicates the strengthened system (C=Control, F=FRP strengthened, T= TRM strengthened), Y indicates the reinforcement ratio (L=0.77%; M=1.54%; H=2.31%) and Z represents the percentage loss of reinforcement steels due to corrosion (0, 5, 10 and 15).

Table 4.1: Test matrix

Group		Specimen notation	ρ (%)	% of ρ_b (ρ_b=3%)	Corrosion level (%)	Strengthening technique
Control	Un-corroded	C-L-0	0.77	26	0	None
		C-M-0	1.54	51	0	None
		C-H-0	2.31	77	0	None
	5% corrosion	C-L-5	0.77	26	5	None
		C-M-5	1.54	51	5	None
		C-H-5	2.31	77	5	None
	10% corrosion	C-L-10	0.77	26	10	None
		C-M-10	1.54	51	10	None
		C-H-10	2.31	77	10	None
	15% corrosion	C-L-15	0.77	26	15	None
		C-M-15	1.54	51	15	None
		C-H-15	2.31	77	15	None
FRP	Un-corroded	F-L-0	0.77	26	0	FRP
		F-M-0	1.54	51	0	FRP
		F-H-0	2.31	77	0	FRP
	5% corrosion	F-L-5	0.77	26	5	FRP
		F-M-5	1.54	51	5	FRP
		F-H-5	2.31	77	5	FRP
	10% corrosion	F-L-10	0.77	26	10	FRP
		F-M-10	1.54	51	10	FRP
		F-H-10	2.31	77	10	FRP
	15% corrosion	F-L-15	0.77	26	15	FRP
		F-M-15	1.54	51	15	FRP
		F-H-15	2.31	77	15	FRP
TRM	Un-corroded	T-L-0	0.77	26	0	TRM
		T-M-0	1.54	51	0	TRM
		T-H-0	2.31	77	0	TRM
	5% corrosion	T-L-5	0.77	26	5	TRM
		T-M-5	1.54	51	5	TRM
		T-H-5	2.31	77	5	TRM
	10% corrosion	T-L-10	0.77	26	10	TRM
		T-M-10	1.54	51	10	TRM
		T-H-10	2.31	77	10	TRM
	15% corrosion	T-L-15	0.77	26	15	TRM
		T-M-15	1.54	51	15	TRM
		T-H-15	2.31	77	15	TRM

The following sections will present and discuss the results obtained in detail. The failure modes, strain analysis, load carrying capacity, displacement and ductility and stiffness behaviour will be discussed in sections 4.3, 4.4 4.5, 4.6 and 4.7, respectively.

4.3 Failure Modes

In the flexural strengthening of a reinforced concrete beam, it is essential to understand the effects of the strengthening systems on the beam failure mode, especially for the development of suitable design guidelines under ultimate loading conditions. Failure of a beam was assumed when concrete compressive strain exceed 3500 $\mu\varepsilon$ or FRP/TRM reached their fracture strain whichever was met first. Table 4.2 listed the failure modes for all the beams, while Fig. 4.1 shows different typical failure modes. The following sections describe the failure modes obtained for the unstrengthened and the strengthened beams.

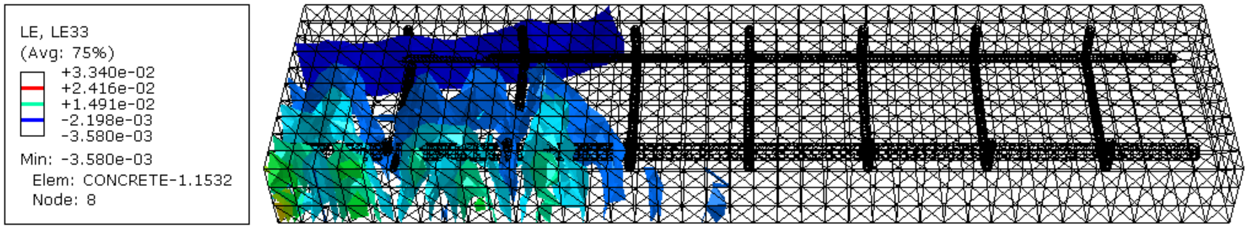

a) Concrete crushing (C-M-0)

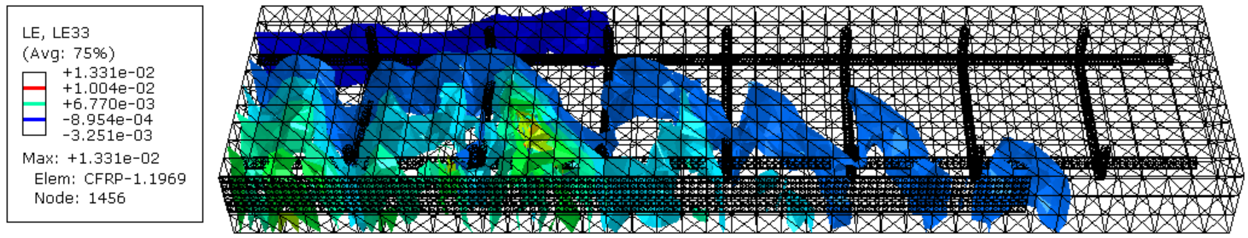

b) FRP rupture (F-L-0)

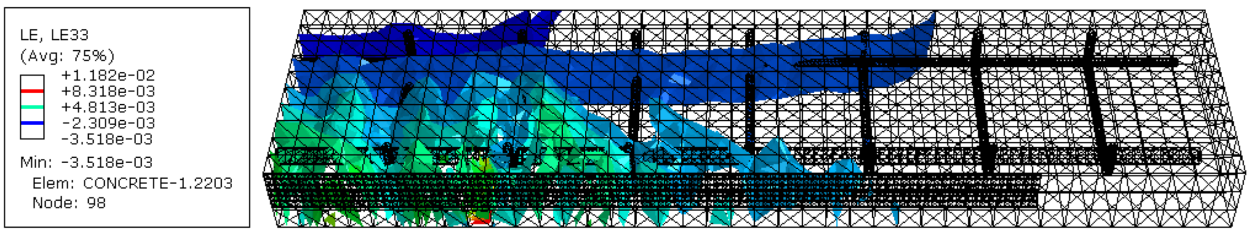

c) Concrete crushing (F-M-0)

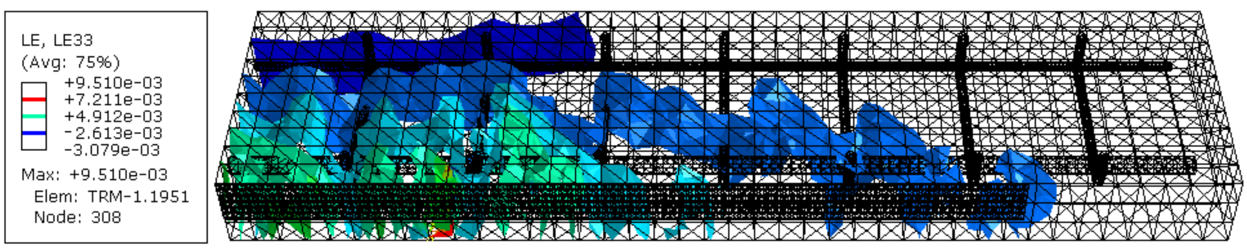

d) TRM rupture (T-M-0)

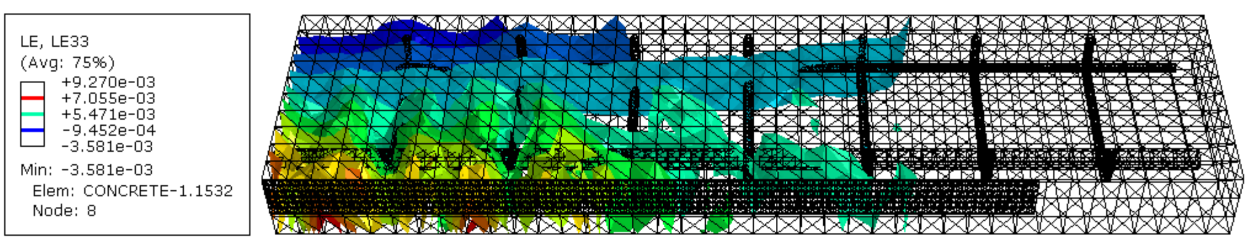

e) Concrete crushing (T-H-0)

Figure 4.1: Typical failure modes of the studied beams

Table 4.2: Failure modes of the specimens

Group		Specimen notation	Failure mode
Control	Un-corroded	C-L-0	Steel yielding followed by concrete crushing
		C-M-0	Steel yielding followed by concrete crushing
		C-H-0	Steel yielding followed by concrete crushing
	5% corrosion	C-L-5	Steel yielding followed by concrete crushing
		C-M-5	Steel yielding followed by concrete crushing
		C-H-5	Steel yielding followed by concrete crushing
	10% corrosion	C-L-10	Steel yielding followed by concrete crushing
		C-M-10	Steel yielding followed by concrete crushing
		C-H-10	Steel yielding followed by concrete crushing
	15% corrosion	C-L-15	Steel yielding followed by concrete crushing
		C-M-15	Steel yielding followed by concrete crushing
		C-H-15	Steel yielding followed by concrete crushing
FRP retrofitted	Un-corroded	F-L-0	Steel yielding followed by FRP rupture
		F-M-0	Steel yielding followed by concrete crushing
		F-H-0	Steel yielding followed by concrete crushing
	5% corrosion	F-L-5	Steel yielding followed by FRP rupture
		F-M-5	Steel yielding followed by concrete crushing
		F-H-5	Steel yielding followed by concrete crushing
	10% corrosion	F-L-10	Steel yielding followed by FRP rupture
		F-M-10	Steel yielding followed by concrete crushing
		F-H-10	Steel yielding followed by concrete crushing
	15% corrosion	F-L-15	Steel yielding followed by FRP rupture
		F-M-15	Steel yielding followed by concrete crushing
		F-H-15	Steel yielding followed by concrete crushing
TRM retrofitted	Un-corroded	T-L-0	Steel yielding followed by TRM rupture
		T-M-0	Steel yielding followed by TRM rupture
		T-H-0	Steel yielding followed by concrete crushing
	5% corrosion	T-L-5	Steel yielding followed by TRM rupture
		T-M-5	Steel yielding followed by TRM rupture
		T-H-5	Steel yielding followed by TRM rupture
	10% corrosion	T-L-10	Steel yielding followed by TRM rupture
		T-M-10	Steel yielding followed by TRM rupture
		T-H-10	Steel yielding followed by TRM rupture
	15% corrosion	T-L-15	Steel yielding followed by TRM rupture
		T-M-15	Steel yielding followed by TRM rupture
		T-H-15	Steel yielding followed by TRM rupture

4.3.1 Control Beams

Depending upon the beam properties, flexural failures may occur in three different ways:

- Tension failure: Steel reinforcement yields before concrete crushes.
- Compression failure: Concrete crushes before steel yields.
- Balanced failure: Concrete crushes and steel yields simultaneously.

For very high reinforcement ratios ($\rho > \rho_b$) failure of the beam can be caused by compressive crushing of the concrete before the tensile steel yields. This failure mode is brittle and undesirable. However, in this study all of the control beams had a reinforcement ratio less than the balanced reinforcement ratio ($\rho < \rho_b$). Hence, as expected, the flexural strength of the control beams was reached with yielding of the tensile steel reinforcement followed by crushing of the concrete in the compression zone (Fig 4.1-a, Table 4.2). It is concluded that for the control beams, the level of corrosion and the level of reinforcement ratio had no effect on the failure mode as long as $\rho < \rho_b$.

4.3.2 FRP Strengthened Beams

The failure mode changed when changing the reinforcement ratio for the FRP strengthened beams. For beams having low reinforcement ratio, the failure was initiated by steel yielding followed by FRP rupture in tension (Fig 4.1-b, Table 4.2). This observation has met the expectation mentioned by Bonacci and Maalej (2001) and Thomsen et al. (2004). For high and medium reinforcement ratios, the strengthened beams failed by concrete crushing in compression after steel yielded with the FRP laminate still intact (Fig. 4.1-c, Table 4.2).

This is because for low reinforcement ratio, the FRP had to resist more load than in the case of medium and high reinforcement ratio. Therefore, the FRP experienced higher strain values compared to its counterpart with medium and high reinforcement ratios leading to its failure before concrete crushing. This was further shown by the crack distribution, for beams with low reinforcement ratio, the cracks were distributed along the entire length; while for beams with high and medium reinforcement ratios, the cracks were concentrated within the middle region.

The transition of the failure mode is depicted in Fig. 4.2 through the strain distribution mechanism. The line XOY' represents the strain distribution at failure. The concrete was crushed (ϵ_{cu}, point X) while the FRP was intact (point Y'). As the reinforcement ratio decreased, the neutral axis shifted upward from point O to point O'. As a consequence, the line X$O'Z'$ representing the strain distribution under the same load as line XOY' now has a higher tensile strain at the bottom of the beam (shifted tensile strain from point Y' to point Z'), thus exceeding the ultimate capacity of the FRP (ϵ_{Fu}, point Z). Therefore, FRP ruptured before concrete crushed (line PO'Z).

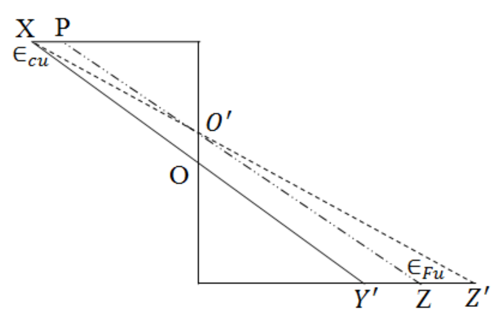

Figure 4.2: Change of failure mode with lowering reinforcement ratio

Based on the parametric study considering the variation of the reinforcement ratio and the material properties used in this study, it can be concluded that for design applications FRP should be applied on beams such that the strengthened beams would not be over reinforced ($\rho_{steel+FRP} < \rho_b$) and at the same time for utilizing the full strength of the FRP, the beams should have steel reinforcement ratio not more than 24% of the balanced reinforcement ratio ($\rho \leq 0.24\,\rho_b$). This value was determined by observing the failure modes of the beams having different reinforcement ratios and is valid for the considered parameters in this study. However, the FRP laminates must be well anchored for this failure to take place to prevent any premature failure due to debonding of the sheets.

4.3.3 TRM Strengthened Beams

Unlike the control beams, all of the TRM strengthened beams but specimen T-H-0, had a tensile flexure failure where the steel yielded followed by tensile rupture of the TRM prior to crushing of the concrete (Fig. 4.1-d, Table 4.2). Only the uncorroded TRM strengthened beam having high reinforcement ratio failed by concrete crushing in compression after steel yielded with the TRM still intact (Fig. 4.1-e).

This was different than the FRP, because the ultimate strain of the TRM system was 40% less than that of the FRP. Therefore, it had lower tensile capacity that led to its rupture prior to concrete reaching its compression capacity. On the other hand, similar to the FRP strengthened beams, cracks distributions were uniform over the length of the TRM strengthened beams when failure was initiated by TRM rupture (Fig. 4.1-d), while it was concentrated in the constant moment region for specimen T-H-0 that failed by concrete crushing (Fig. 4.1-e).

Hence, it could be conclude that similar to the FRP strengthened beam, TRM should be applied on the beams such that the strengthened beams would not be over reinforced ($i.e.\ \rho_{steel+TRM} < \rho_b$). At the same time for utilizing the full strength of the TRM that used in this study, the beams should have steel reinforcement ratio not more than 73% of the balanced reinforcement ratio ($\rho \leq 0.73\,\rho_b$) and the TRM system should be anchored to prevent any premature failure. This value was determined by observing the failure modes of the beams having different reinforcement ratios and is valid for the considered parameters in this study.

4.4 Strain Analysis

Strain analysis was conducted to examine the behaviour of the concrete, steel and FRP/TRM at yield and ultimate conditions. The stress did not vary too much between the yield and ultimate state; hence, performing strain analysis seemed more rational. Strain was read along the length of the quarter beam from the boundary end to the loading end as shown in Fig. 4.3. Concrete strain was noted at the level that surrounds the longitudinal tensile steel. Steel strain was taken at the bottom rebar elements and FRP/TRM strain was measure at the soffit of the beam. The strain distributions in the concrete, steel and FRP/TRM of all of the studied beams are shown in Appendix B, C and D, respectively.

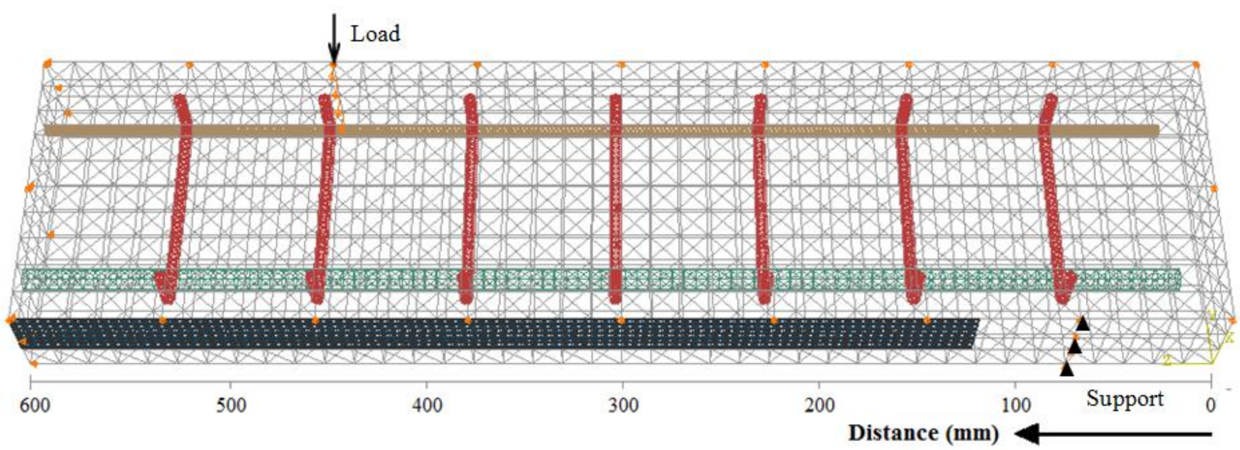

Figure 4.3: Distance convention for the strain analysis

4.4.1 Concrete versus Steel Strain

Tensile load caused equal strains in the concrete and steel in a beam prior to cracking. The strains increased with increasing load until the cracking strain of the concrete is reached. Then at the crack location, the applied tensile load was resisted totally by the rebar. Adjacent to the cracks, there was a local slip between the concrete and the rebar that controlled the crack width. The slip caused some forces to be transferred from the rebar to the concrete by means of bond stress acting on the perimeter of the bar. Therefore, the concrete between the cracks resisted some of the tensile forces. This bond-slip mechanism caused aperiodic variation of the strains in the concrete and steel along the length of the member, as indicated in the Fig. 4.4. The same pattern was also described by CEB/FIP (1990); Konig and Tue (1992); and Carino and Clifton (1995). Thus, at a crack, the steel strain was maximum and the concrete strain was zero (Fig. 4.4). In between cracks, the steel strain was minimum and the concrete strain was maximum. The same pattern was observed for all studied beams.

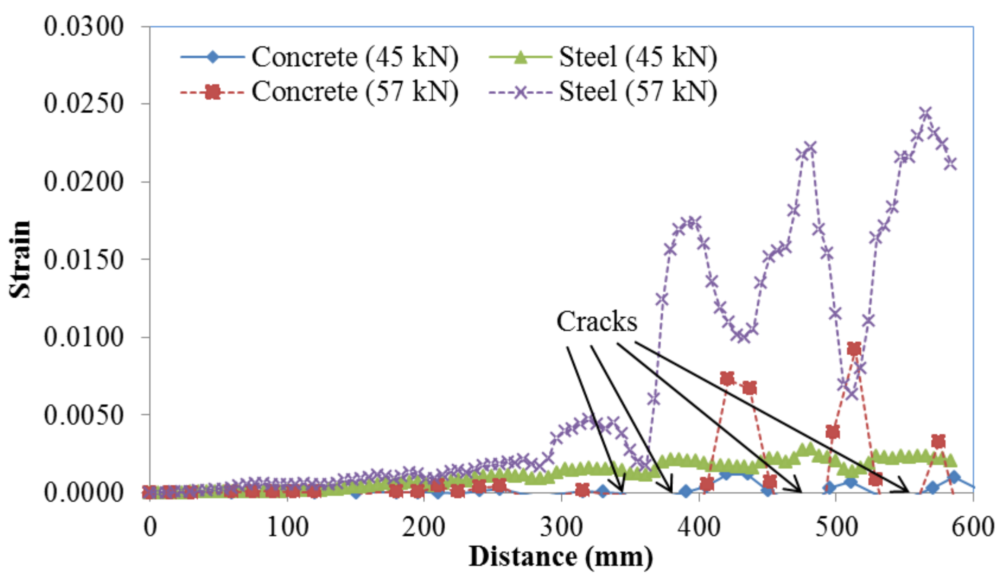

Figure 4.4: Typical train distribution in concrete and steel along the length (specimen C-M-0)

4.4.2 FRP/TRM System versus Steel Strain

Fig. 4.5 shows the strain distribution between the FRP/TRM and the steel for a typical beam. It shows that up to yielding of the steel, the FRP/TRM strain was slightly more than the steel strain due to its position relative to the neutral axis. However, after yielding the gap between the FRP/TRM and the steel strains increased which indicated that the FRP/TRM's contribution to resisting tensile load has increased. This is because the considered stress-strain behaviour for the steel, FRP and TRM in the FE model. In case of steel after reaching the yield stress at 445 MPa, stress did not increase, while the stress of the FRP and the TRM was increasing continuously until it reaches the failure stress at 960 MPa and 777 MPa, respectively. This trend was observed for all strengthened beams.

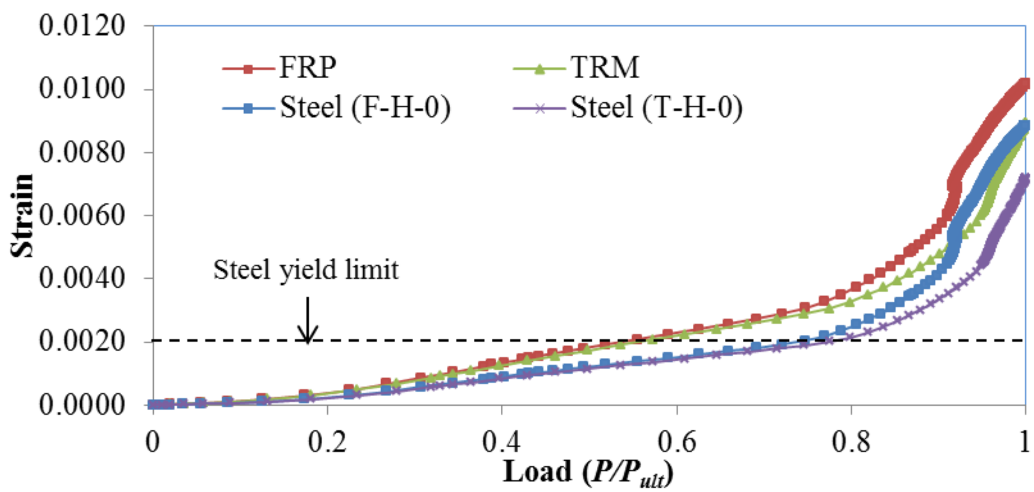

Figure 4.5: Typical strain distribution in FRP/TRM and steel (specimen F-H-0 and T-H-0)

4.4.3 FRP versus TRM System Strain

Typical strain distribution in the FRP and the TRM systems are shown in Fig. 4.6 and 4.7. Up to the yield load, the strains of both systems were almost the same (Fig. 4.6 and 4.7). This is because from section 4.4.2 it was observed that, steel was the major contributor in resisting the tensile load up to the yield point. However, from the yield load to the ultimate load, strain was quite higher in the FRP than that in the TRM system (maximum 40%). This is because the elastic modulus was 13% lower in the FRP compared to the TRM. Hence, for the same load increase, the FRP experienced higher strain. The same trend was observed for all strengthened beams.

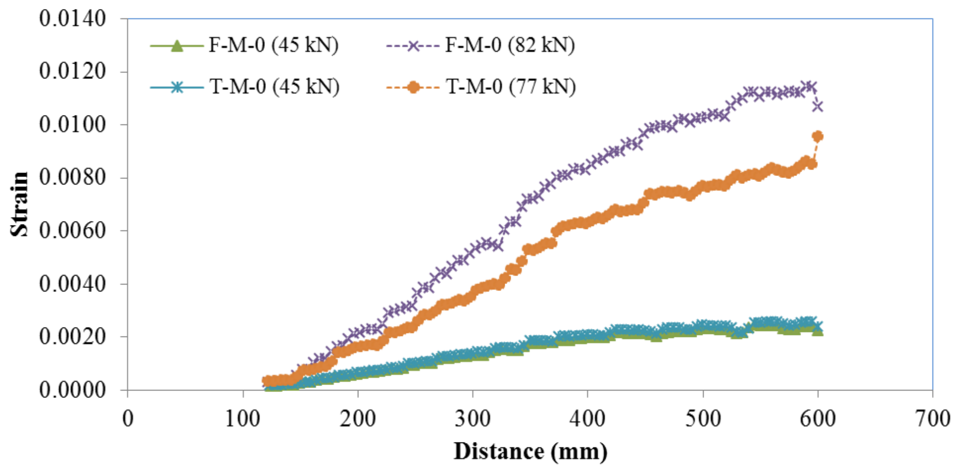

Figure 4.6: Typical strain distribution in FRP/TRM (specimen F-M-0 and T-M-0)

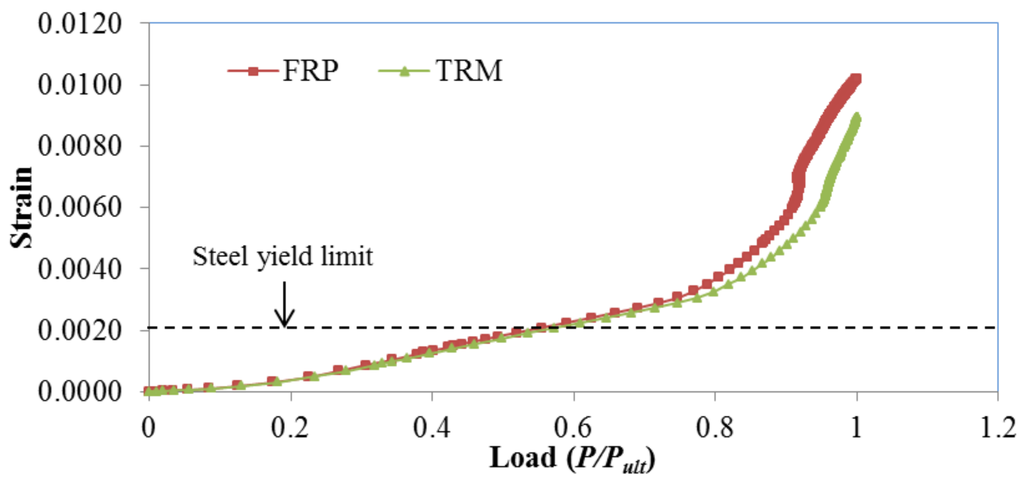

Figure 4.7: Typical strain distribution in FRP/TRM over load (specimen F-M-0 and T-M-0)

4.4.4 Variation of Strain Distribution when Changing the Reinforcement Ratio

Fig. 4.8 and 4.9 depict typical strain distribution in the steel and FRP/TRM along the length of a beam having high and low reinforcement ratios. As expected, in the beam having low reinforcement ratio, the steel has experienced higher strain than that of a beam having high reinforcement ratio. This contributed to a shift in the neutral axis position upward. Thus, in the FRP/TRM beam having low reinforcement ratio, Fig 4.8 and 4.9 show that cracks started from around 125 mm from the support i.e. cracks were distributed along the entire length of the FRP/TRM system which also resembled the failure mode shown in the Fig. 4.1-b and d.

In addition, it was observed that for a beam having high reinforcement ratio at the ultimate load the FRP/TRM strain was higher than the steel strain which was expected while for a beam having low reinforcement ratio, the case was reversed. This is because the beam having low reinforcement ratio had a flexure failure where the steel yielded followed by tensile rupture of the FRP/TRM while the beam with high reinforcement ratio failed by steel yielding followed by concrete crushing.

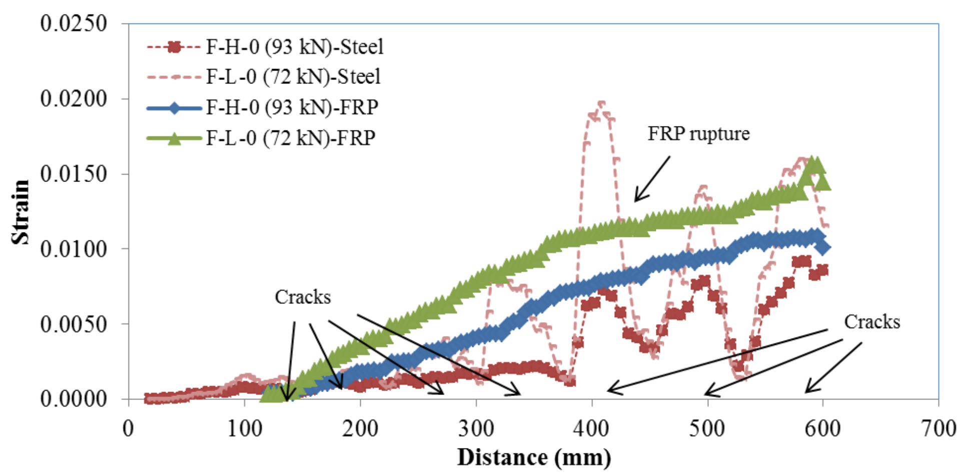

Figure 4.8: Typical strain distribution in steel and FRP (specimen F-H-0 and F-L-0)

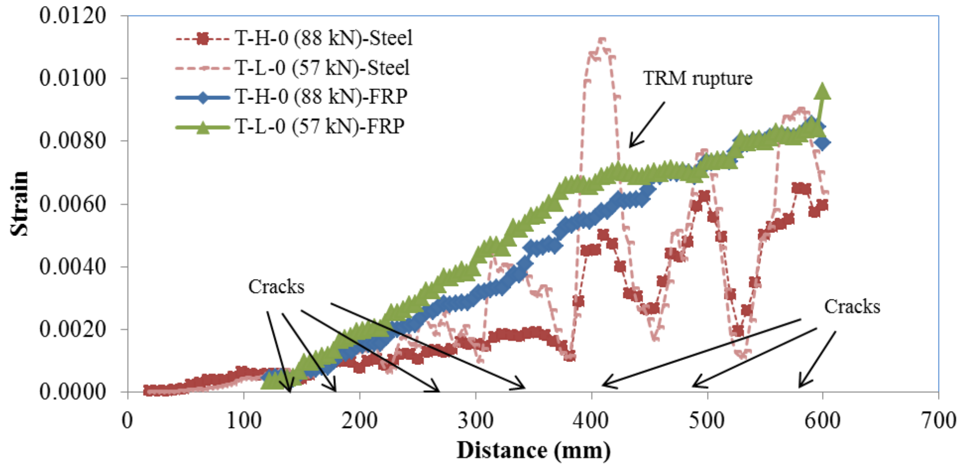

Figure 4.9: Typical strain distribution in steel and TRM (specimen T-H-0 and T-L-0)

4.4.5 Variation of Strain Distribution with the Corrosion Level

With changing corrosion level from 0% to 15%, Fig. 4.10 and 4.11 depict the strain distribution in the steel and FRP/TRM along the length of the beam having high reinforcement ratio. Fig. 4.10 and 4.11 depict that the sudden increase of the steel strain was higher in the high corrosion level. This is because less steel area was available to resist the tensile force causing the neutral axis to shift upward which eventually increased the rebar strain. Moreover, the aperiodic distribution of the steel strain follows the cause of bond-slip mechanism (section 4.4.1). The same pattern was observed for all studied beams.

On the other hand, it was observed that as long as the beam failed by steel yielding prior to concrete crushing, the FRP/TRM strain was higher than the steel strain which was expected. This is indicated in all depicted beams behaviour but specimen T-H-15 where steel strain exceeded the TRM strain at distance of 400 mm from the support. This is because as stated earlier, Beam T-H-15 failed by steel yielding followed by TRM rupture (Table 4.2).

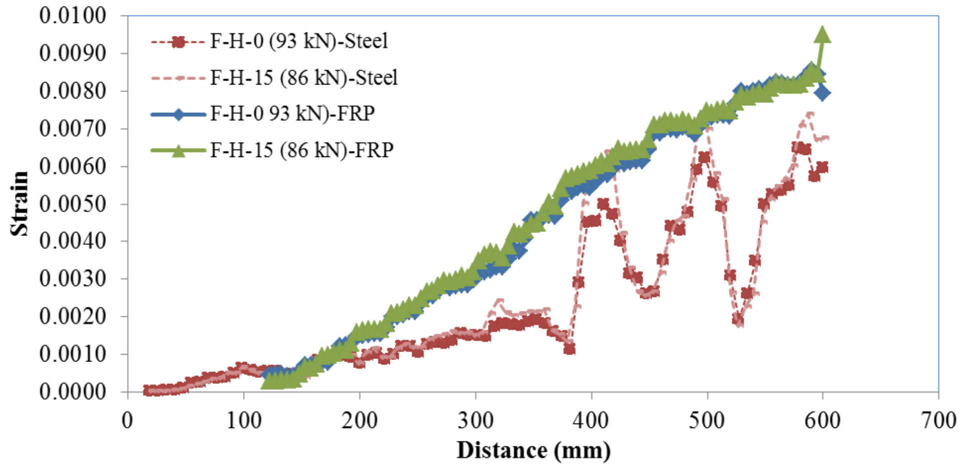

Figure 4.10: Typical strain distribution in steel and FRP (specimen F-H-0 and F-H-15)

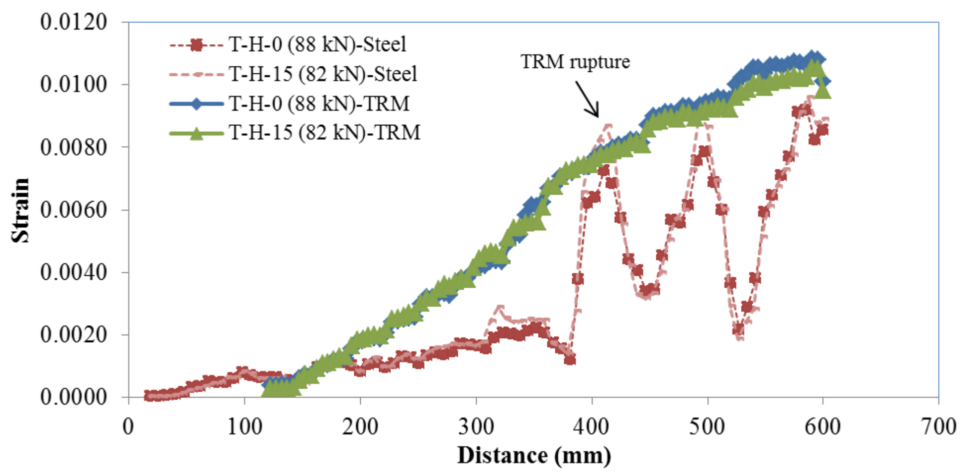

Figure 4.11: Typical strain distribution in steel and TRM (specimen T-H-0 and T-H-15)

4.4.6 Variation of Strain Distribution with the Strengthening Technique

Fig. 4.12 and 4.13 depict the strain distribution in the concrete and steel along the length of the beam having medium reinforcement ratio. Both strengthening systems enhanced the tensile capacity of the specimen and increased the moment of inertia (*I*). Since deflection of a member is inversely proportion to *I*, hence, both strengthening systems reduced deflection compared to the control beam and reduced the crack propagation. Therefore, deflection was limited for the strengthened beams which led to form more narrow cracks to release the energy. Thus, strengthening systems helped to distribute the cracks along the entire length of the beam rather than in a concentrated zone with wide cracks as shown in Fig. 4.13. The same pattern was observed for all studied beams.

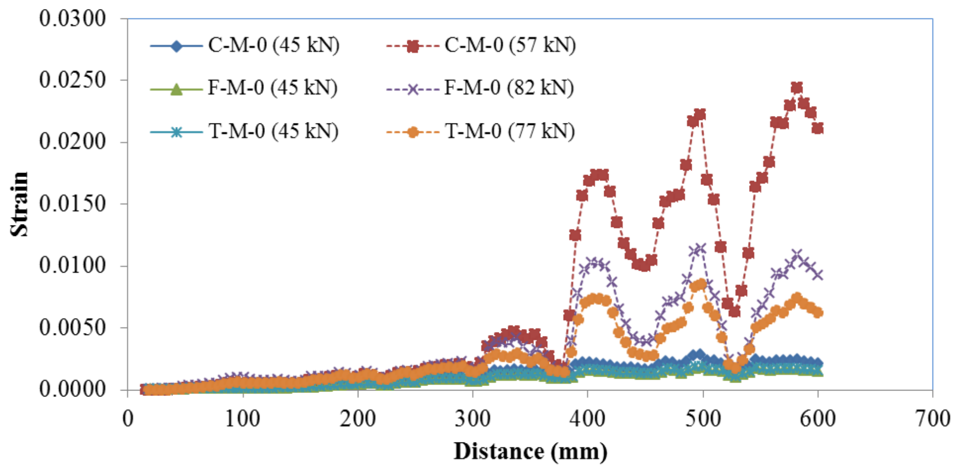

Figure 4.12: Typical strain distribution in steel (specimen C-M-0, F-M-0 and T-M-0)

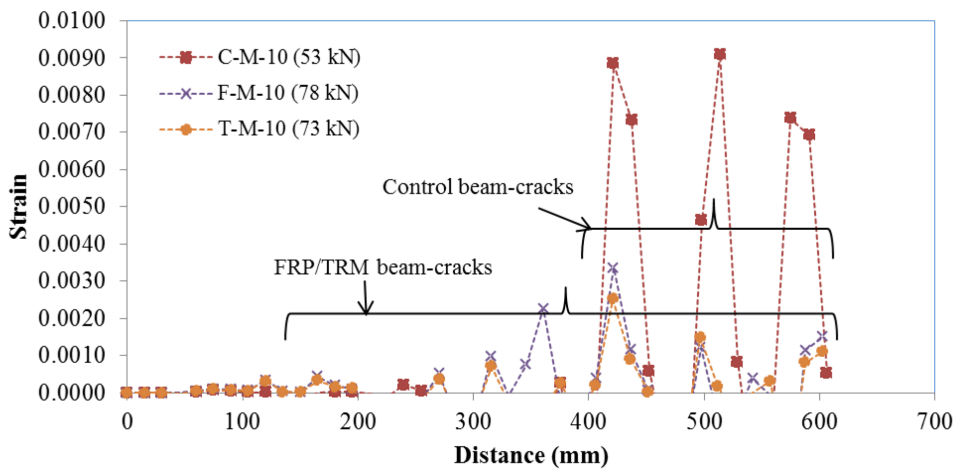

Figure 4.13: Typical strain distribution in concrete (specimen C-M-10, F-M-10 and T-M-10)

4.5 Load Carrying Capacity

The load-midspan deflection curve of the FRP and TRM strengthened beams over the control specimens with changing reinforcement ratios and corrosion levels are represented in Fig. 4.14. The individual load-deflection behaviour for each group of beams is shown in Appendix E. The load carrying capacity was studied by measuring and comparing the load at the onset of concrete crack, steel yield and failure either by concrete crushing or FRP/TRM fracture. Following the study conducted by Carino and Clifton (1995), concrete cracking was defined at a tensile strain of 140 $\mu\varepsilon$ obtained at the bottom face of the concrete specimen. The yield point of a beam was determined according to FEMA 356 (2000) guideline. A beam specimen was considered to fail when either the concrete compressive strain of 3500 $\mu\varepsilon$ was reached at the top layer or the strengthening system reached its ultimate strain, whichever was occurred first. In general, the load carrying capacity was improved by adding both strengthening systems and deteriorated with increasing corrosion levels.

Table 4.3 summaries the results of the simulated specimens in terms of the predicted crack, yield and ultimate loads. It also shows the effect of changing the reinforcement ratio. Within the considered range, in all corrosion levels for both unstrengthened and strengthened specimens load carrying capacity has increased with increasing reinforcement ratio. The effect of the three variables- corrosion level, reinforcement ratio and existence of strengthening material on the cracking, yield and ultimate loads is described in details in the following sections.

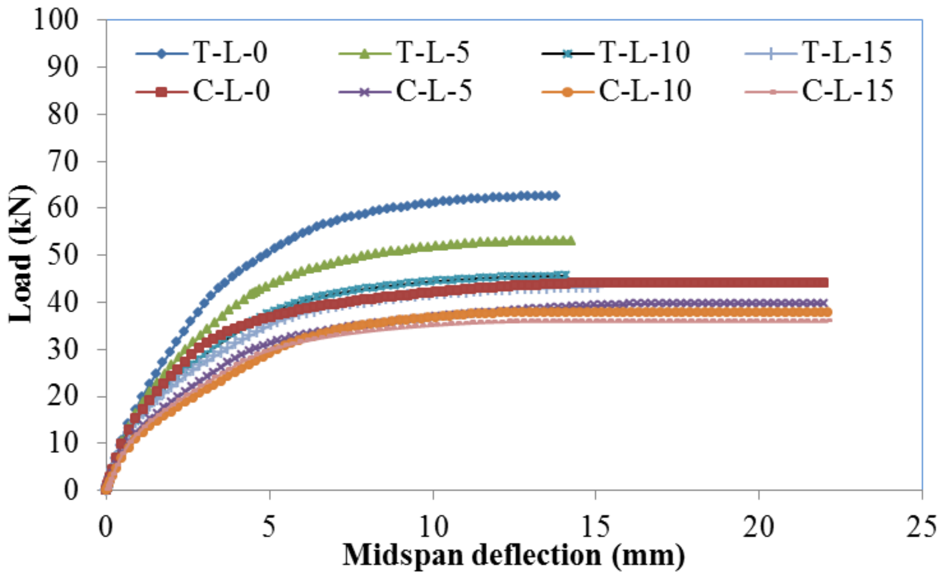

a) TRM strengthened

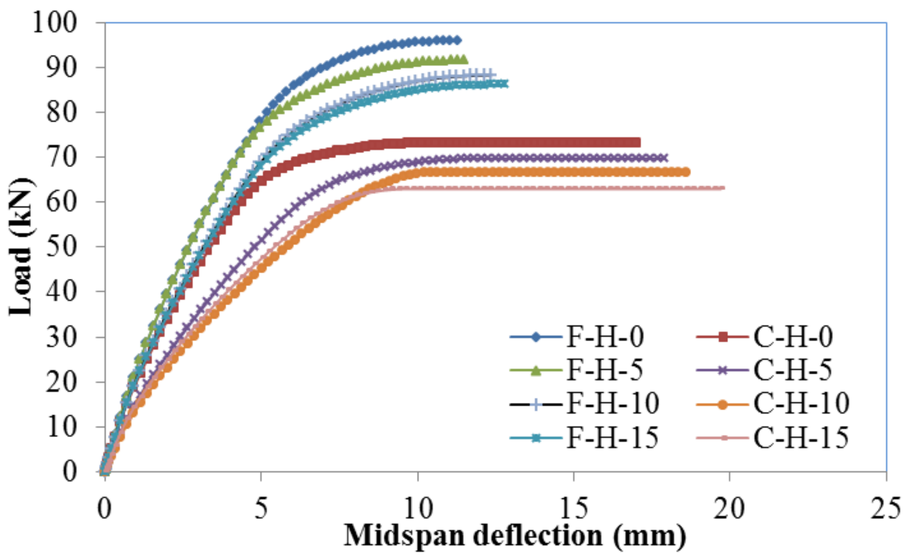

b) FRP strengthened

Figure 4.14: Load–deflection curves of strengthened and unstrengthened beams

Table 4.3: Effect of reinforcement ratio on the load carrying capacity

Group		Specimen	Load (kN)					
			Cracking	% Change	Yield	% Change	Ult.	% Change
Control	C-0	C-L-0	18.20	-	34.93	-	44.20	-
		C-M-0	21.11	16.0	45.16	29.3	56.53	27.9
		C-H-0	23.34	28.2	53.74	53.8	73.25	65.7
	C-5	C-L-5	18.03	-	31.28	-	39.77	-
		C-M-5	20.89	15.9	42.55	36.0	55.74	40.2
		C-H-5	23.02	27.7	48.46	54.9	69.78	75.5
	C-10	C-L-10	17.86	-	26.71	-	37.92	-
		C-M-10	20.59	15.3	37.51	40.4	53.14	40.1
		C-H-10	22.73	27.2	43.92	64.4	66.79	76.1
	C-15	C-L-15	17.68	-	26.54	-	35.89	-
		C-M-15	20.33	15.0	30.99	16.7	46.77	30.3
		C-H-15	22.39	26.6	41.86	57.7	62.99	75.5
FRP	F-0	F-L-0	20.15	-	51.36	-	71.84	-
		F-M-0	22.84	13.3	63.88	24.4	82.44	14.8
		F-H-0	24.92	23.6	71.19	38.6	96.09	33.8
	F-5	F-L-5	20.00	-	48.98	-	68.36	-
		F-M-5	22.64	13.2	61.44	25.4	79.67	16.6
		F-H-5	24.62	23.1	71.01	45.0	91.68	34.1
	F-10	F-L-10	19.84	-	48.37	-	67.94	-
		F-M-10	22.36	12.7	59.65	23.3	77.70	14.4
		F-H-10	24.35	22.7	67.06	38.6	88.41	30.1
	F-15	F-L-15	19.68	-	47.99	-	66.51	-
		F-M-15	22.12	12.4	54.92	14.4	73.88	11.1
		F-H-15	24.03	22.1	66.20	37.9	86.24	29.7
TRM	T-0	T-L-0	20.16	-	46.48	-	62.58	-
		T-M-0	22.85	13.3	58.06	24.9	76.25	21.8
		T-H-0	24.93	23.6	66.12	42.3	94.12	50.4
	T-5	T-L-5	20.01	-	39.54	-	53.17	-
		T-M-5	22.49	12.4	54.28	37.3	71.32	34.1
		T-H-5	24.63	23.1	65.07	64.6	86.57	62.8
	T-10	T-L-10	19.86	-	33.06	-	45.57	-
		T-M-10	22.37	12.7	46.60	41.0	63.50	39.3
		T-H-10	24.36	22.7	58.47	76.8	80.08	75.7
	T-15	T-L-15	19.69	-	31.16	-	43.22	-
		T-M-15	22.13	12.4	46.02	47.7	63.10	46.0
		T-H-15	24.04	22.1	58.15	86.6	79.56	84.1

4.5.1 Cracking Load

It was stated earlier that the concrete crack was considered when tensile strain reached 140 με.

4.5.1.1 Effect of reinforcement ratio

Fig. 4.15 depicts the effect of reinforcement ratio on the cracking load of a beam. In Fig. 4.15, cracking load of a beam having medium or high reinforcement ratio was normalized with that of a beam of low reinforcement ratio. At all corrosion levels, all unstrengthened and strengthened beams exhibited almost the same increase in cracking load of 13% and 24% with changing reinforcement ratio to medium and high, respectively (Table 4.3).

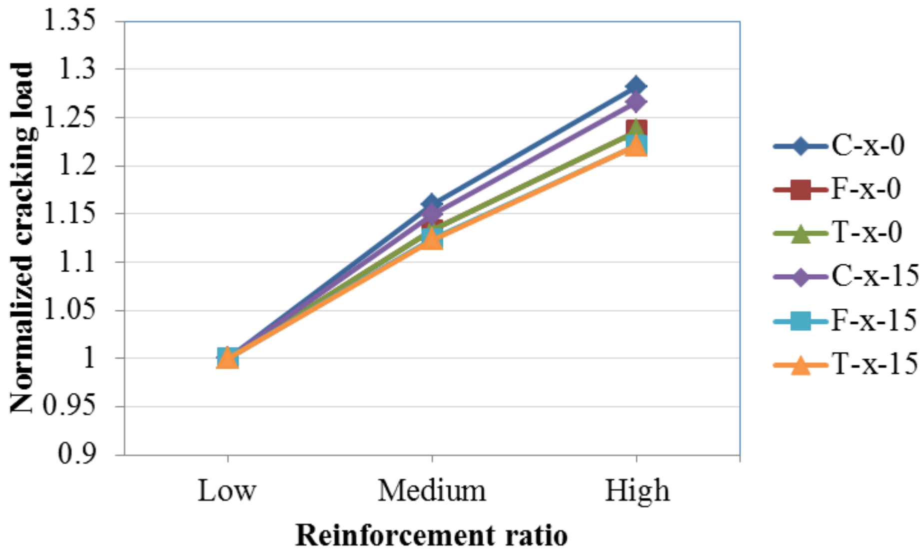

Figure 4.15: The effect of reinforcement ratio on the cracking load

The cause of the effect of changing reinforcement ratio is depicted in Fig. 4.16 through the strain distribution. Under a load the line POC represents a state where the concrete was cracked (ϵ_{cr}, point C) and passed through the neutral axis, point O. As the reinforcement ratio decreased, the neutral axis shifted upward from point O to point O' (Fig. 4.16). As a consequence, line P$O'C'$ in Fig. 4.16 represents the strain distribution under the same load as line POC. The tensile strain was increased at the bottom of the beam (shifted tensile strain from point C to point C') and exceeded the cracking strain of the concrete (ϵ_{cr}, point C). Therefore, the cracking strain of the concrete (ϵ_{cr}, point C) was reached under lower load which decreased the concrete compressive strain from point P to point Q.

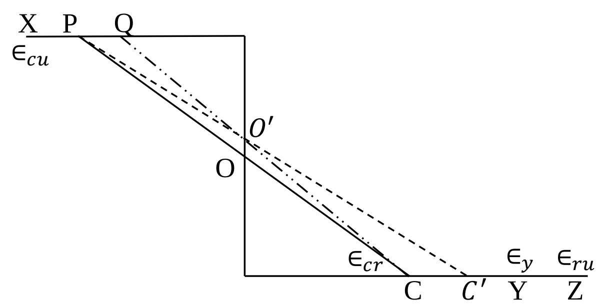

Figure 4.16: Typical cracking load behaviour with changing tensile reinforcement

4.5.1.2 Effect of corrosion level

In Table 4.4 and Fig. 4.17, cracking load of a damaged beam was normalized with respect to the cracking load of uncorroded beam specimen. As the corrosion level increased a slight decrease (maximum 4%) in the cracking load was observed.

As corrosion level increased, the available steel reinforcement area decreased, effectively decreasing the available reinforcement ratio. Therefore, as the corrosion level increased, the cracking load decreased as described in section 4.5.1.1.

Table 4.4: Effect of corrosion level on the load carrying capacity

Group	Reinf. ratio	Specimen	Load (kN)					
			Cracking	% Change	Yield	% Change	Ult.	% Change
Control	Low	C-L-0	18.20	-	34.93	-	44.20	-
		C-L-5	18.03	-0.94	31.28	-10.46	39.77	-10.03
		C-L-10	17.86	-1.84	26.71	-23.53	37.92	-14.20
		C-L-15	17.68	-2.84	26.54	-24.01	35.89	-18.79
	Medium	C-M-0	21.11	-	45.16	-	56.53	-
		C-M-5	20.89	-1.06	42.55	-5.78	55.74	-1.41
		C-M-10	20.59	-2.45	37.51	-16.93	53.14	-6.00
		C-M-15	20.33	-3.69	30.99	-31.37	46.77	-17.28
	High	C-H-0	23.34	-	53.74	-	73.25	-
		C-H-5	23.02	-1.37	48.46	-9.82	69.78	-4.74
		C-H-10	22.73	-2.62	43.92	-18.27	66.79	-8.82
		C-H-15	22.39	-4.07	41.86	-22.11	62.99	-14.00
FRP	Low	F-L-0	20.15	-	51.36	-	71.84	-
		F-L-5	20.00	-0.78	48.98	-4.64	68.36	-4.85
		F-L-10	19.84	-1.53	48.37	-5.83	67.94	-5.42
		F-L-15	19.68	-2.35	47.99	-6.57	66.51	-7.41
	Medium	F-M-0	22.84	-	63.88	-	82.44	-
		F-M-5	22.64	-0.89	61.44	-3.82	79.67	-3.36
		F-M-10	22.36	-2.10	59.65	-6.61	77.70	-5.74
		F-M-15	22.12	-3.15	54.92	-14.02	73.88	-10.38
	High	F-H-0	24.92	-	71.19	-	96.09	-
		F-H-5	24.62	-1.19	71.01	-0.24	91.68	-4.59
		F-H-10	24.35	-2.29	67.06	-5.80	88.41	-7.99
		F-H-15	24.03	-3.56	66.20	-7.01	86.24	-10.25
TRM	Low	T-L-0	20.16	-	46.48	-	62.58	-
		T-L-5	20.01	-0.78	39.54	-14.94	53.17	-15.04
		T-L-10	19.86	-1.52	33.06	-28.87	45.57	-27.18
		T-L-15	19.69	-2.34	31.16	-32.95	43.22	-30.93
	Medium	T-M-0	22.85	-	58.06	-	76.25	-
		T-M-5	22.49	-1.58	54.28	-6.51	71.32	-6.47
		T-M-10	22.37	-2.10	46.60	-19.73	63.50	-16.73
		T-M-15	22.13	-3.15	46.02	-20.73	63.10	-17.25
	High	T-H-0	24.93	-	66.12	-	94.12	-
		T-H-5	24.63	-1.18	65.07	-1.58	86.57	-8.02
		T-H-10	24.36	-2.28	58.47	-11.58	80.08	-14.91
		T-H-15	24.04	-3.55	58.15	-12.05	79.56	-15.47

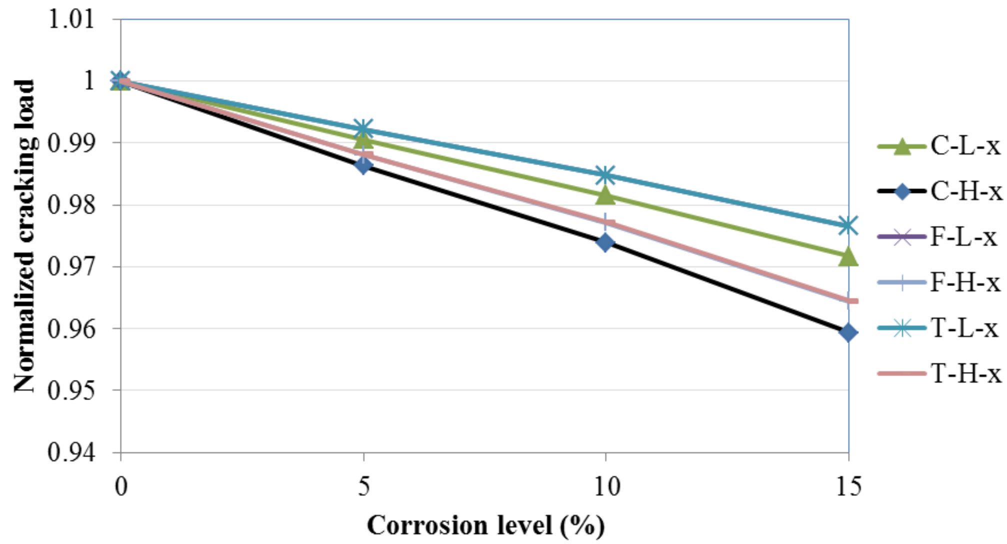

Figure 4.17: The effect of corrosion level on the cracking load

4.5.1.3 Effect of strengthening system

Fig. 4.18 shows the strengthening effect on the cracking load for a beam having low reinforcement ratio. In Table 4.5 and Fig. 4.18, cracking load of a strengthening beam was normalized with that of unstrengthened beam for each reinforcement ratio. The strengthening effect on the beams having medium and high reinforcement ratio are shown in Appendix F.

Compared to the respective unstrengthened beams, cracking loads of the undamaged and damaged FRP beams were increased on average by 11%, 8% and 7% for beams with low, medium and high reinforcement ratio, respectively (Table 4.5). Adding a strengthening system effectively increased the reinforcement ratio of the beam, thus causing the cracking load to increase as described in section 4.5.1.1. The TRM strengthened beams had a similar behaviour to the FRP strengthened beams in terms of the cracking load (Fig 4.18, Table 4.5).

Table 4.5 shows the comparative effectiveness between the TRM and the FRP systems. The ratio of the cracking loads of the TRM to the FRP strengthened beams were almost 1 for all beams considered, which indicates that both systems are equally effective in terms of increasing the cracking load.

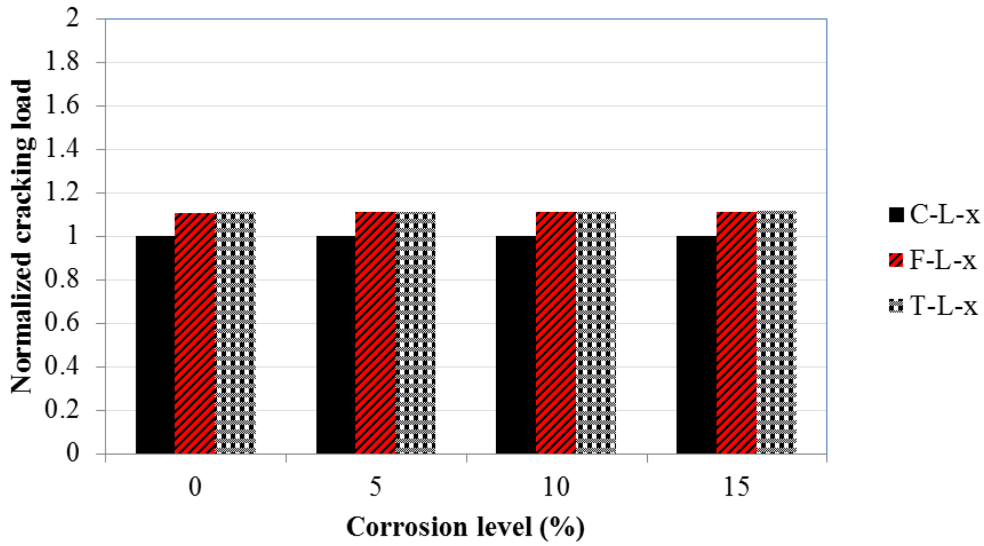

Figure 4.18: The effect of strengthening system on the cracking load

Table 4.5: Effectiveness of the strengthening systems on the load carrying capacity

Corrosion	Reinf. ratio	Cracking load			Yield load			Ultimate load		
		FRP/ Control	TRM/ Control	TRM/ FRP	FRP/ Control	TRM/ Control	TRM/ FRP	FRP/ Control	TRM/ Control	TRM/ FRP
0%	Low	1.11	1.11	1.00	1.47	1.33	0.90	1.63	1.42	0.87
	Medium	1.08	1.08	1.00	1.41	1.29	0.91	1.46	1.35	0.92
	High	1.07	1.07	1.00	1.32	1.23	0.93	1.31	1.28	0.98
5%	Low	1.11	1.11	1.00	1.57	1.26	0.81	1.72	1.34	0.78
	Medium	1.08	1.08	0.99	1.44	1.28	0.88	1.43	1.28	0.90
	High	1.07	1.07	1.00	1.47	1.34	0.92	1.31	1.24	0.94
10%	Low	1.11	1.11	1.00	1.81	1.24	0.68	1.79	1.20	0.67
	Medium	1.09	1.09	1.00	1.59	1.24	0.78	1.46	1.19	0.82
	High	1.07	1.07	1.00	1.53	1.33	0.87	1.32	1.20	0.91
15%	Low	1.11	1.11	1.00	1.81	1.17	0.65	1.85	1.20	0.65
	Medium	1.09	1.09	1.00	1.77	1.49	0.84	1.58	1.35	0.85
	High	1.07	1.07	1.00	1.58	1.39	0.88	1.37	1.26	0.92

4.5.2 Yield Load

To calculate the effective yield strength of the beams the procedure described in FEMA 356 (2000) and Priestley (2000) was followed. First, a horizontal line was drawn on the idealized load-displacement curve for the ultimate load and then the slope of line ABC (Fig. 4.19) was changed such that the area between the straight line and the load-displacement curve (ABA in Fig. 4.19) is equal to the area between the straight line and the load-displacement curve (BCDB in Fig. 4.19). Once this is done, point B was defined as the yield load. This was done using an iterative graphical procedure.

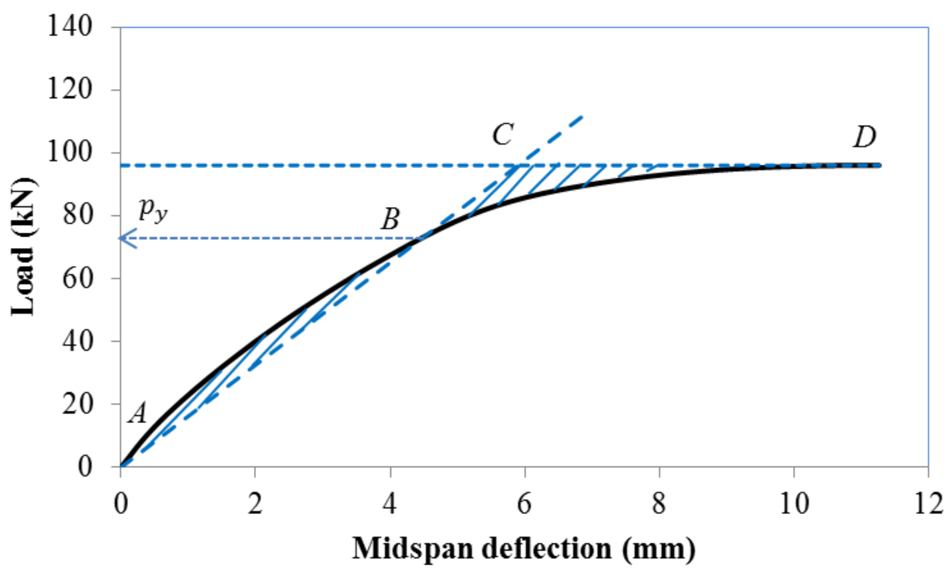

Figure 4.19: Yield load determination of a typical beam (F-H-0)

4.5.2.1 Effect of reinforcement ratio

In Fig. 4.20, the yield load of a beam having medium or high reinforcement ratio was normalized with that of a beam with low reinforcement ratio. The yield loads of the undamaged and damaged control beams increased on average by 31% and 57% when the reinforcement ratio increased by 2 and 3 times, respectively. For the FRP beams this increase was 22% and 40%, respectively while TRM beams exhibited higher increase of 38% and 68%, respectively (Table 4.3).

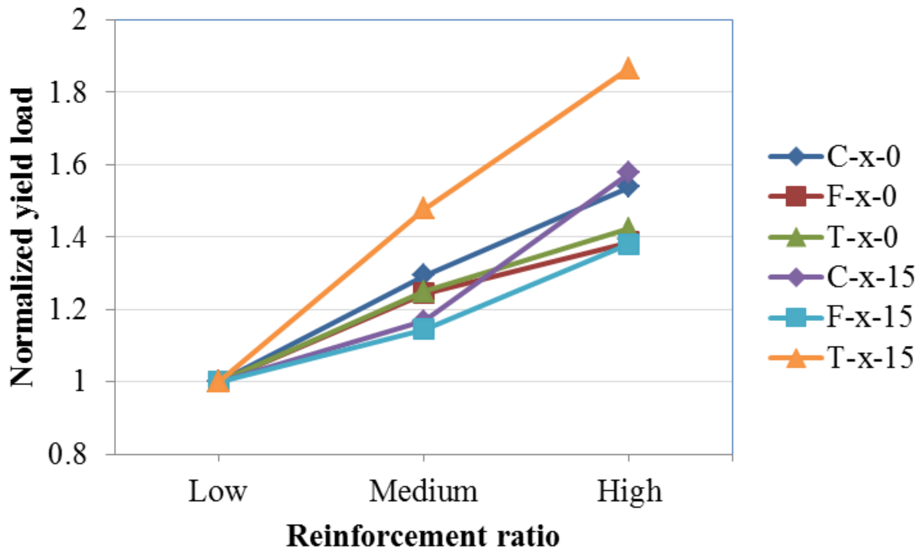

Figure 4.20: The effect of reinforcement ratio on the yield load

The cause of the effect of changing reinforcement ratio on the yield load is depicted in Fig. 4.21 through the strain distribution mechanism. Under a load, the line POY represents a state where the steel was yielded (ϵ_y, point Y) and passed through the neutral axis, point O. As the reinforcement ratio decreased, the neutral axis shifted upward from point O to point O' (Fig. 4.21). As a consequence, line P$O'Y'$ in Fig. 4.21 represents the strain distribution under the same load as line POY with an increased strain at the bottom of the beam (shifted tensile strain from point Y to point Y') which exceeded the yield strain (line QO'Y). Therefore, the yield strain of the steel (ϵ_y, point Y) was reached under a lower load.

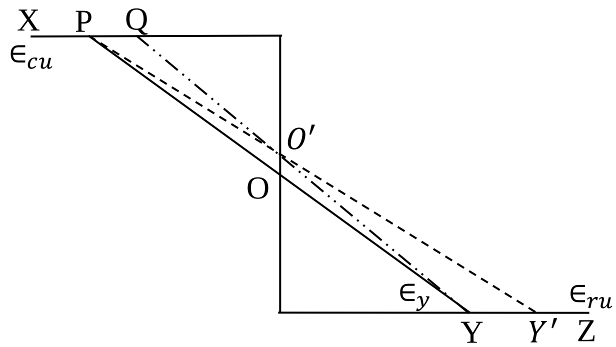

Figure 4.21: Typical yield load behaviour with changing tensile reinforcement

4.5.2.2 Effect of corrosion level

In Fig. 4.22, the yield load of a damaged beam was normalized with respect to the yield load of an uncorroded beam specimen in each of the groups. The yield load dropped on average by 8%, 20% and 26% for beams with corrosion levels 5%, 10% and 15%, respectively, compared to the uncorroded counterparts for all unstrengthened beams (Fig. 4.22). The yield load of the FRP and the TRM strengthened beams decreased in a range of 3% to 20% depending on the considered corrosion levels (Table 4.4).

As the corrosion level increased, the available steel reinforcement area decreased, effectively decreasing the available reinforcement ratio. Therefore, as the corrosion level increased, the yield load decreased as described in section 4.5.2.1.

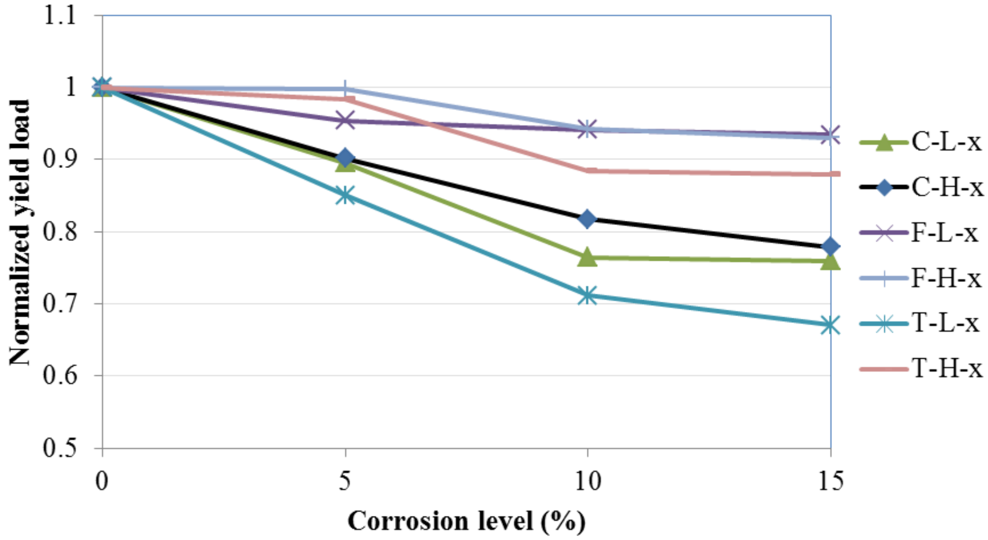

Figure 4.22: The effect of corrosion level on the yield load

4.5.2.3 Effect of strengthening system

In Fig. 4.23, the yield load of a strengthening beam having low reinforcement ratio was normalized with that of a control beam. The strengthening effect on the beams having medium and high reinforcement ratio are shown in Appendix F.

The yield load has increased on average by 66%, 55% and 48% for the undamaged and damaged FRP strengthened beams having low, medium and high reinforcement ratio, respectively, compared to the respective control beams (Table 4.5). The yield load of the TRM strengthened beams has increased by a range of 17% to 49% compared to the control beams (Table 4.5). Adding a strengthening system effectively increased the reinforcement ratio of the beam, thus causing the yield load to increase as described in section 4.5.2.1.

Table 4.5 represents the comparative effectiveness between the TRM and FRP strengthened beams over the control beams. It shows that the TRM system is less effective than the FRP system by 9% for control, 19% for 5% corrosion level and up to 35% for high corrosion level in terms of increasing the yield load. However, as the reinforcement ratio was increased the gap between the TRM and FRP systems was decreased.

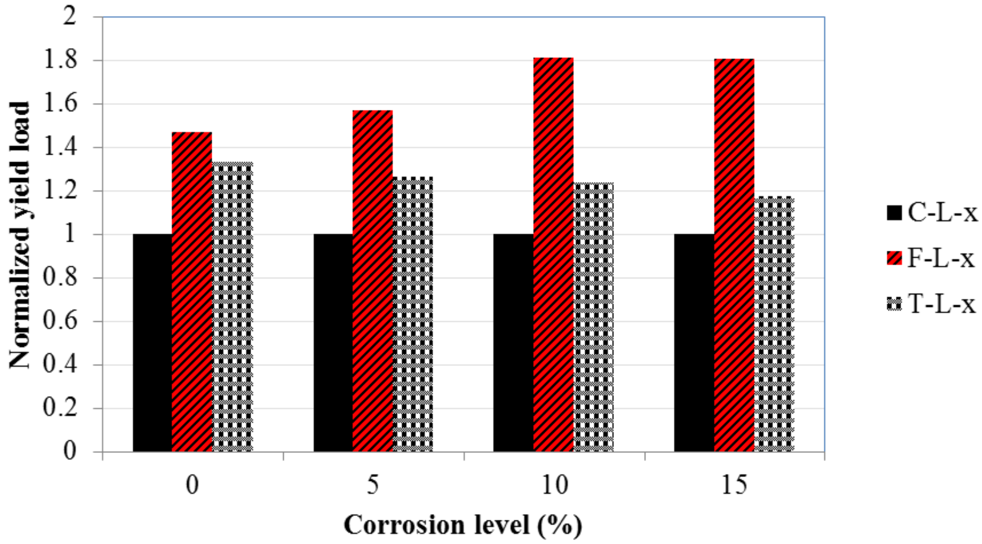

Figure 4.23: The effect of strengthening system on the yield load

4.5.3 Ultimate Load

The ultimate load was considered when a compressive strain of a beam reached a 3500 με or when the FRP/TRM reached their ultimate strain whichever was occurred first.

4.5.3.1 Effect of reinforcement ratio

In Fig. 4.24, the ultimate load of a beam having medium or high reinforcement ratio was normalized with that of a beam with low reinforcement ratio. The ultimate loads of the undamaged and damaged control beams increased on average by 35% and 73% when the reinforcement ratio increased by 200% and 300%, respectively. For the FRP strengthened beams this increase was 14% and 32%, respectively while TRM strengthened beams exhibited higher increase of 38% and 68%, respectively (Table 4.3).

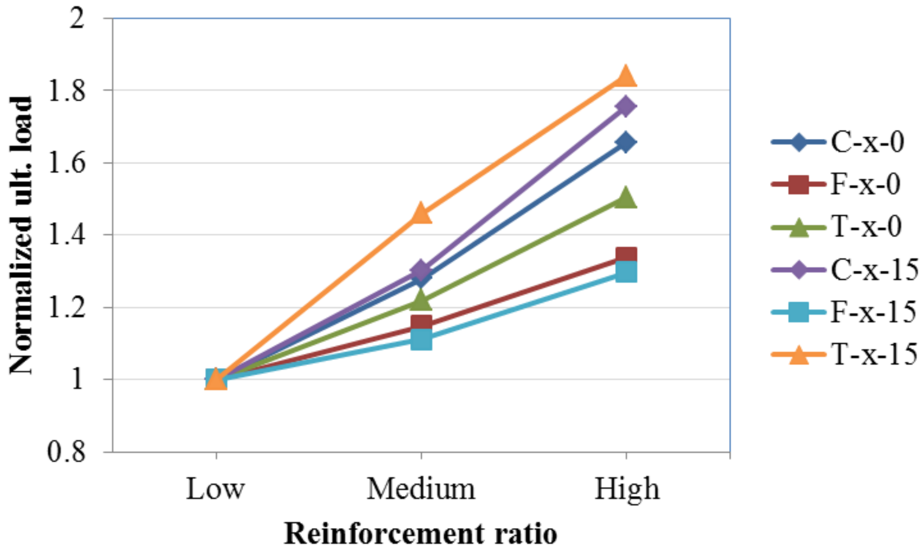

Figure 4.24: The effect of reinforcement ratio on the ultimate load

The cause of the effect of changing reinforcement ratio on the ultimate load when failure was initiated by steel yielding followed by concrete crushing is depicted in Fig. 4.25 through the strain distribution mechanism. Under a load, line XOY' in Fig. 4.25 represents a state where the concrete was crushed (ϵ_{cu}, point X) while the FRP/TRM was intact (strain at point Y' was less than the fracture strain of the FRP/TRM, ϵ_{ru} at point Z) and passed through the neutral axis, point O. As the reinforcement ratio decreased, the neutral axis shifted upward from point O to point O' (Fig. 4.25). As a consequence, (line $XO'Y''$) the concrete crushing strain (ϵ_{cu}, point X) was reached under the lower load.

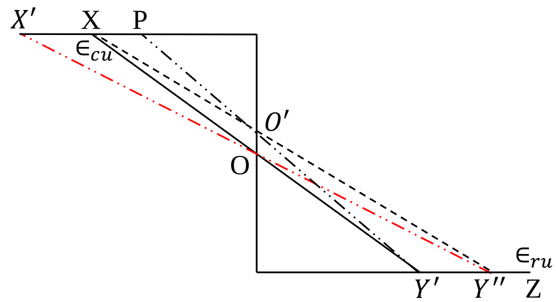

Figure 4.25: Typical ultimate load behaviour with changing tensile reinforcement (failure mode- concrete crushing)

The cause of the effect of changing reinforcement ratio on the ultimate load when failure was initiated by steel yielding followed by FRP/TRM rupture is depicted in Fig. 4.26 through the strain distribution mechanism. Under a load, the line POZ in Fig. 4.26 represents a strain distribution where the FRP/TRM was ruptured (ϵ_{ru}, point Z) while the concrete was uncrushed and passed through the neutral axis, point O. As the reinforcement ratio decreased, the neutral axis shifted upward from point O to point O' (Fig. 4.26). In this case, (line QO'Z in Fig. 4.26) the fracture strain of the FRP/TRM (ϵ_{ru}, point Z) was reached under a lower load causing the concrete compressive strain represented by point Q. Thus, the original beam resisted more loads to reach its failure point at point Z. Thereby, the ultimate loads was decreased with decreasing tensile reinforcement ratio of the beams.

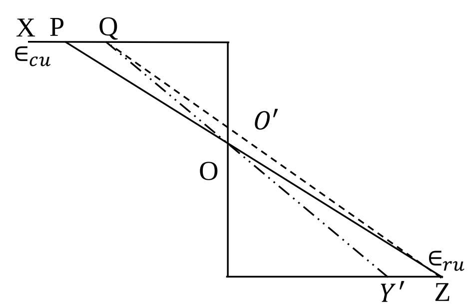

Figure 4.26: Typical ultimate load behaviour with changing tensile reinforcement (failure mode- FRP/TRM rupture)

4.5.3.2 Effect of corrosion level

In Fig. 4.27, the ultimate load of a damaged beam was normalized with respect to the ultimate load of the uncorroded beam specimen. The ultimate loads decreased on average by 9%, 20% and 26% for beams with corrosion levels 5%, 10% and 15%, respectively, compared to the uncorroded counterparts for all unstrengthened beams (Fig. 4.27). The ultimate loads of the FRP and the TRM strengthened beams decreased in a range of 1% to 33% with corresponding to the considered corrosion levels (Table 4.4).

As corrosion level increased, the available steel reinforcement area decreased, effectively decreasing the available reinforcement ratio. Therefore, as the corrosion level increased, the ultimate load decreased as described in section 4.5.3.1.

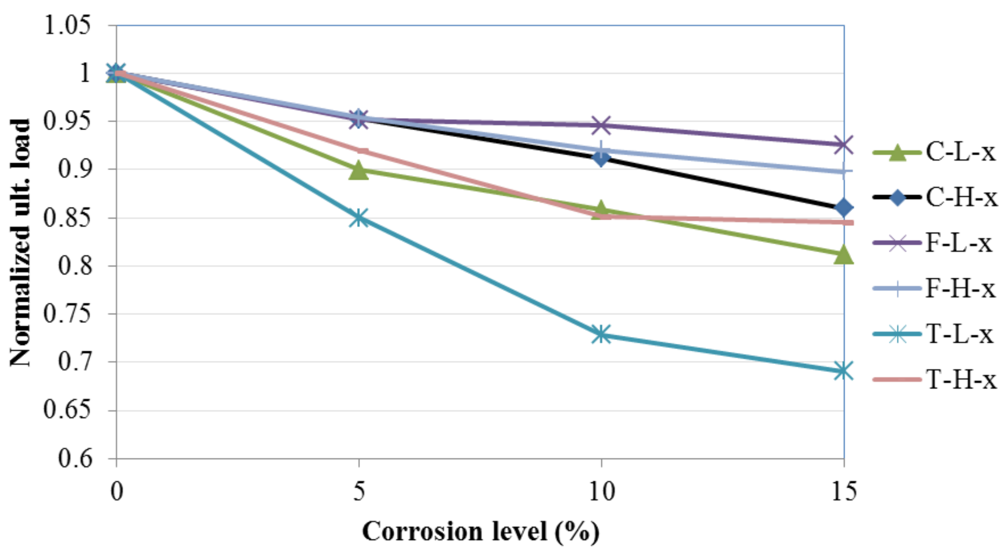

Figure 4.27: The effect of corrosion level on the ultimate load

4.5.3.3 *Effect of strengthening system*

In Fig. 4.28, the ultimate load of a strengthening beam having low reinforcement ratio was normalized with that of a control beam. The strengthening effect on the beams having medium and high reinforcement ratio are shown in Appendix F.

The ultimate load has increased on average by 75%, 48% and 33% for the undamaged and damaged FRP strengthened beams having low, medium and high reinforcement ratio, respectively, compared to the respective control beams (Table 4.5). The ultimate load of the TRM strengthened beams has increased by a range of 19% to 42% compared to the control beams. Adding a strengthening system effectively increased the reinforcement ratio of the beam, thus causing the ultimate load to increase as described in section 4.5.3.1.

Table 4.5 represents the strengthening effect of the TRM system compared to the FRP system. It shows that the TRM system is as effective as the FRP system at high reinforcement ratio in terms of increasing the ultimate load carrying capacity. However, when decreasing the reinforcement ratio, the TRM effectiveness decreased and became about 45% of that of the FRP. This attributes to the lower fracture strain (9500 $\mu\varepsilon$) of the TRM system which resulted in lower capacity.

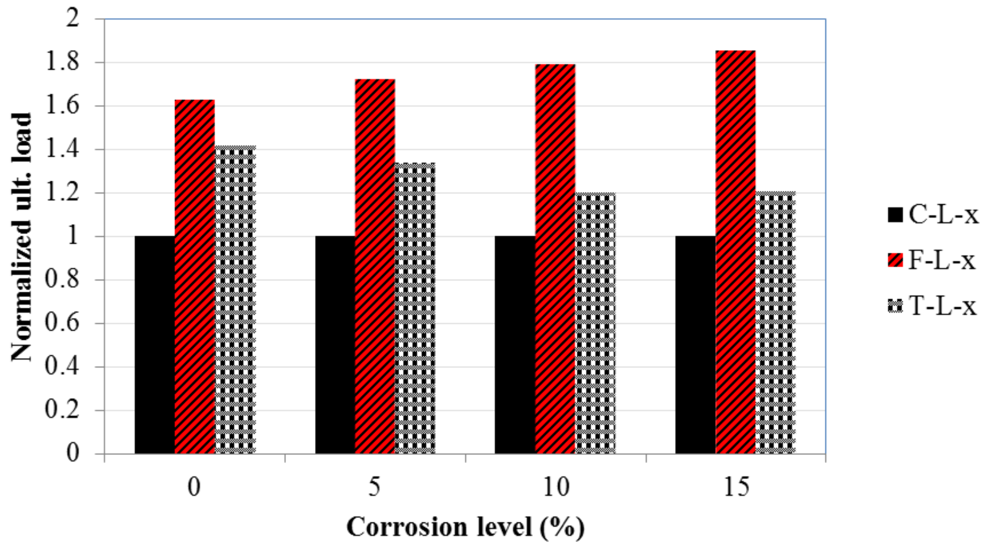

Figure 4.28: The effect of strengthening system on the ultimate load

4.6 Displacement and Ductility

The overall displacement behaviour is shown in Fig. 4.14 and Appendix E for the TRM and FRP strengthened beams compared to the control beams with changing reinforcement ratios and corrosion levels. Displacement behaviour is described by measuring the displacement of a specimen at yield and at failure loads. As described earlier, the displacement at the yield load was determined from the intersection point of the nonlinear load-displacement curve and the idealized bilinear curve (point B) as shown in Fig. 4.29 (FEMA 356, 2000; Priestley, 2000). In addition, the displacement at failure was considered when concrete compressive strain reach a value of 3500 $\mu\varepsilon$ at top layer or the FRP/TRM reach their ultimate strain, whichever was met first. In general, displacement values of the strengthened beams were lower than that of the control beams.

On the other hand, ductility (μ_d) is a structure's ability to deform plastically under tensile stress without failure. It can be defined as the ratio of the displacement at maximum load, Δ_{max} to the displacement corresponding to the yield load, Δ_y as shown in the Fig. 4.29 (FEMA 356, 2000; Priestley, 2000).

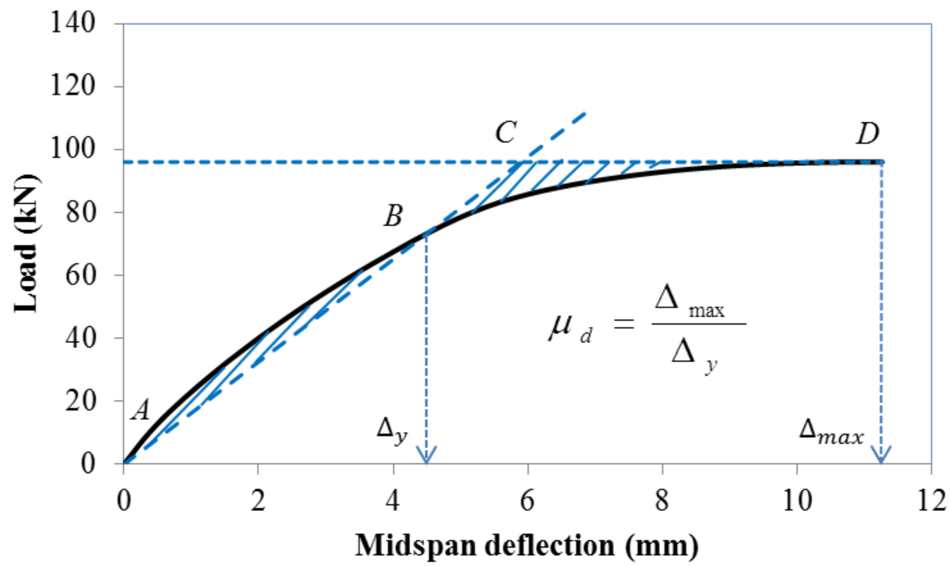

Figure 4.29: Measurement of ductility for a typical beam

Table 4.6 summaries the results of the simulated specimens in terms of the predicted displacement at the yield and ultimate loads and ductility, it also shows the effect of changing reinforcement ratio. Within the considered range, in all corrosion levels for both unstrengthened and strengthened specimens the ultimate displacement and ductility were decreased with increasing reinforcement ratio. The effect of the three variables- corrosion level, reinforcement ratio and existence of strengthening material on the displacement and ductility is described in details in the following sections.

Table 4.6: Effect of reinforcement ratio on the displacement and ductility

Group		Specimen	Displacement (mm)			Ductility	% Change
			Yield	Ult.	% Change		
Control	C-0	C-L-0	4.16	22.00	-	5.29	-
		C-M-0	4.94	20.15	-8.41	4.08	-22.87
		C-H-0	4.71	16.98	-22.82	3.61	-31.83
	C-5	C-L-5	4.03	22.39	-	5.56	-
		C-M-5	4.80	20.37	-9.02	4.24	-23.62
		C-H-5	4.77	17.91	-20.01	3.75	-32.42
	C-10	C-L-10	4.04	22.99	-	5.69	-
		C-M-10	4.71	20.73	-9.83	4.40	-22.66
		C-H-10	4.79	18.59	-19.14	3.88	-31.80
	C-15	C-L-15	3.94	23.11	-	5.87	-
		C-M-15	4.37	21.21	-8.22	4.85	-17.25
		C-H-15	4.46	19.70	-14.76	4.42	-24.69
FRP	F-0	F-L-0	3.87	13.67	-	3.53	-
		F-M-0	3.75	11.26	-17.63	3.00	-15.01
		F-H-0	4.31	11.24	-17.78	2.61	-26.06
	F-5	F-L-5	3.76	13.74	-	3.65	-
		F-M-5	3.87	11.92	-13.25	3.08	-15.62
		F-H-5	4.31	11.50	-16.30	2.67	-26.85
	F-10	F-L-10	3.98	14.66	-	3.68	-
		F-M-10	4.07	12.66	-13.64	3.11	-15.49
		F-H-10	4.63	12.35	-15.76	2.67	-27.45
	F-15	F-L-15	4.27	15.96	-	3.74	-
		F-M-15	4.54	14.29	-10.46	3.15	-15.78
		F-H-15	4.74	12.79	-19.86	2.70	-27.81
TRM	T-0	T-L-0	4.08	13.79	-	3.38	-
		T-M-0	4.09	11.05	-19.87	2.70	-20.12
		T-H-0	3.88	9.50	-31.12	2.45	-27.51
	T-5	T-L-5	3.94	14.08	-	3.57	-
		T-M-5	3.94	11.07	-21.42	2.81	-21.29
		T-H-5	3.89	9.79	-30.48	2.52	-29.41
	T-10	T-L-10	3.91	14.25	-	3.64	-
		T-M-10	3.91	12.00	-15.74	3.07	-15.66
		T-H-10	4.09	10.39	-27.06	2.54	-30.22
	T-15	T-L-15	4.00	14.83	-	3.71	-
		T-M-15	3.91	12.05	-18.77	3.08	-16.98
		T-H-15	4.11	10.43	-29.70	2.54	-31.54

4.6.1 Effect of Reinforcement Ratio

In Fig. 4.30-a and 4.30-b, the ultimate displacement and ductility of a beam having medium and high reinforcement ratio were normalized to those of a beam having low reinforcement ratio, respectively. The ultimate displacements of all the strengthened and unstrengthened beams were decreased on average by 15% and 20% for increasing the reinforcement ratio to medium and high, respectively, at various corrosion levels (Fig. 4.30, Table 4.6). This reduction influenced the ductility behaviour of a beam. Thus, the ductility of the unstrengthened and strengthened beams was decreased on average by 13% and 28% with increasing reinforcement ratio to medium and high, respectively, at all considered corrosion levels (Fig. 4.36, Table 4.8). This similar relationship between the ductility and the reinforcement ratio was observed in many studies (Park and Ruitong, 1989; Ashour, 2000; Agussalim, 2004; Olivia and Mandal, 2005; Maghsoudi and Akbarzadeh, 2007; Ashrafi et al., 2012).

This decrease can be explained as follows. Adding tensile reinforcement decreased the tensile stress and increased the depth of the neutral axis resulting higher compression area, lower tensile strain and, thus, lower displacement. Moreover, the curvature ductility (ratio of the curvature at ultimate to the curvature when the tension reinforcement first reaches the yield strength) is inversely proportional to the depth of the neutral axis. It is to be noted that the curvature ductility and displacement ductility are almost the same (Olivia and Mandal, 2005; Maghsoudi and Akbarzadeh, 2007). Thus, with increasing reinforcement ratio, curvature was decreased which reduced the ultimate displacement that led to lower ductility.

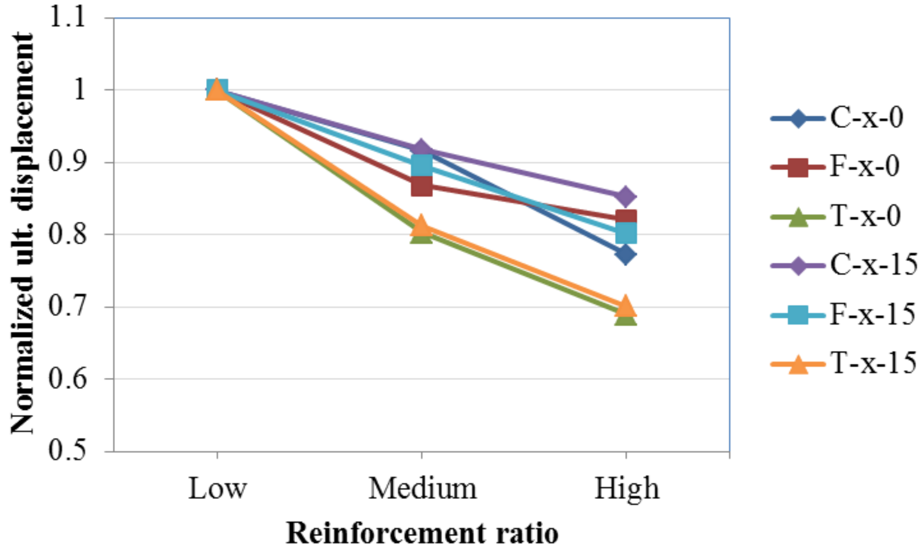

a) Ultimate displacement

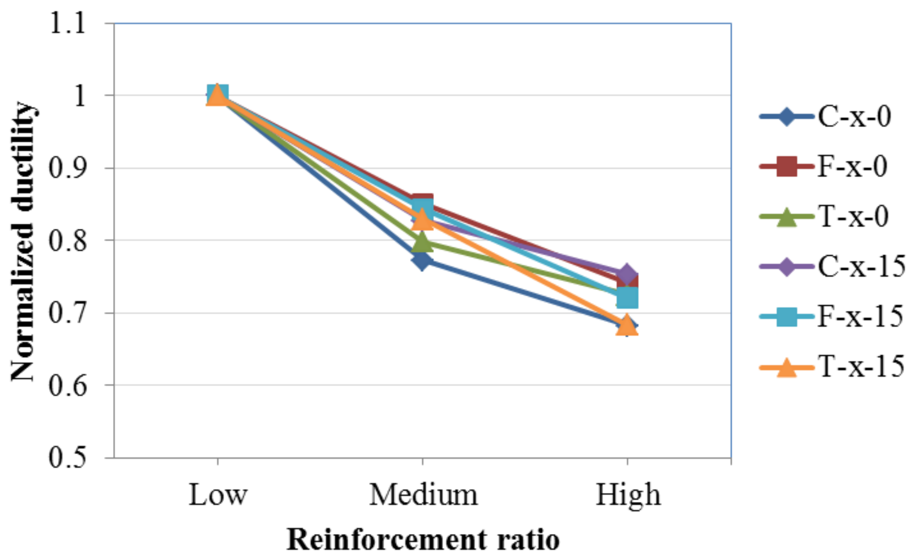

b) Ductility

Figure 4.30: The effect of reinforcement ratio on the displacement and ductility

4.6.2 Effect of Corrosion Level

In Fig. 4.31-a and 4.31-b, the ultimate displacement and ductility of a damaged beam were normalized with respect to the ultimate displacement and ductility of the uncorroded beam specimen, respectively. The ultimate displacements increased on average by 3%, 6% and 11% for all unstrengthened beams with corrosion levels 5%, 10% and 15%, respectively, compared to the uncorroded counterparts (Fig. 4.31, Table 4.7). The ultimate displacements of the FRP and the TRM strengthened beams increased in a range of 1% to 27% with corresponding to the considered corrosion levels (Table 4.7). This effects on the ductility as well. The ductility of the strengthened and unstrengthened beams having high, medium and low reinforcement ratios was increased on average by 2%, 6% and 17% with increasing corrosion level to 5%, 10% and 15%, respectively (Fig. 4.31, Table 4.7).

As corrosion level increased, the available steel reinforcement area decreased, effectively decreasing the available reinforcement ratio. Therefore, as the corrosion level increased, the ultimate displacement was increased that led to higher ductility as described in section 4.6.1.

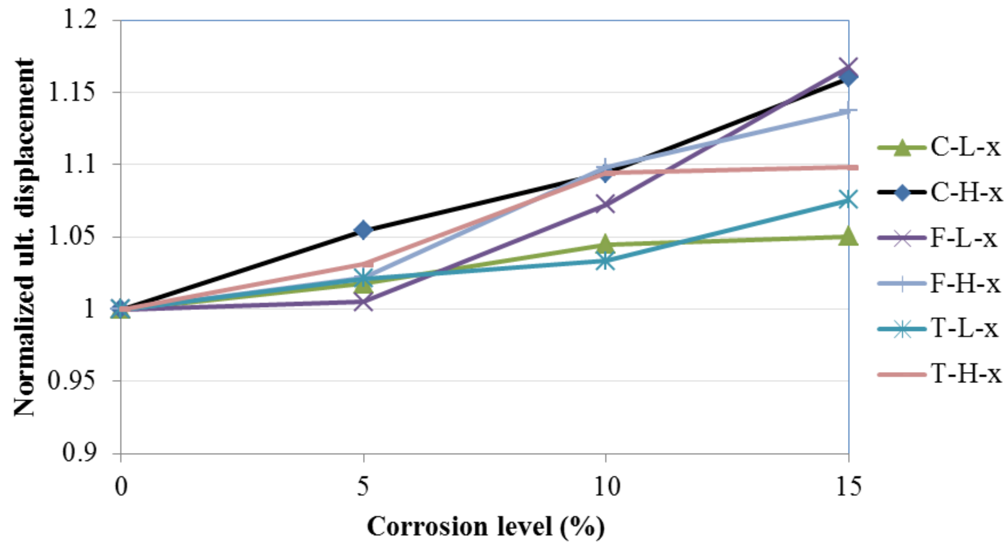

a) Ultimate displacement

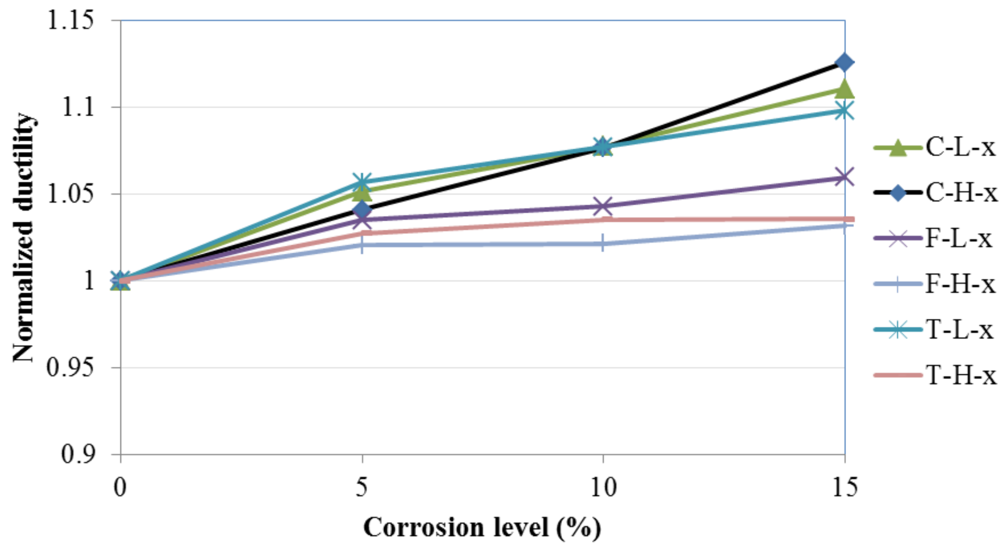

b) Ductility

Figure 4.31: The effect of corrosion level on the displacement and ductility

Table 4.7: Effect of corrosion level on the displacement and ductility

Group	Reinf. ratio	Specimen	Displacement (mm)			Ductility	% Change
			Yield	Ult.	% Change		
Control	Low	C-L-0	4.16	22.00	-	5.29	-
		C-L-5	4.03	22.39	1.77	5.56	5.06
		C-L-10	4.04	22.99	4.50	5.69	7.60
		C-L-15	3.94	23.11	5.05	5.87	10.91
	Medium	C-M-0	4.94	20.15	-	4.08	-
		C-M-5	4.80	20.37	1.09	4.24	4.04
		C-M-10	4.71	20.73	2.88	4.40	7.90
		C-M-15	4.37	21.21	5.26	4.85	18.99
	High	C-H-0	4.71	16.98	-	3.61	-
		C-H-5	4.77	17.91	5.48	3.75	4.15
		C-H-10	4.79	18.59	9.48	3.88	7.65
		C-H-15	4.46	19.70	16.02	4.42	22.52
FRP	Low	F-L-0	3.87	13.67	-	3.53	-
		F-L-5	3.76	13.74	0.51	3.65	3.40
		F-L-10	3.98	14.66	7.24	3.68	4.25
		F-L-15	4.27	15.96	16.75	3.74	5.95
	Medium	F-M-0	3.75	11.26	-	3.00	-
		F-M-5	3.87	11.92	5.86	3.08	2.67
		F-M-10	4.07	12.66	12.43	3.11	3.67
		F-M-15	4.54	14.29	26.91	3.15	5.00
	High	F-H-0	4.31	11.24	-	2.61	-
		F-H-5	4.31	11.50	2.31	2.67	2.30
		F-H-10	4.63	12.35	9.88	2.67	2.30
		F-H-15	4.74	12.79	13.79	2.70	3.45
TRM	Low	T-L-0	4.08	13.79	-	3.38	-
		T-L-5	3.94	14.08	2.13	3.57	5.62
		T-L-10	3.91	14.25	3.32	3.64	7.69
		T-L-15	4.00	14.83	7.57	3.71	9.76
	Medium	T-M-0	4.09	11.05	-	2.70	-
		T-M-5	3.94	11.07	0.17	2.81	4.07
		T-M-10	3.91	12.00	8.65	3.07	13.70
		T-M-15	3.91	12.05	9.06	3.08	14.07
	High	T-H-0	3.88	9.50	-	2.45	-
		T-H-5	3.89	9.79	3.09	2.52	2.86
		T-H-10	4.09	10.39	9.42	2.54	3.67
		T-H-15	4.11	10.43	9.79	2.54	3.67

4.6.3 Effect of Strengthening System

In Fig. 4.32-a and 4.32-b, the ultimate displacement and ductility of a strengthened beam were normalized with that of an unstrengthened beam, respectively. Compare to the control beams, the ultimate displacements of the FRP beams having low, medium and high reinforcement ratios were decreased on average by 34%, 46% and 35%, respectively, at all corrosion levels (Fig. 4.32, Table 4.8). Their TRM counterparts had a decrease of 45%, 48% and 35%, respectively. On the other hand, compared to the respective control beams, the ductility of the strengthened beams having low, medium and high reinforcement ratios were decreased on average by 33%, 35% and 32%, respectively, at all corrosion levels (Fig. 4.38).

This is because the FRP/TRM system was acted as a supplement to the tensile reinforcement along with the steel. Thereby, with increasing tensile capacity tensile stress was decreased and this increased the depth of the neutral axis. As a consequence, under the same load, tensile strain was reduced which resulted in lower displacement. Moreover, the curvature ductility was decreased due to shifting the neutral axis of the section downward. Thus, both strengthening systems reduced the ultimate displacement and ductility as well.

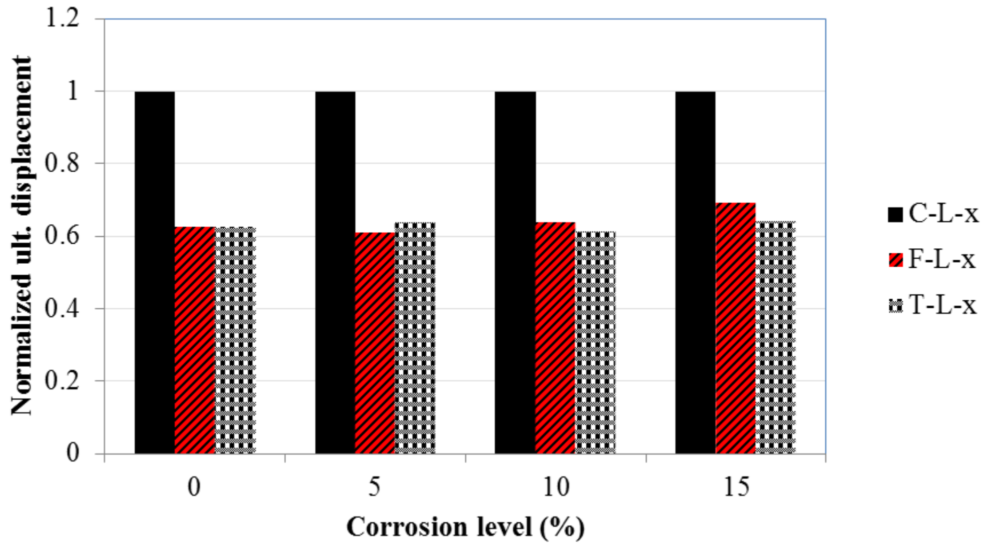

a) Ultimate displacement

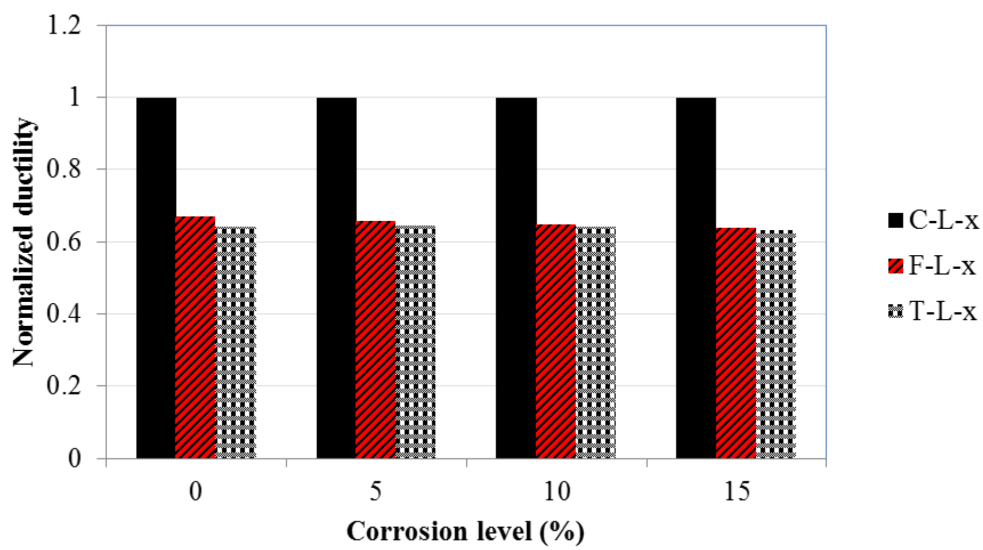

b) Ductility

Figure 4.32: The effect of strengthening system on the displacement and ductility

Table 4.8 represents the comparative effectiveness of the strengthening systems over the control beams with respect to the ultimate displacement and ductility. With respect to the ultimate displacement, the TRM system was slightly lower than the FRP system (about 7%) for uncorroded and corroded up to 10%, however, at 15% corrosion level this was increased to 14%. Besides, the ultimate displacement of the TRM beams with low reinforcement ratio was slightly lower (about 3%) compared to its FRP beams counterpart and with high reinforcement ratio this was increased to 18%. On the other hand, the TRM strengthened beams having different reinforcement ratio showed slightly lower (about 5%) ductility than the FRP beams at all corrosion levels. The FRP's superiority could be attributed to its ultimate strain capacity, which was 40% higher than the TRM's.

Table 4.8: Effectiveness of the strengthening systems on the displacement and ductility

Corrosion	Reinf. ratio	Ultimate displacement				Ductility			
		FRP/ Control	TRM/ Control	TRM/ FRP	Avg.	FRP/ Control	TRM/ Control	TRM/ FRP	Avg.
0%	Low	0.62	0.63	1.01	0.94	0.67	0.64	0.96	0.93
	Medium	0.56	0.55	0.98		0.74	0.66	0.90	
	High	0.66	0.56	0.84		0.72	0.68	0.94	
5%	Low	0.61	0.63	1.02	0.93	0.66	0.64	0.98	0.94
	Medium	0.59	0.54	0.93		0.73	0.66	0.91	
	High	0.64	0.55	0.85		0.71	0.67	0.94	
10%	Low	0.64	0.62	0.97	0.92	0.65	0.64	0.99	0.98
	Medium	0.61	0.58	0.95		0.71	0.70	0.99	
	High	0.66	0.56	0.84		0.69	0.65	0.95	
15%	Low	0.69	0.64	0.93	0.86	0.64	0.63	0.99	0.97
	Medium	0.67	0.57	0.84		0.65	0.63	0.98	
	High	0.65	0.53	0.82		0.61	0.58	0.94	

4.7 Stiffness Behaviour

Stiffness is the rigidity of a beam used to describe the force required to achieve a certain deformation (Baumgart 2000). Stiffness capacity was determined by measuring the slope of the line AB on the load-displacement curve shown in the Fig. 4.33. Due to the non-linearity of the load-displacement curve line AB was assumed as the equivalent initial straight line portion present in the load-displacement curve. The advantage of this assumption is to compare the stiffness of different beams on the same standard. Here, points A and B are directly dependant on the yield point of the beam and were fixed as the first (25th percentile) and third (75th percentile) quartile values of the yield load, respectively (Favre and Charif, 1994). The yield point of a beam was determined according to FEMA 356 (2000) guideline.

Table 4.9 summaries the results of the simulated specimens in terms of the predicted stiffness. It also shows the effect of changing reinforcement ratio. The effect of the three variables- corrosion level, reinforcement ratio and existence of strengthening material on stiffness has described in the following sections.

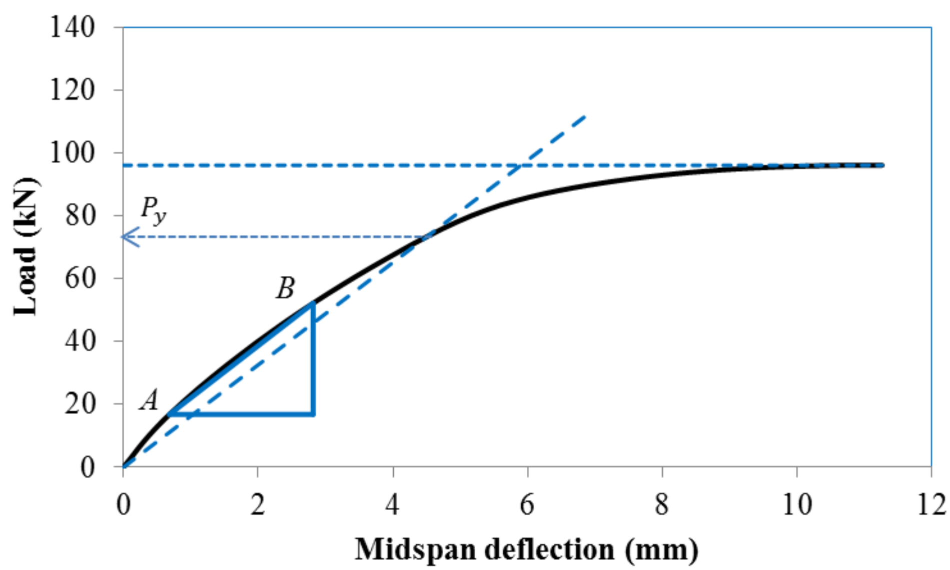

Figure 4.33: Determination of stiffness for a typical beam

Table 4.9: Effect of reinforcement ratio on the stiffness

Group		Specimen	Stiffness (kN/mm)	% Change
Control	C-0	C-L-0	09.97	-
		C-M-0	11.53	15.6
		C-H-0	14.47	45.1
	C-5	C-L-5	06.42	-
		C-M-5	08.74	36.2
		C-H-5	10.15	58.3
	C-10	C-L-10	06.43	-
		C-M-10	08.86	37.7
		C-H-10	08.99	39.8
	C-15	C-L-15	06.02	-
		C-M-15	06.97	15.9
		C-H-15	08.83	46.7
FRP	F-0	F-L-0	11.56	-
		F-M-0	13.44	16.3
		F-H-0	16.59	43.6
	F-5	F-L-5	11.45	-
		F-M-5	12.55	9.70
		F-H-5	15.63	36.6
	F-10	F-L-10	9.74	-
		F-M-10	12.24	25.7
		F-H-10	14.17	45.4
	F-15	F-L-15	09.26	
		F-M-15	10.96	18.4
		F-H-15	13.97	50.8
TRM	T-0	T-L-0	12.08	-
		T-M-0	14.95	23.8
		T-H-0	17.37	43.8
	T-5	T-L-5	11.03	-
		T-M-5	14.48	31.3
		T-H-5	17.05	54.6
	T-10	T-L-10	09.39	-
		T-M-10	11.91	26.8
		T-H-10	14.33	52.6
	T-15	T-L-15	08.69	-
		T-M-15	11.68	34.4
		T-H-15	14.31	64.6

4.7.1 Effect of Reinforcement Ratio

In Fig. 4.34, the stiffness of a beam having medium or high reinforcement ratio was normalized with that of a beam having low reinforcement ratio. The stiffness of all the unstrengthened and strengthened beams was increased on average by 26% and 47% with increasing reinforcement ratio to two and three times, respectively, at all corrosion levels (Fig. 4.34, Table 4.9).

The modulus of elasticity of the steel was higher compared to the concrete, therefore, stiffness was expected to increase with increasing reinforcement ratio. Moreover, for a cracked section, the moment of inertia ($I_{cracked}$) increases as the reinforcement ratio (ρ) increases ($I_{cracked} \propto \rho$) which results in increasing the beam stiffness.

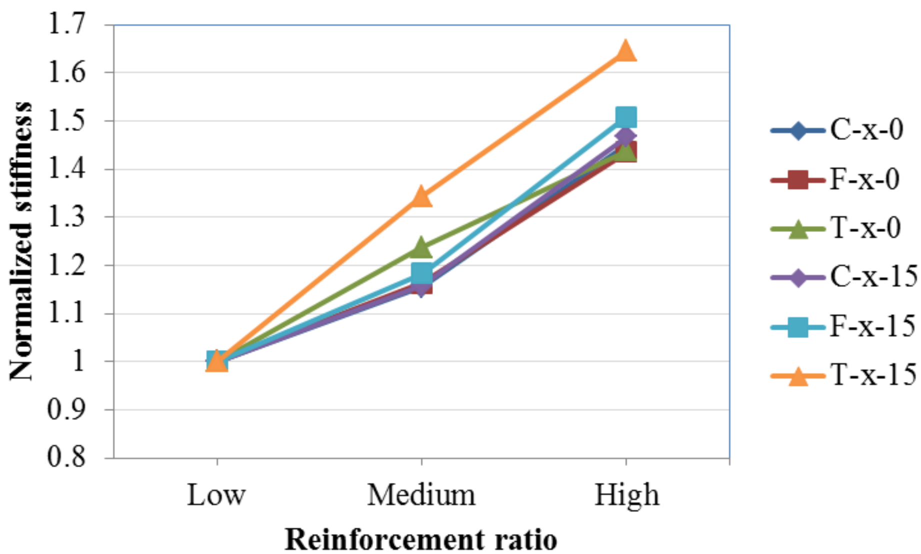

Figure 4.34: The effect of reinforcement ratio on the stiffness

4.7.2 Effect of Corrosion Level

In Fig. 4.35, the stiffness of a damaged beam was normalized with respect to stiffness of the uncorroded beam specimen. The stiffness of the unstrengthened beams having different reinforcement ratios was decreased on average by 23%, 34% and 40% with increasing corrosion level to 5%, 10% and 15%, respectively. Their strengthened beams counterpart had a decrease of 5%, 15% and 21%, respectively (Fig. 4.35, Table 4.10). As described in section 4.7.1, with increasing corrosion level (decreasing available steel area), the moment of inertia of a cracked section decreases, thus, stiffness decreased.

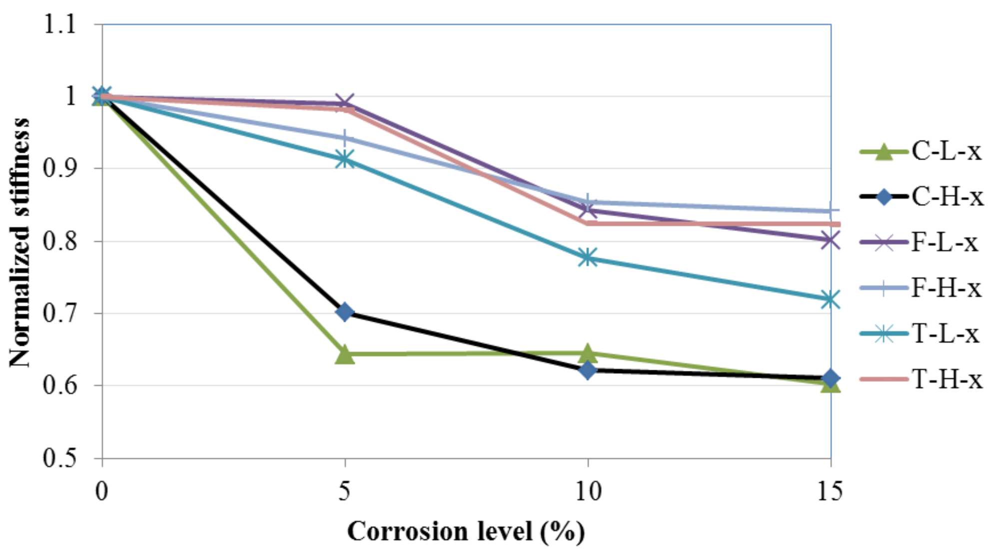

Figure 4.35: The effect of corrosion level on the stiffness

Table 4.10: Effect of corrosion level on the stiffness

Group	Reinf. ratio	Specimen	Stiffness (kN/mm)	% Change
Control	Low	C-L-0	9.97	-
		C-L-5	6.42	-35.61
		C-L-10	6.43	-35.51
		C-L-15	6.02	-39.62
	Medium	C-M-0	11.53	-
		C-M-5	8.74	-24.20
		C-M-10	8.86	-23.16
		C-M-15	6.97	-39.55
	High	C-H-0	14.47	-
		C-H-5	10.15	-29.85
		C-H-10	8.99	-37.87
		C-H-15	8.83	-38.98
FRP	Low	F-L-0	11.56	-
		F-L-5	11.45	-0.950
		F-L-10	9.74	-15.74
		F-L-15	9.26	-19.90
	Medium	F-M-0	13.44	-
		F-M-5	12.55	-6.620
		F-M-10	12.24	-8.930
		F-M-15	10.96	-18.45
	High	F-H-0	16.59	-
		F-H-5	15.63	-5.790
		F-H-10	14.17	-14.59
		F-H-15	13.97	-15.79
TRM	Low	T-L-0	12.08	-
		T-L-5	11.03	-8.690
		T-L-10	9.39	-22.27
		T-L-15	8.69	-28.06
	Medium	T-M-0	14.95	-
		T-M-5	14.48	-3.140
		T-M-10	11.91	-20.33
		T-M-15	11.68	-21.87
	High	T-H-0	17.37	-
		T-H-5	17.05	-1.840
		T-H-10	14.33	-17.50
		T-H-15	14.31	-17.62

4.7.3 *Effect of Strengthening System*

In Fig. 4.36, the stiffness of a strengthened beam was normalized with that of an unstrengthened beam for each corrosion level. Compared to the respective control beams, the stiffness of the FRP beams having low, medium and high reinforcement ratios were increased on average by 50%, 39% and 46%, respectively, at all corrosion levels (Fig. 4.36, Table 4.11). On the other hand, the stiffness of the TRM beams having high, medium and low reinforcement ratios were increased on average by 52%, 49% and 45% compared to the control beams, respectively, at all corrosion levels (Fig. 4.36, Table 4.11).

The cause of this increase attributes to the high tensile modulus of the FRP/TRM with respect to the concrete which makes a beam stiffer. Besides, attaching the FRP/TRM on the soffit of a beam increased the moment of inertia (I) of a beam cross-section. Since deflection of a member is inversely proportion to I, hence, both strengthening systems reduced deflection of the control beam which eventually increased the stiffness. However, the increase was higher in case of FRP having low reinforcement ratio compared to high reinforcement ratio because the full strength of the FRP laminates was utilized in this case.

The stiffness of both TRM and FRP strengthened beams were generally the same for 10% and 15% corrosion level (Table 4.11) with slightly higher for TRM when corrosion level was lower (0% and 5%). This is because the failure modes observed were different in the FRP and the TRM strengthened beams.

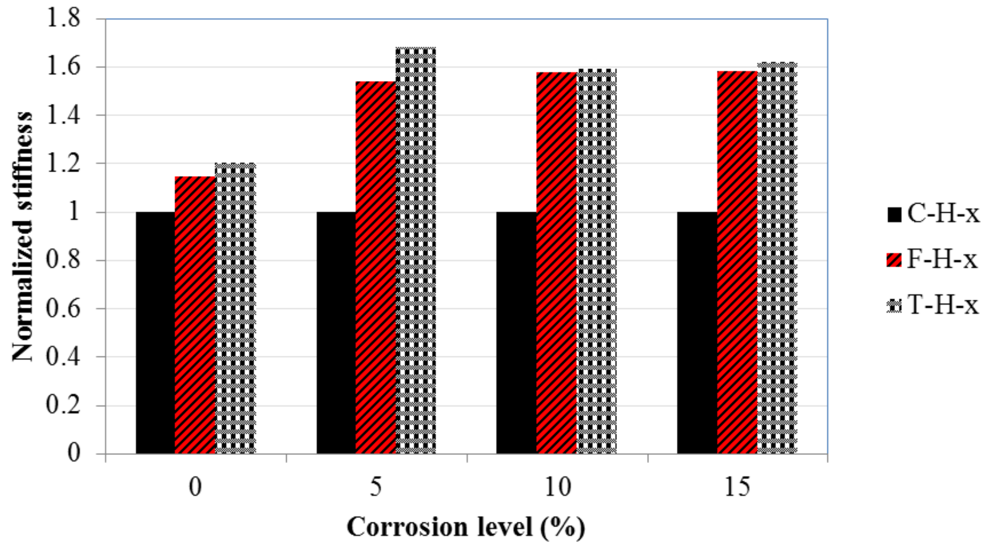

Figure 4.36: The effect of strengthening system on the stiffness

Table 4.11: Effectiveness of the strengthening systems on the stiffness

Corrosion	Reinf. ratio	FRP/Control	TRM/Control	TRM/FRP	Avg.
0%	Low	1.16	1.21	1.05	1.07
	Medium	1.17	1.30	1.11	
	High	1.15	1.20	1.05	
5%	Low	1.78	1.72	0.96	1.07
	Medium	1.44	1.66	1.15	
	High	1.54	1.68	1.09	
10%	Low	1.51	1.46	0.96	0.98
	Medium	1.38	1.34	0.97	
	High	1.58	1.59	1.01	
15%	Low	1.54	1.44	0.94	1.01
	Medium	1.57	1.68	1.07	
	High	1.58	1.62	1.02	

4.8 Summary

The parametric study gave an in depth understanding of the strengthening effect in corrosion damaged RC beams. From the FE analyses, the load carrying capacity, displacement, ductility and stiffness behaviours were examined and failure modes were observed. Strain analysis was conducted for understanding the cause of the effects. Both strengthening systems reduced ductility and enhanced stiffness. For the given material properties, the TRM system showed better performance with respect to stiffness compared to the FRP system while the FRP was better in terms of load carrying capacity, displacement and ductility behaviours except for beams having high tensile steel reinforcement ratio. In such case, the TRM system showed almost equal effectiveness as the FRP system. Given the scope of this study, it is suggested that the full strength of the FRP and TRM systems could be achieved if the unstrengthen beam have tensile steel reinforcement ratio less than 24% and 73% of its balanced reinforcement ratio, respectively.

CHAPTER 5: CONCLUSIONS AND FUTURE RECOMMENDATIONS

In this study, the structural performance of corrosion-damaged reinforced concrete beams strengthened with externally bonded FRP and TRM systems was numerically investigated. Thirty six 3D nonlinear FE models were developed to simulate the response of corrosion damaged RC beams, 100 x 150 x 1200 mm each, strengthened in flexure. Eight FE models were validated against the experimentally measured data in Soudki and Sherwood, (2000). In addition, the parametric study used 28 additional models. The parametric study varied the reinforcement ratio, the corrosion level and the existence of the strengthening techniques and its type. The numerical study considered different material constitutive laws for concrete in compression (crushing) and tension (cracking), steel yielding and isotropic material properties for the FRP and the TRM composite systems. The results presented are in terms of the load carrying capacity, displacement, stiffness, ductility and failure modes. Moreover, strain analysis was conducted to link the cause and effect of the studied parameters. Finally, a comparison between the effectiveness of FRP and TRM systems was conducted.

Based on the results and discussion presented in the previous chapter, the following conclusions can be drawn.

5.1 Effect of Reinforcement Ratio

- The yield loads of all beams increased on average by 31% and 56% when the reinforcement ratio increased by 2 and 3 times, respectively.
- The ultimate loads of the undamaged and damaged control beams increased on average by 35% and 73% when the reinforcement ratio increased by 200% and 300%,

respectively. For the FRP beams this increase was 14% and 32%, respectively while the TRM beams had an increase of 38% and 68%, respectively.

- The ductility of the unstrengthened and strengthened beams was decreased on average by 13% and 28% with increasing reinforcement ratio to medium and high, respectively, at all considered corrosion levels. Moreover, the ultimate displacements of all beams having medium and high reinforcement ratios were decreased by almost the same amount when compared to low reinforcement ratio.
- The stiffness of all the unstrengthened and strengthened beams was increased on average by 26% and 47% with increasing reinforcement ratio to medium and high, respectively, at all corrosion levels.

5.2 Effect of Corrosion Level

- The considered corrosion levels had negligible effect on the cracking load of the studied beams.
- The yield loads dropped on average by 8%, 20% and 26% for all unstrengthened and strengthened beams with corrosion levels 5%, 10% and 15%, respectively, compared to the uncorroded counterparts. The ultimate loads of all corroded beams were decreased by almost the same percentage when compared to the uncorroded counterparts.
- The ultimate displacements increased on average by 3%, 6% and 11% for all beams with corrosion levels 5%, 10% and 15%, respectively, compared to their uncorroded counterparts. Moreover, the ductility of all corroded beams increased by almost the same amount when compared to the uncorroded counterparts.

- The stiffness of the unstrengthened beams having different reinforcement ratios was decreased on average by 23%, 34% and 40% with increasing corrosion level to 5%, 10% and 15%, respectively. Their strengthened beams counterpart had a decrease of 5%, 15% and 21%, respectively.

5.3 Effect of Strengthening System

- The yield load was increased on average by 66%, 55% and 48% for the undamaged and damaged strengthened beams having low, medium and high reinforcement ratio, respectively, compared to the respective virgin beams.
- The ultimate load was increased on average by 75%, 48% and 33% for the undamaged and damaged strengthened beams having low, medium and high reinforcement ratio, respectively, compared to the respective control beams.
- Compare to the control beams, the ultimate displacements of the strengthened beams having low, medium and high reinforcement ratios were decreased on average by 34%, 46% and 35%, respectively, at all corrosion levels. The ductility of the strengthened beams was reduced almost by same amount when compared to the virgin beams.
- Compared to the respective control beams, the stiffness of the strengthened beams having low, medium and high reinforcement ratios were increased on average by 50%, 39% and 46%, respectively, at all corrosion levels.

5.4 TRM versus FRP Systems

- Both systems are equally effective in terms of increasing the cracking load.

- The TRM system is less effective than the FRP system by 9% for control, but up to 35% for high corrosion level in terms of increasing the yield load.

- The TRM system is as effective as the FRP system at high reinforcement ratio in terms of increasing the ultimate load carrying capacity, however, when decreasing the reinforcement ratio, the TRM effectiveness decreased and became about 45% that of the FRP.

- With respect to the ultimate displacement, the TRM strengthened beam was slightly lower than the FRP strengthened beam (about 7%) for uncorroded beams and 10% for corroded beams. However, at 15% corrosion level this was increased to 14%.

- The TRM strengthened beams having different reinforcement ratio showed slightly lower (about 5%) ductility than the FRP beams at all corrosion levels.

- The stiffness of both TRM and FRP strengthened beams were generally the same for 10% and 15% corrosion level with slightly higher for TRM when corrosion level was low (0% and 5%).

- Based on the above conclusion, it can be deduced that the TRM system is effective in strengthening damaged beams at different corrosion level and with different reinforcement ratio. It is however, slightly less effective than the FRP system.

- Given the scope of this study, it is suggested that the full strength of the FRP and TRM systems could be achieved if the unstrengthen beam have tensile steel reinforcement ratio less than 24% and 73% of its balanced reinforcement ratio, respectively.

5.5 Future Research Scope

The current research work has brought a better understanding on how the structural behaviour of reinforced concrete beams having different reinforcement ratios changed when they are exposed to corrosion at various degrees. It also contributed to the understanding of the viability of using externally bonded TRM system to repair corroded reinforced concrete beams. Thus, new developments concerning the structural performance of uncorroded, corroded and FRP/TRM strengthened beams having different reinforcement ratio were introduced. However, further investigation and validation are required for some topics. Recommendations for future researches are:

- Experimental validation of these models which will help to develop the TRM design guidelines.
- A steel-concrete bond model can be incorporated in the FE models.
- It has been identified that TRM systems can fail either by fracture of the textile fibres or by debonding of the TRM layer from the substrate concrete. Debonding failure is a brittle failure as well as it does not allow the full use of TRM strength. Very little research has been reported on the TRM debonding problem. For a full understanding of the behaviour of the TRM system, the study of the debonding failure mode can be great interest in the future. The same interest should also be brought to FRP system.
- The developed FE models can be used further to investigate the behaviour of RC beams externally strengthened in flexure with FRP/TRM system having different parameters such as concrete strength, steel strength and FRP/TRM properties.

REFERENCES

ABAQUS. (2013). ABAQUS Theory Manual, version 6.11. Simulia, a Dassault Systemes Brand, Velizy-Villacoublay, France.

ACI 222R. (2001). Protection of metals in concrete against corrosion. American Concrete Institute, ACI Committee 222, Farmington Hills, Michigan.

ACI 318. (2002). Building code requirements for structural concrete (ACI 318-02) and commentary (ACI 318R-02). American Concrete Institute.

ACI 318. (2005). Building code requirements for structural concrete. American Concrete Institute, ACI Committee 318, Farmington Hills, Michigan.

ACI 440.1R. (2006). Guide for the Design and Construction of Structural Concrete Reinforced with FRP Bars. American Concrete Institute, ACI Committee 440, Farmington Hills, Michigan.

ACI 506.1R. (2008). State-of-the-art report on fibre reinforced shotcrete. American Concrete Institute, ACI Committee 506, Farmington Hills, Michigan.

ACI 544.3R. (1998). Guide for specifying, proportioning, mixing, placing and finishing steel fibre reinforced concrete. American Concrete Institute, ACI Committee 544, Farmington Hills, Michigan.

ACI 544.4R. (1999). Design considerations for steel fibre reinforced concrete. American Concrete Institute, ACI Committee 544, Farmington Hills, Michigan.

ACI 546R. (2001). Concrete Repair Guide. American Concrete Institute, ACI Committee 546, Farmington Hills, Michigan.

Agussalim, A. B. (2004). Effect of compression reinforcement arrangement on ductility of reinforced concrete beams. 29th Conference on our world in concrete and structures, Singapore, 103-108.

Ahmad, Zaki. (2006). Principles of Corrosion Engineering and Corrosion Control. Published by Elsevier, UK.

Alhaddad, M. S., Siddiqui, N. A. and Abadel, A. A. (2012). Numerical Investigations on the Seismic Behavior of FRP and TRM Upgraded RC Exterior Beam-Column Joints, Journal of Composites for Construction, 16(3), 308–321. doi:10.1061/(ASCE)CC.1943-5614.0000265.

Al-Hammoud, R., Soudki, K. and Topper, T.H. (2011). Fatigue flexural behavior of corroded reinforced concrete beams repaired with CFRP sheets. Journal of Composites for Construction, 15(1): 42-51.

Almusallam, A., Al-Gahtani, A.S., Aziz, A. R., Dakhil, F. and Rasheeduzzafar. (1996). Effect of reinforcement corrosion on flexural behavior of concrete slabs, ASCE Journal of Materials in Civil Engineering, 8(3), 123-127.

Al-Sulaimani, G. J., Kaleemullah, M., Basunbul, I. A. and Rasheeduzzafar. (1990). Influence of corrosion and cracking on bond behavior and strength of reinforced concrete members. ACI Structural Journal, 87(2), 220-231.

Ambrisi, A. D., Feo, L. and Focacci, F. (2012). Composites : Part B Experimental analysis on bond between PBO-FRCM strengthening materials and concrete. Journal of Composites Part B: Engineering, 22–25. doi:10.1016/j.compositesb.2012.03.011

Ambrisi, A.D., Feo, L. and Focacci, F. (2013). Experimental analysis on bond between PBO-FRCM strengthening materials and concrete. Journal of Composites Part B: Engineering, 44(1), 524–532. doi:10.1016/j.compositesb.2012.03.011

Amir, S. L., Raphael, C., Emmanuel, F. and Patrice, H. (2010). Flexural Strengthening of Reinforced Concrete Beams with Textile Reinforced Concrete (TRC), CICE 2010 - The 5th International Conference on FRP Composites in Civil Engineering, Beijing, China. 665-667.

Ashrafi, H.R., Behsan, H. and Esmaeili, N. (2012). Comparison of analytical and experimental results of ductility factor in reinforced concrete structures, Journal of Life Science, 9(4), 2721–2734.

Ashour, S. A. (2000). Effect of compressive strength and tensile reinforcement ratio on flexural behavior of high-strength concrete beams. Journal of Engineering Structures, 22(5), 413–423. doi:10.1016/S0141-0296(98)00135-7

ASTM A615. (1995). Standard specification for deformed and plain billet steel bars for concrete reinforcing. American society for testing and material. Annual book of ASTM standard.

Basalo, F.J.D.C.Y, Matta, F and Nanni, A. (2012). Fibre reinforced cement-based composite system for concrete confinement. Journal of Construction and Building Materials, 32(2012), 55-65.

Baumgart, F. (2000). Stiffness-an unknown world of mechanical science. International Journal of the care of the Injured, 31(2): 14-23.

Binici, B. (2005). An analytical model for stress–strain behavior of confined concrete. Journal of Engineering Structures, 27 (2005), 1040–1051.

Bonacci, J. F. and Maalej, M. (2000). Externally bonded fibre reinforced polymer for rehabilitation of corrosion damaged concrete beams. ACI Structural Journal, 97(5), 703-711.

Bonacci, J. F. and Maalej, M. (2001). Behavioral trends of RC beams strengthened with externally bonded FRP. Journal of Composites for Construction, 5(2), 102–113.

Borgand, B., Warren, C., Somayagi, S. and Heidersbach, R. (1990). Mechanisms of corrosion of steel in concrete. Published by N. S. Berke, V. Chaker and D. Whiting, Philadelphia, 174-188.

Bournas, D.A., Lontou, P.V., Papanicolaou, C.G. and Triantafillou, T.C. (2007). Textile-reinforced mortar versus fibre-reinforced polymer confinement in reinforced concrete columns. ACI Structural Journal, 104(6): 740-748.

Bournas, D.A. and Triantafillou, T. C. (2008). Innovative seismic retrofitting of old-type RC columns through jacketing: textile-reinforced mortars (TRM) versus fibre-reinforced polymers (FRP). The 14th World Conference on Earthquake Engineering, Beijing, China, 1-8.

Bournas, D. A., Triantafillou, T. C., Zygouris, K. and Stavropoulos, F. (2009). Textile-Reinforced Mortar versus FRP Jacketing in Seismic Retrofitting of RC Columns with Continuous or Lap-Spliced, Journal of Composites for Construction, 13(5), 360–371.

Bournas, D. A. and Triantafillou, T. C. (2011). Bond Strength of Lap-Spliced Bars in Concrete Confined with Composite Jackets, Journal of Composites for Construction, 15(2), 156–167. doi:10.1061/(ASCE)CC.1943-5614.0000078.

Bousias, S. N., Triantafillou, T. C., Fardis, M. N., Spathis, L. and Regan, B. A. O. (2005). Fiber-reinforced polymer retrofitting of rectangular reinforced concrete columns with or without corrosion, Journal of Composites for Construction, 101(4), 512-520.

Brameshuber, W. (2006). Textile reinforced concrete. RILEM Publications SARL.

Broomfield, J.P. (1997). Corrosion of steel in concrete: understanding, investigation and repair. Published by E and FN Spon, London and New York.

Bruckner, A., Ortlepp, R. Curbach, M. (2006). Textile reinforced concrete for strengthening in bending and shear. Journal of Materials and Structures, (2006) 39:741–748

Bruckner, A., Ortlepp, R. Curbach, M. (2008). Textile reinforced concrete for strengthening in bending and shear. Journal of Materials and Structures, (2008) 41:407–418

Cabrera J. G. (1996). Deterioration of concrete due to reinforcement corrosion. Journal of Cement and Concrete Research, 18(1), 47-59.

Cairns, J. and Zhao, Z. (1993). Behaviour of concrete beams with exposed reinforcement. Proceedings of the Institution of Civil Engineers: Structures and Buildings. 99(2), 141-154.

Carino, N. J. and Clifton, J. R. (1995). Prediction of Cracking in Reinforced Concrete Structures. Report, NISTIR 5634, U.S. department of commerce.

Carstensen, J.V. (2011). Material Modelling of Reinforced Concrete at Elevated Temperatures, MSc Thesis, Technical University of Denmark, Denmark.

CEB/FIP Model Code. (1990). Final Draft, Information Bulletin 204, Comite Euro-International du Beton, Lausanne, Switzerland, Chapters 4-10.

CEP. (2012). Civil Engineering Disasters – Collapse Of Bridges, online available from <http://www.engineeringcivil.com/civil-engineering-disasters-collapse-of-bridges.html>

Chaudhari, S. V. and Chakrabarti, M. A. (2012). Modeling of Concrete for Nonlinear Analysis using Finite Element Code ABAQUS. International Journal of Computer Applications, 44(7), 14–18. doi:10.5120/6274-8437

Collins, M.P. and Mitchell, D., (1997). Prestressed concrete structure, Response publication, Toronto, Canada.

Colombo, I., Colombo, M., Magri, A., Zani, G. and Di Prisco, M. (2011). Textile Reinforced Mortar at High Temperatures. Journal of Applied Mechanics and Materials, 82, 202–207. doi:10.4028/www.scientific.net/AMM.82.202

Contamine, R., Si Larbi, a. and Hamelin, P. (2011). Contribution to direct tensile testing of textile reinforced concrete (TRC) composites. Journal of Materials Science and Engineering: A, 528(29-30), 8589–8598. doi:10.1016/j.msea.2011.08.009

Contamine, R., Si Larbi, a. and Hamelin, P. (2013). Identifying the contributing mechanisms of textile reinforced concrete (TRC) in the case of shear repairing damaged and reinforced concrete beams. Journal of Engineering Structures, 46, 447–458. doi:10.1016/j.engstruct.2012.07.024

CSA A23.3. (2004). Design of concrete structures. Canadian Standards Association. Rexdale, Ontario, Canada.

CSA S806. (2002). Design and construction of building components with fibre reinforced polymers. Canadian Standards Association. Rexdale, Ontario, Canada.

CSA S807. (2010). Specification for fibre reinforced polymers. Canadian Standards Association. Rexdale, Ontario, Canada.

David, E. and Djelal, C. (1998). Repair and strengthening of reinforced concrete beams using composite materials. 2nd Int. PhD Symposium in Civil Engineering, Budapest, 1–8.

Dimas, J. V., Ehsani, M. R. and Saadatmanesh, H. (1996). Strengthening of RC beams in a nuclear power plant. Second International Conference on Advanced Composite Materials in Bridges and Structures, ACMBS, Montreal, Quebec, Canada, 613-620.

Ebead, U.A. and Marzouk, H. (2005). Tension-Stiffening Model for FRP-Strengthened Concrete Two-Way Slabs, Journal of Material and Structures/Materiaux at Constructions, RILEM, Paris, 38(2005), 193-200.

El-Maaddawy, T.A.Z.E. (2004). Performance of corrosion-damaged reinforced concrete beams repaired with CFRP laminates. PhD thesis. The University of Waterloo, Ontario, Canada.

El-Maaddawy, T. and Soudki, K. (2005). Carbon fiber reinforced polymer repair to extend service life of corroded reinforced concrete beams. Journal of Composites for Construction, 9(2), 187-194.

El-Maaddawy, T., Soudki, K. and Topper, T. (2005). Analytical model to predict nonlinear flexural behavior of corroded reinforced concrete beams, ACI Structural Journal, 102(4), 550-559.

El-Maaddawy, T., Soudki, K. and Topper, T. (2007). Performance evaluation of carbon fiber reinforced polymer repaired beams under corrosive environmental conditions, ACI Structural Journal, 104(1), 3-11.

Esfahani M, Kianoush M, Tajari A. (2007). Flexural behavior of reinforced concrete beams strengthened by CFRP sheets. Journal of Engineering Structure. 29:2428–44.

Favre., R. and Charif, H. (1994). Basic Model and Simplified Calculations of Deformations According to the CEB-FIP Model Code 1990. ACI Structural Journal. 91(2), 169-177.

FEMA 356. (2000). Prestandard and commentary for the seismic rehabilitation of buildings.

Gadve, S., Mukherjee, A. and Malhotra, S. N. (2009). Corrosion of steel reinforcements embedded in FRP wrapped concrete. Journal of Construction and Building Materials, 23(1), 153–161. doi:10.1016/j.conbuildmat.2008.01.008

Gao, Y. F. and Bower, a F. (2004). A simple technique for avoiding convergence problems in finite element simulations of crack nucleation and growth on cohesive interfaces. Journal of Modelling and Simulation in Materials Science and Engineering, 12(3), 453–463. doi:10.1088/0965-0393/12/3/007

Gjorv, O.E. (2009). Durability design of concrete structures in severe environments. Published by Taylor and Francis, USA.

GEOCISA and Toroja Institute. (2004). CONTECVET A validated Users Manual for assessing the residual service life of concrete structures, Manual for assessing corrosion-affected concrete structures. <http://www.ietcc.csic.es/files/manual_ingles.pdf>

Gonzalez, J.A. Andrade, C., Alonso, C., Feliu, S. (1995). Comparison of rates of general corrosion and maximum pitting penetration on concrete embedded steel reinforcement, Journal of Cement and Concrete Research, 25(2), 257-264.

Guo, Z. and Zhang, X. (1987). Investigation of complete stress- deformation curves for concrete in tension, ACI Materials Journal, 84(4), 278-285.

Harajli, M., and El-Khatib, H. (n.d.). Experimental Evaluation of the Behaviour of Masonry Walls Strengthened Using Textile-Mortar System. Online available from (http://webfea.fea.aub.edu.lb/fea/cee/research/research_programs.aspx#r1)

Hartig, J., Combe, U.H. and Schicktanz, K. (2008). Influence of bond properties on the tensile behaviour of Textile Reinforced Concrete. Journal of Cement and Concrete Composites. 30(2008), 898-906.

Hashemi, S. and Mahaidi, R.A. (2010). Investigation of bond strength and flexural behaviour of FRP-strengthened reinforced concrete beams using cement-based adhesives. Australian Journal of Structural Engineering, 11(2):129-139.

Hashemi, S. and Mahaidi, R.A. (2012). Flexural performance of CFRP textile-retrofitted RC beams using cement-based adhesives at high temperature. Journal of Construction and Building Materials, 28(2012), 791-797.

Hawileh, R. A., Naser, M. Z. and Abdalla, J. A. (2013). Finite element simulation of reinforced concrete beams externally strengthened with short-length CFRP plates. Journal of Composites Part B: Engineering, 45(1), 1722–1730. doi:10.1016/j.compositesb.2012.09.032

Hegger, J. and Voss, S. (2005). Textile reinforced concrete – bearing behavior, design, applications. Composites in Construction 2005, Third International Conference, France, Lyon: 1139-1146.

Hegger, J. and Voss, S. (2008). Investigations on the bearing behaviour and application potential of textile reinforced concrete. Journal of Engineering Structures, 30(7), 2050–2056. doi:10.1016/j.engstruct.2008.01.006

Hinzen, M., Hatting, A. and Brameshuber, W. (2012). Influence of Textile Alignment, Moisture and Shape of Specimens on First Crack Load and Load Bearing Behavior of Textile Reinforced Concrete Containing Short Fibers, HPFRCC6, RILEM, 455–462.

Holler, S., Butenweg, C., Noh, S.-Y. and Meskouris, K. (2004). Computational model of textile-reinforced concrete structures. Journal of Computers and Structures, 82(23-26), 1971–1979. doi:10.1016/j.compstruc.2004.03.076

Isecke, B., (1982). Failure analysis of the collapse of the Berlin Congress Hall. Journal of material performance. 1982(12): 36-46.

Jun, P. and Mechtcherine, V. (2010). Behaviour of Strain-hardening Cement-based Composites (SHCC) under monotonic and cyclic tensile loading. Journal of Cement and Concrete Composites, 32(10), 801–809. doi:10.1016/j.cemconcomp.2010.07.019

Khomwan, N., Foster, S. J. and Smith, S. T. (2010). FE Modeling of FRP-Repaired Planar Concrete Elements Subjected to Monotonic and Cyclic Loading. Journal of Composites for Construction, 14(6), 720–729.

Kmiecik, P. and Kamiński, M. (2011). Modelling of reinforced concrete structures and composite structures with concrete strength degradation taken into consideration, Archives of civil and mechanical engineering, XI(3).

Konig, G. and Tue, N. (1992). Crack Width Control for Concrete Constmctions," Journal of Darmstadt Concrete, 7(1992), 231-245

Kutarba, M.P., Brown, J.R., Hamilton, H.R. (2007). Repair of corrosion damaged concrete beams with carbon fiber-reinforced polymer composites. Composites Research Journal, 1(4): 36-46.

Lee, H., Tomosawa, F., Masuda, Y. and Kage, T. (1997). Effect of CFRP sheets on flexural strengthening of RC beams damaged by corrosion of tension rebar. Third International Symposium on Non-Metallic FRP Reinforcement for Concrete Structures, Sapporo, Japan, 435-442.

LeRose, C. (2001). The Collapse of the Silver Bridge. West Virginia Historical Society Quarterly, xv(4), < http://www.wvculture.org/history/wvhs1504.html >

Lin, Y. and Scanlon, A. (2010). Tension stiffening model for reinforced concrete based on bond stress slip relation. MSc Thesis, Pennsylvania State University, PA, USA.

Liu, Y. and Weyers, R. (1998). Modeling the time-to-corrosion cracking in chloride contaminated reinforced concrete structures, ACI Materials Journal, 95(6), 675-681.

Lodygowski, T. and Jankowiak, T., (2005). Identification of Parameters of a Concrete Damage Plasticity Constitutive Model. Journal of Foundations of Civil and Environmental Engineering, 6(2005), 54-69.

Maghsoudi, A. A. and Akbarzadeh, B. H. (2007). Effect of tension and compression reinforcements on the serviceability of HSC beams with relatively small shear span to depth ratio, The Arabian Journal for Science and Engineering, 32(2), 219–238.

Mailvaganam, N.P. (2004). Concrete repair and rehabilitation: issues and trends. NRCC-47293, 1(1): 1-9.

Marzouk, H. and Chen, Z.M., (1993). Finite element analysis of high strength concrete slabs, ACI Structural Journa1, 90(5), 505-513.

Marzouk, H. and Chen, Z.M., (1995). Fracture energy and tension properties of high strength concrete, Journal of Materials in Civil Engineering, 7(2), 108-116.

Masoud, S. G. and Soudki, K. A. (2002). Post-repair performance of corrosion-damaged reinforced concrete beams repaired with FRP sheets. International Conference on Durability of Composites for Construction, CDCC, Sherbrooke, Quebec, Canada, 113-125.

Mobasher, B. and Raji, B. (2007). Rehabilitation of concrete structures. A Joint Publication of NCSEA, CASE and SEI, Online available from (http://www.structuremag.org/article.aspx?articleID=424)

Moniruzzman, P.K.M. and Rteil, A. (2012). Numerical Comparison between FRP and TRM for Seismic Retrofitting. 3rd International Structural Specialty Conference, CSCE, Edmonton, Alberta.

Neale, K., Ebead, U., Abdel Baky, H., Elsayed, W. and Godat, A. (2005). Modeling of debonding phenomena in FRP-strengthened concrete beams and slabs. Proceedings of the international symposium on bond behaviour of FRP in structures (BBFS). Hong Kong, China, 45-54.

Obaidat Y. (2011). Structural retrofitting of concrete beams using FRP- Debonding Issues. PhD Thesis, Lund University, Lund, Sweden.

Okada, K., Kobayashi, K. and Miyagawa, T. (1988). Influence of longitudinal cracking due to reinforcement corrosion on characteristics of reinforced concrete members. ACI Structural Journal, 85(2), 134-140.

Olivia, M. and Mandal, P. (2005). Curvature ductility of reinforced concrete beam, Journal of Teknik Sipil, 6(1),1–13.

Ortlepp, R., Hampel, U. and Curbach, M. (2006). A new approach for evaluating bond capacity of TRC strengthening. Journal of Cement and Concrete Composites, 28(7), 589–597. doi:10.1016/j.cemconcomp.2006.05.003

Papanicolaou, C.G., Triantafillou, T. C. and Karlos, K., Papathanasiou, M. (2007). Textile-reinforced mortar (TRM) versus FRP as strengthening material of URM walls : in-plane cyclic loading, Journal of Materials and Structures, 2007(40),1081–1097. doi:10.1617/s11527-006-9207-8

Papanicolaou, C.G., Triantafillou, T.C., Papathanasiou, M. and Karlos, K. (2008). Textile reinforced mortar (TRM) versus FRP as strengthening material of URM walls: out-of-plane cyclic loading. Journal of Materials and Structures, 40(10): 1081-1097.

Papanicolaou, C.G. and Papantoniou, I.C. (2010). Mechanical behavior of textile reinforced concrete (TRC) / concrete composite elements. Journal of Advanced Concrete Technology, 8(1): 35-47.

Park, R. and Ruitong, D. (1989). Ductility of Doubly Reinforced Concrete Beam Sections, ACI Structural Journal, (85), 217–225.

PCA. (2013). Corrosion of Embedded Metals. Portland Cement Association, Skokie, Illinois, USA. < http://www.cement.org/tech/cct_dur_corrosion.asp >

Peled, A. and Bentur, A. (2000). Geometrical characteristics and efficiency of textile fabrics for reinforcing cement composites. Journal of Cement and Concrete Research, 30(2000): 781-790.

Piggott, M. (2002). Load bearing fibre composites, 2nd Edition. Kluwer Academic Publishers, Boston, Dordrecht, London.

Potisuk, T., Higgins, C. C., Miller, T. H. and Yim, S. C. (2011). Finite Element Analysis of Reinforced Concrete Beams with Corrosion Subjected to Shear. Journal of Advances in Civil Engineering, 2011, 1–14. doi:10.1155/2011/706803

Priestley, M.J.N. (2000). Performance based seismic design, Conference proceeding of 12th WCEE, Auckland, New-Zealand, 0756.

Rami A. Hawileh, Mohannad Z. Naser, Jamal A. Abdalla. (2012). Finite element simulation of reinforced concrete beams externally strengthened with short-length CFRP plates, Journal of Composites Part B: Engineering, 45(1), 1722-1730.

Rteil, Ahmad. (2012). Corrosion of steel reinforcement in concrete structures. Lectures note of the Rehabilitation of Concrete Structures, UBC, Kelowna. Chapter 1, 1-10.

Roberts, C.C. (2012). Minneapolis Bridge Collapse. Online report, <http://www.croberts.com/minneapolis-bridge-collapse.htm>

Ro driguez, J., Ortega, L. M. and Casal, J. (1997). Load carrying capacity of concrete structures with corroded reinforcement. Journal of Construction and Building Materials, 11(4), 239-248.

Saether, I. and Sand, B. (2012). FEM simulations of reinforced concrete beams attacked by corrosion, Nordic Concrete Research, 39(2), 15–32. <http://www.tekna.no/ikbViewer/Content/789311/N53%20-%20S%E6ther%202009-05-15_FINAL.pdf>

Schladitz, F., Frenzel, M., Ehlig, D. and Curbach, M. (2012). Bending load capacity of reinforced concrete slabs strengthened with textile reinforced concrete. Journal of Engineering Structures, 40, 317–326. doi:10.1016/j.engstruct.2012.02.029

Sherwood, E.G. and Soudki, K.A. (2000). Rehabilitation of Corrosion Damaged Concrete Beams with CFRP Laminates- Pilot Study, Journal of Composites Part B: Engineering, 31(2000), 453-459.

SiLarbi, A., Contamine, R. and Hamelin, P. (2012). TRC and hybrid solutions for repairing and/or strengthening reinforced concrete beams. Journal of Engineering Structures, 45, 12–20. doi:10.1016/j.engstruct.2012.06.002

Smith, S.T. and Foster, S.Z. (2006). Finite Element Modelling of RC Beams Strengthened in Shear with FRP Composites. Proceedings of the 2nd International Congress, Naples, Italy, 1-11.

Soudki, K. A. and Sherwood, T. G. (2000). Behaviour of reinforced concrete beams strengthened with carbon fibre reinforced polymer laminates subjected to corrosion damage. Canadian Journal of Civil Engineering, 27(5), 1005–1010. doi:10.1139/cjce-27-5-1005

Soudki, K.A., Sherwood, T.G. and Masoud S. (2000). FRP repair of corrosion-damaged reinforced concrete beams. Report, Department of Civil Engineering, University of Waterloo, Waterloo, Canada, 1–13. <http://quakewrap.com/frp%20papers/FRP-Repair-of-Corrosion-Damaged-Reinforced-Concrete-Beams.pdf >

Tachibana, Y., Maeda, K. I., Ka jikawa, M. (1990). Mechanical behavior of RC beams damaged by corrosion of reinforcement. Third International Symposium on Corrosion of Reinforcement in Concrete Construction, UK, 178-187.

Teng, J.G., Chen, J.F., Smith, S.T. and Lam, L. (2001). FRP Strengthening RC Structures. John Wiley and Sons publications: 147-211.

Thomsen, H., Spacone, E., Limkatanyu, S. and Camata, G. (2004). Failure mode analyses of reinforced concrete beams strengthened in flexure with externally bonded fiber reinforced polymers. Journal of Composites for Construction, 8(2), 123-131.

Triantafillou, T.C., Papanicolaou, C.G., Zissimopoulou, P., Laourdekis, T. 2005. Concrete confinement with textile reinforced mortar (TRM) jackets. ACI Structural Journal, 103(4).

Tullmin, M. (2007). Costs Related to Corrosion. Corrosion Club, Online available from < http://www.corrosion-club.com/costs.htm >

Uomoto. T., Tsuji, K. and Kakizawa, T. (1984). Deterioration mechanism of concrete structures caused by corrosion of reinforcing bars. Transactions of Japan Concrete Institute, 6(1984), 163-170.

Uomoto. T. and Misra. (1988). Behavior of concrete beams and columns in marine environment when corrosion of reinforcing takes place, ACI Special Publication , ACI SP-109, 127-146.

Wang, Y., Li, V. C. and Backer, S. (1990). Tensile properties of synthetic fiber reinforced mortar. Journal of Cement and Concrete Composites, 12(1), 29–40. doi:10.1016/0958-9465(90)90033-T

Wang, C., Shih, C., Hong, S. and Hwang, W. (2004). Rehabilitation of Cracked and Corroded Reinforced Concrete Beams with Fiber-Reinforced Plastic Patches, Journal of Composites for Construction, 8(3), 219–228.

West, J. (1999). Durability Design of Post-Tensioned Bridge Substructures, PhD thesis, University of Texas at Austin, Texas, USA.

Whitmore, D.W. and Ball, J.C., (2004). Corrosion Management, ACI Concrete International, 26(12), 82-85.

Yang, Z. J., Chen, J. F. and Proverbs, D. (2003). Finite element modelling of concrete cover separation failure in FRP plated RC beams. Journal of Construction and Building Materials, 17(1), 3–13. doi:10.1016/S0950-0618(02)00090-9

Yin, S. and Xu, S. (2011). An experimental study on improved mechanical behavior of textile reinforced concrete. Journal of Advanced Material Research, 168(170): 1850-1853.

Yu, X. and Huang, Z. (2008). An embedded FE model for modelling reinforced concrete slabs in fire. Journal of Engineering Structures, 30(11), 3228–3238. doi:10.1016/j.engstruct.2008.05.004

Zeweben, C., Hahn, H.T. and Chou, T. (1989). Mechanical Behavior and Properties of Composite Materials. Journal of Delaware Composites Design Encyclopedia, Technonic, Lancaster, 1(1989): 3-45.

APPENDICES

APPENDIX A: CONCRETE DAMAGE PLASTICITY MODEL

The stress-strain curve of concrete can be defined beyond the ultimate stress, into the strain-softening branch. As shown in Fig. A.1, when the concrete specimen is unloaded from any point on the strain softening branch of the stress-strain curves, the unloading response is observed to be weakened: the elastic stiffness of the material appears to be damaged (or degraded).

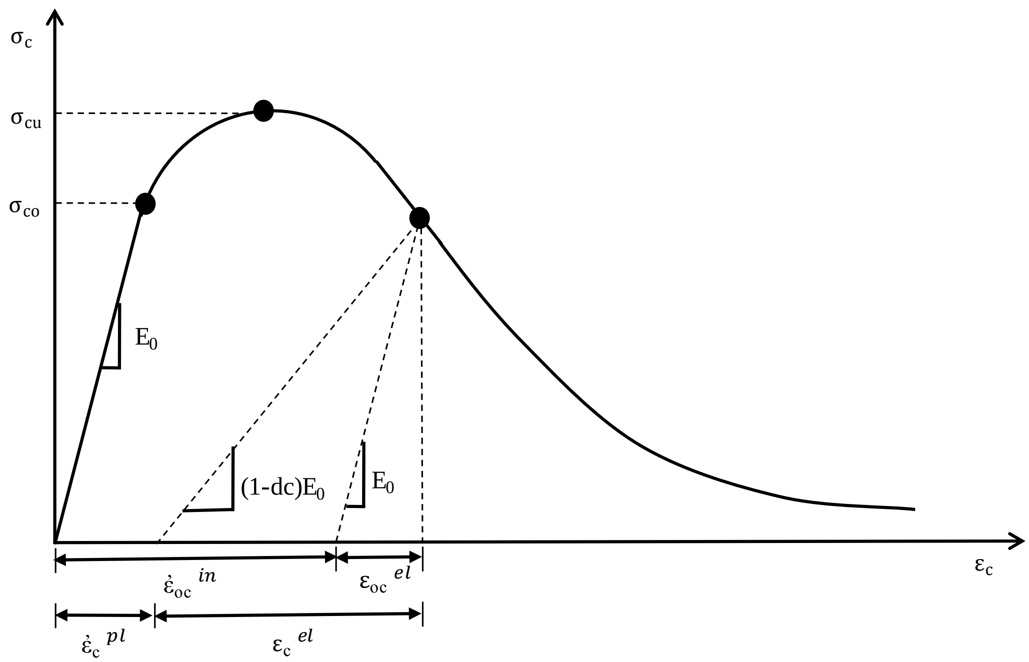

Figure A.1: Response of concrete to uniaxial loading in compression

The compressive inelastic strain ($\dot{\varepsilon}_{oc}{}^{in}$) is defined as the total strain (ε_c) minus the elastic strain ($\varepsilon_{oc}{}^{el}$) as follows.

$$\dot{\varepsilon}_{oc}{}^{in} = \varepsilon_c - \varepsilon_{oc}{}^{el} \tag{A.1}$$

The uniaxial degradation variable (d_c) is an increasing function of the equivalent plastic strain ($\dot{\varepsilon}_c{}^{pl}$). The same relationship is applicable for concrete behaviour under tension.

APPENDIX B: CONCRETE STRAIN DISTRIBUTION

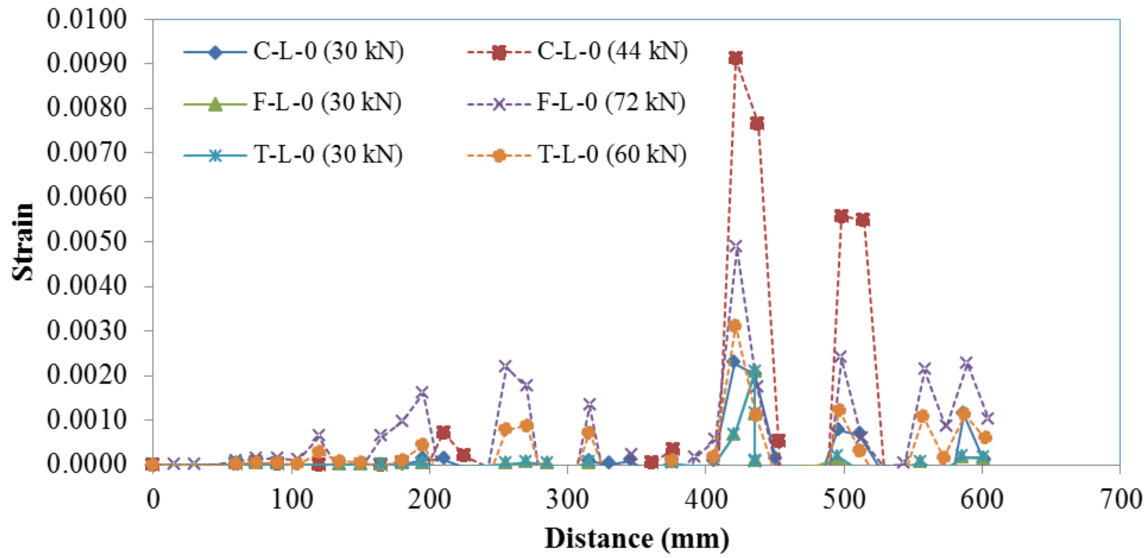

Figure B.1: Concrete strain distribution along the length of the beam (x-L-0)

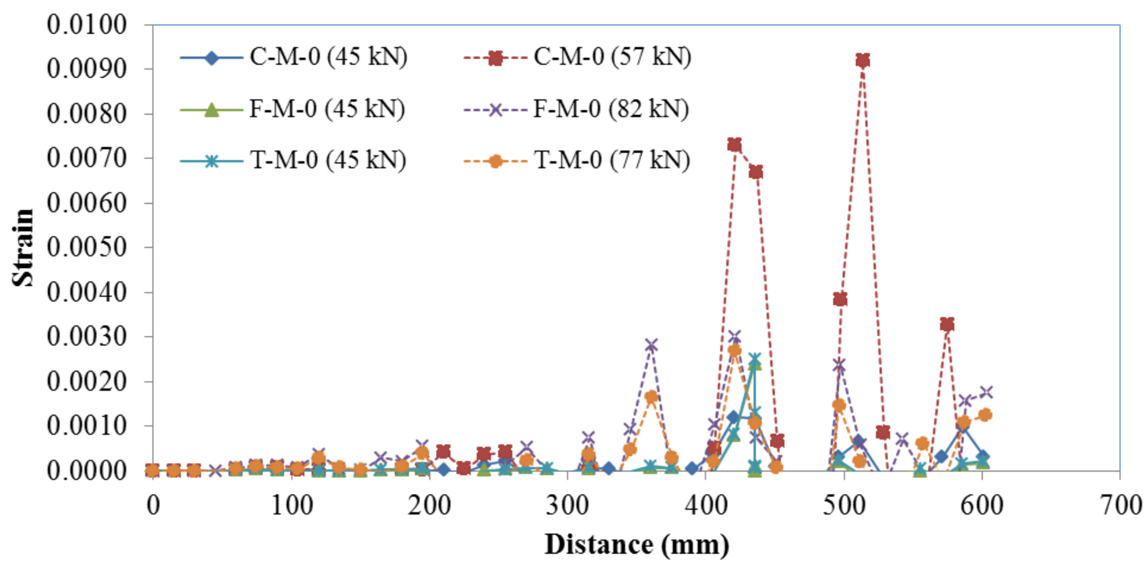

Figure B.2: Concrete strain distribution along the length of the beam (x-M-0)

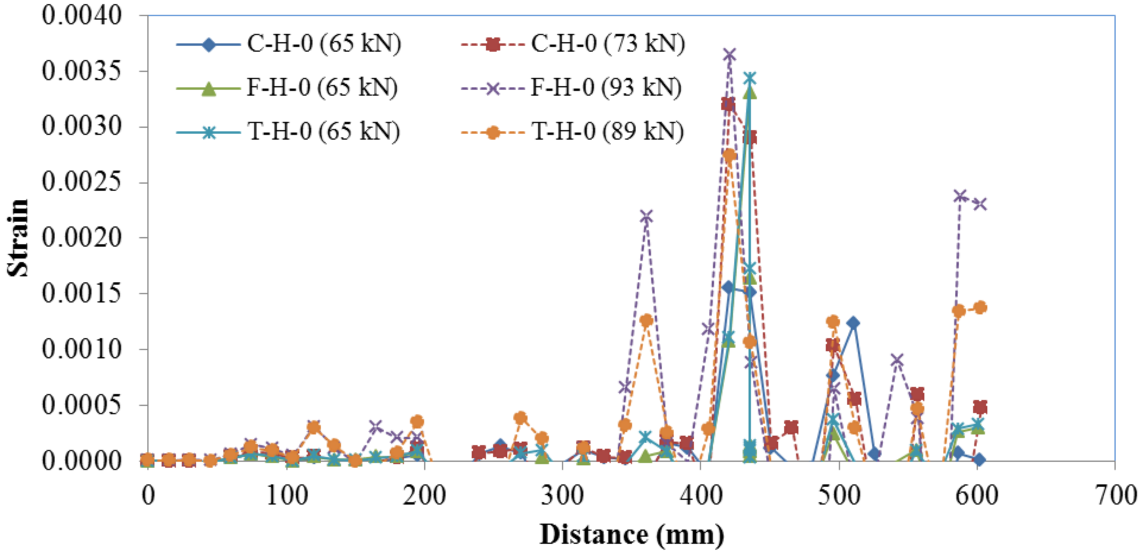

Figure B.3: Concrete strain distribution along the length of the beam (x-H-0)

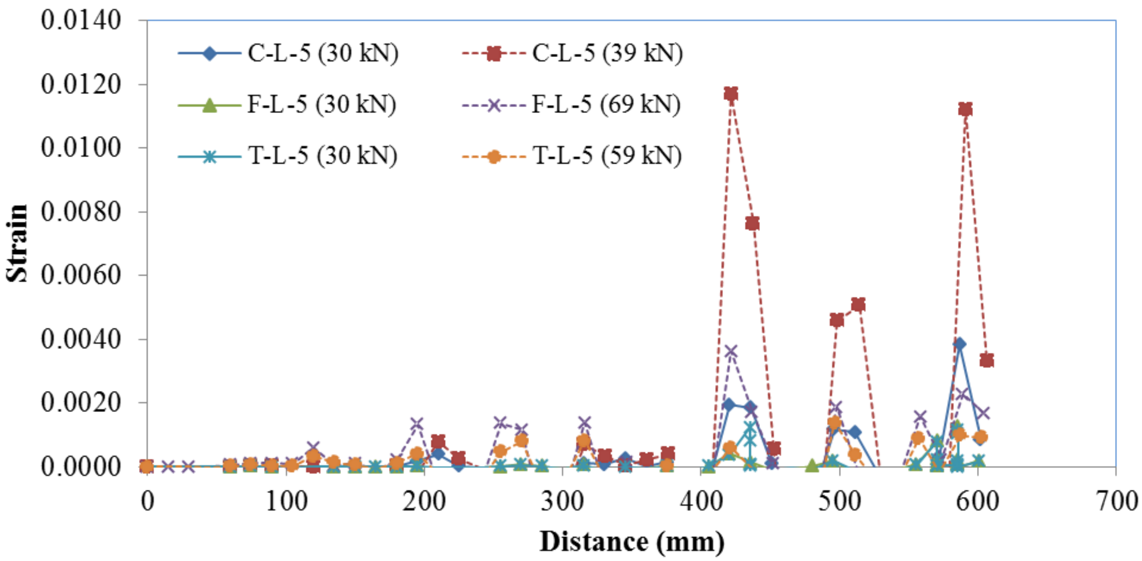

Figure B.4: Concrete strain distribution along the length of the beam (x-L-5)

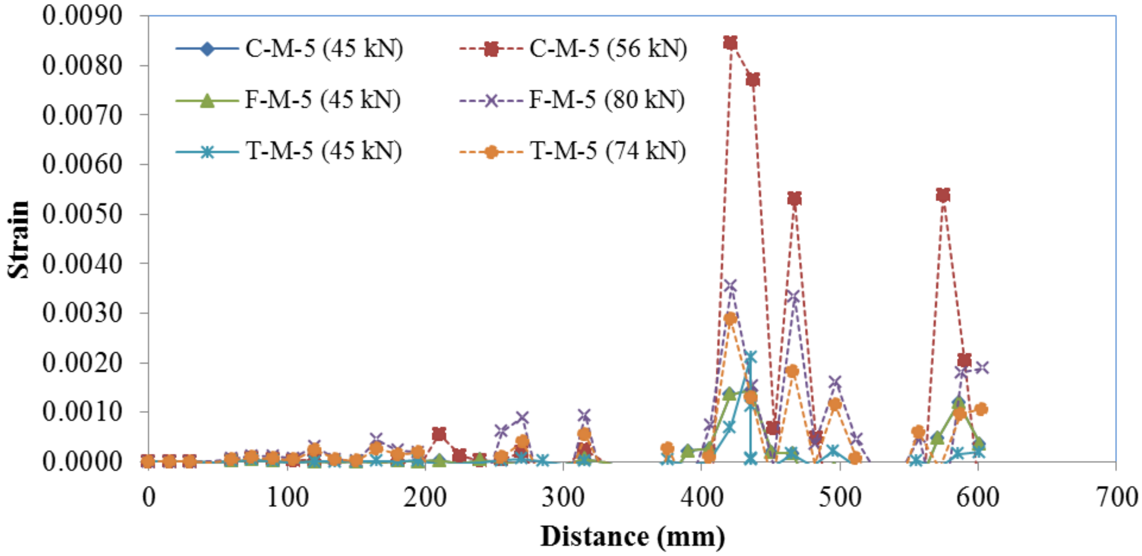

Figure B.5: Concrete strain distribution along the length of the beam (x-M-5)

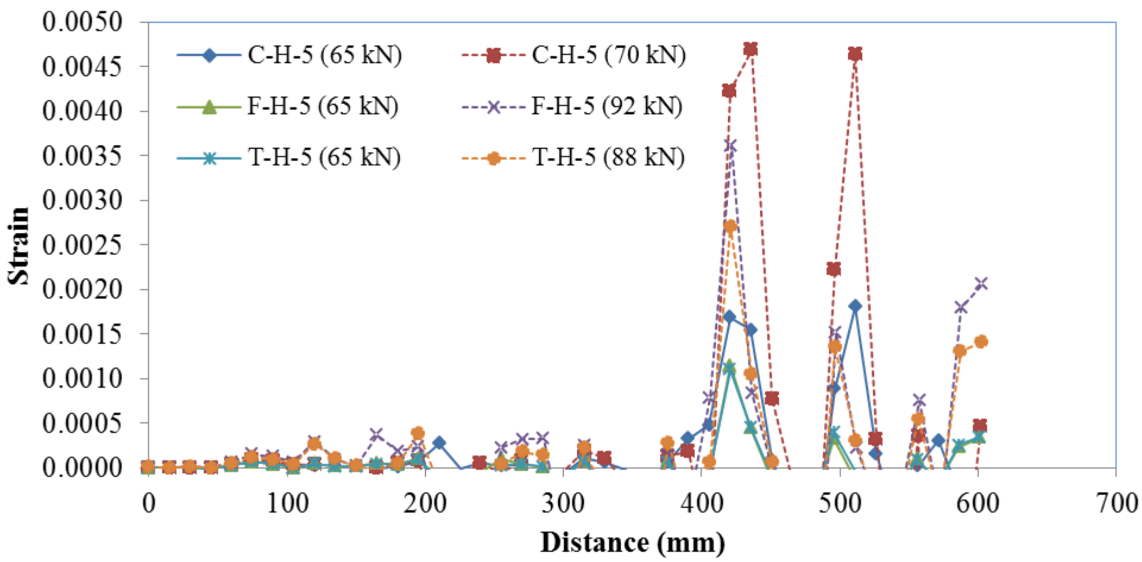

Figure B.6: Concrete strain distribution along the length of the beam (x-H-5)

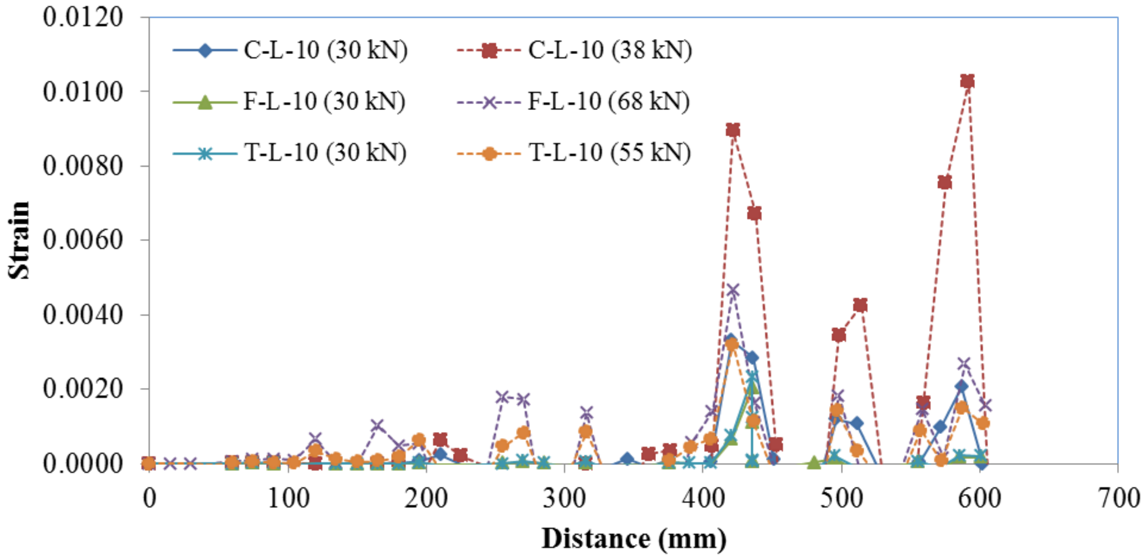

Figure B.7: Concrete strain distribution along the length of the beam (x-L-10)

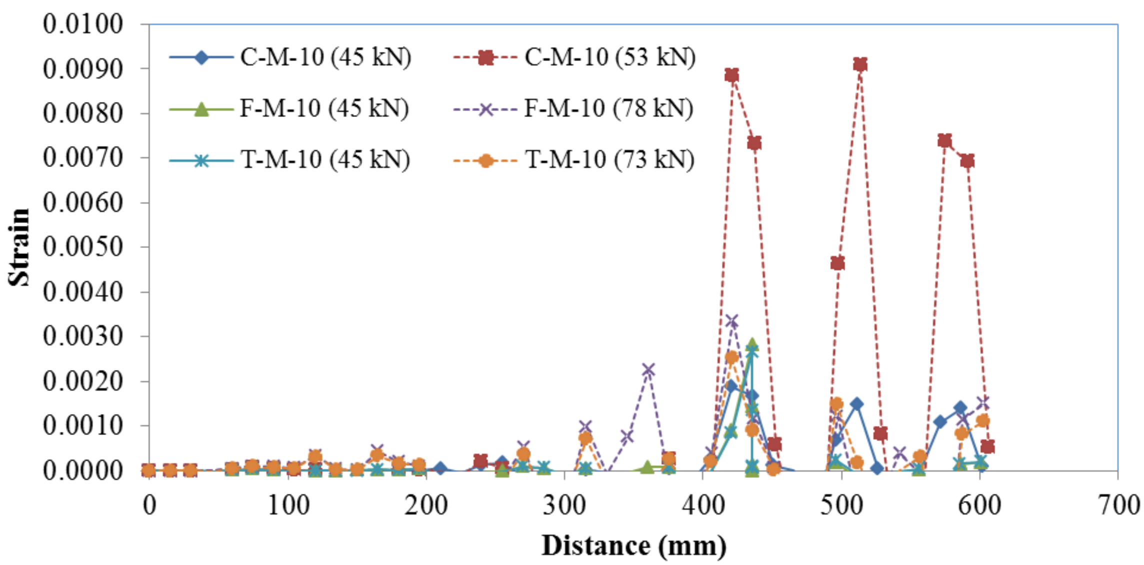

Figure B.8: Concrete strain distribution along the length of the beam (x-M-10)

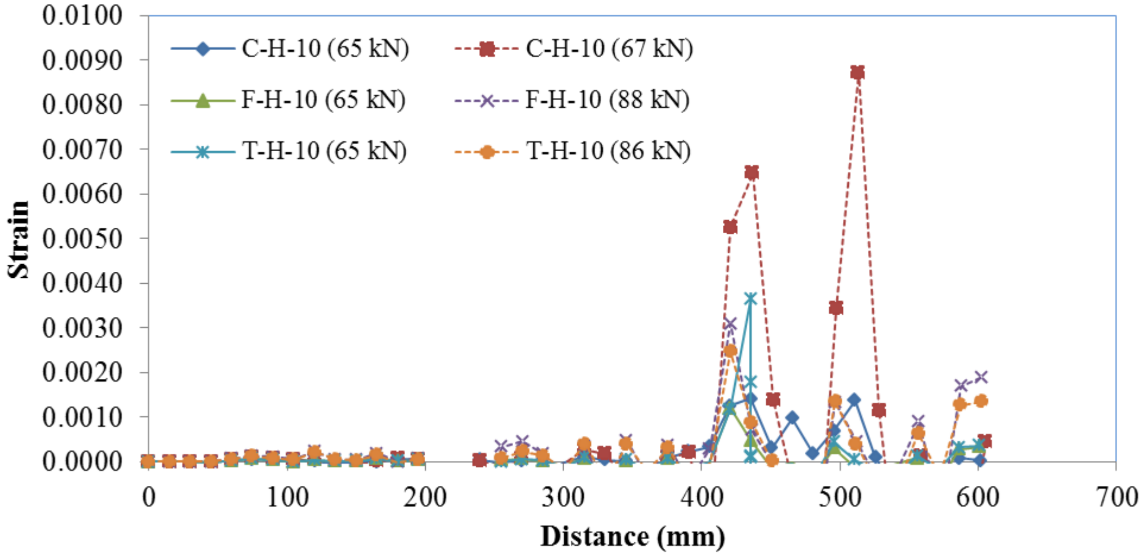

Figure B.9: Concrete strain distribution along the length of the beam (x-H-10)

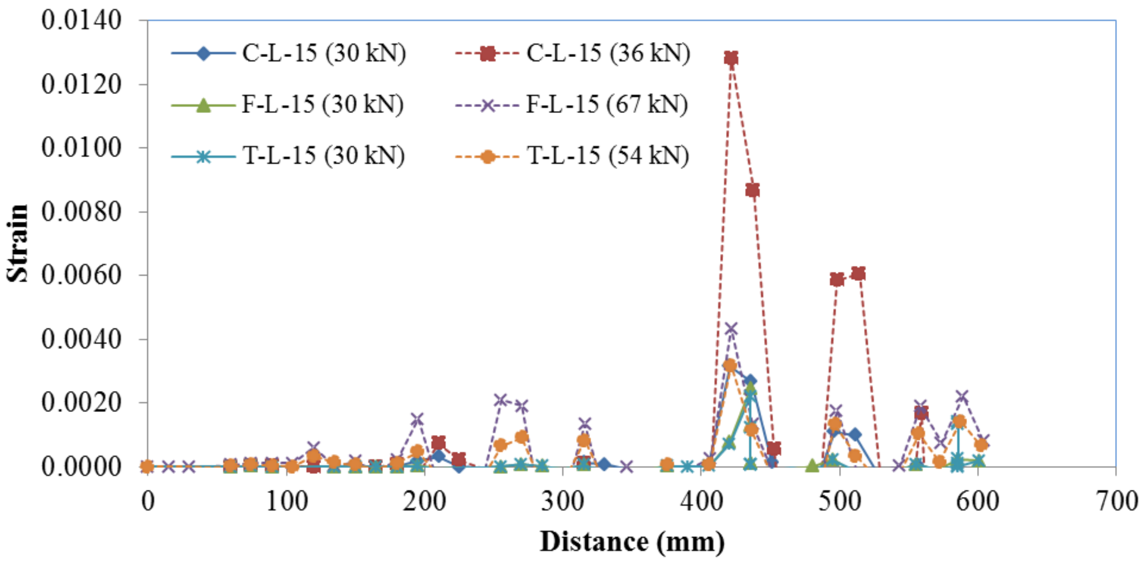

Figure B.10: Concrete strain distribution along the length of the beam (x-L-15)

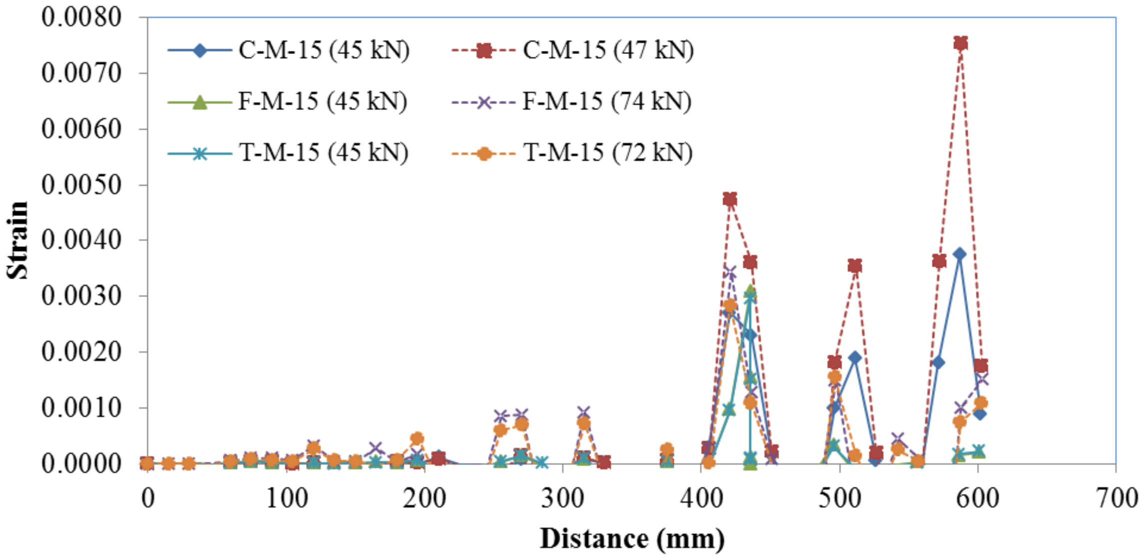

Figure B.11: Concrete strain distribution along the length of the beam (x-M-15)

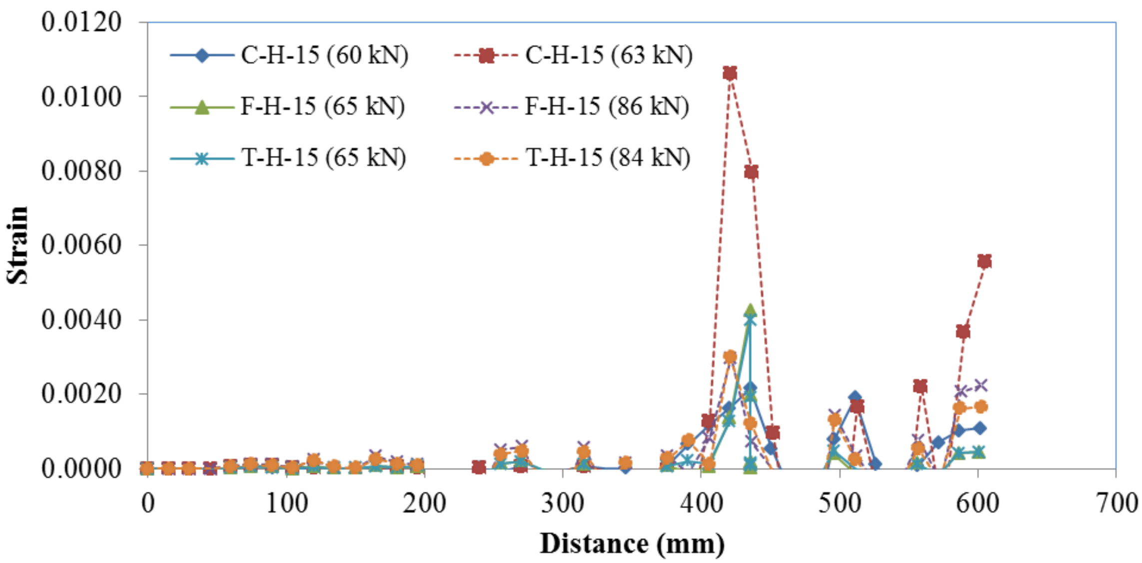

Figure B.12: Concrete strain distribution along the length of the beam (x-H-15)

APPENDIX C: STEEL STRAIN DISTRIBUTION

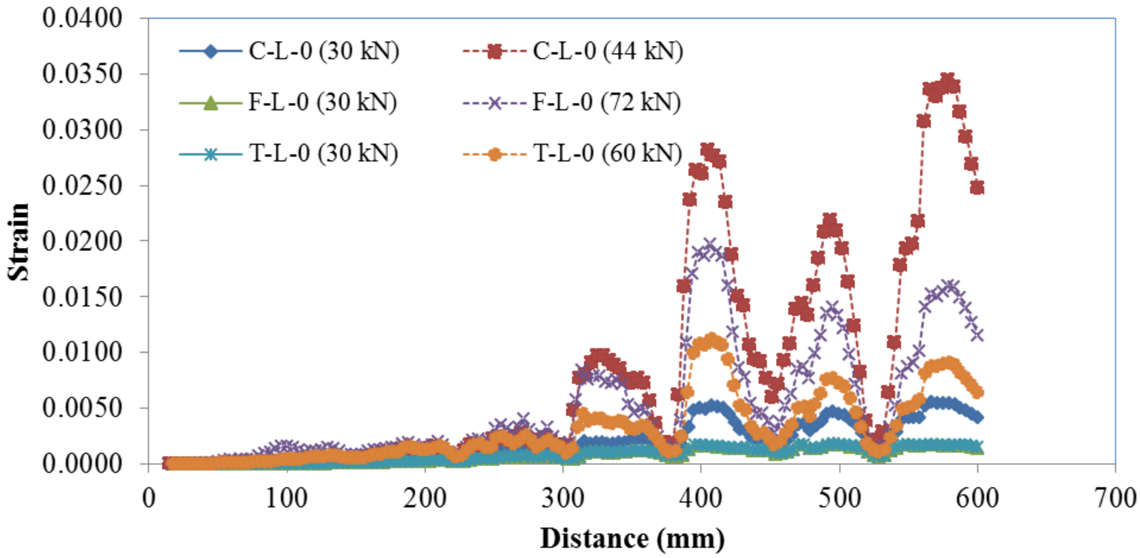

Figure C.1: Steel strain distribution along the length of the beam (x-L-0)

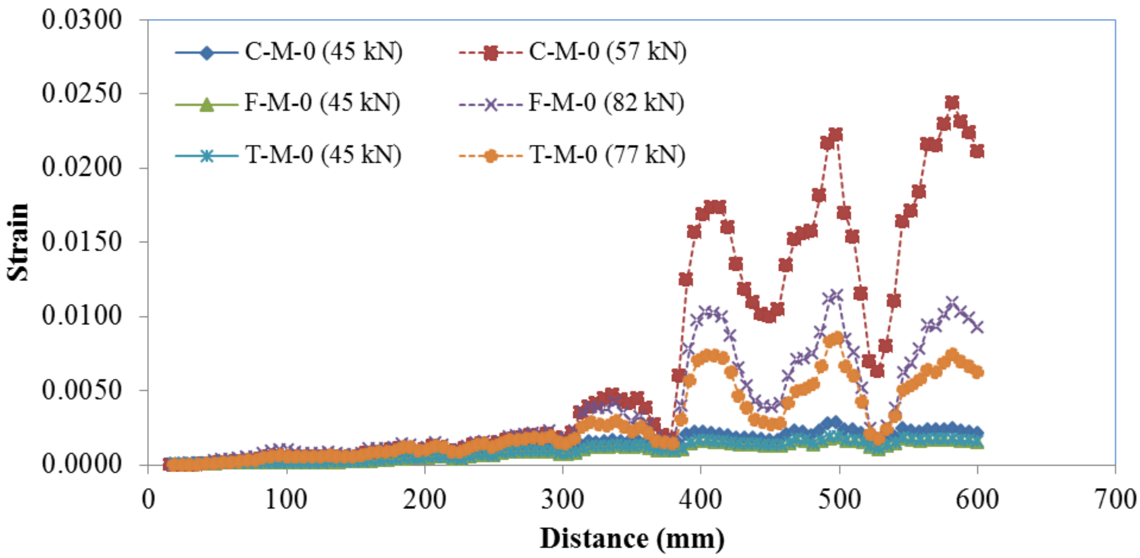

Figure C.2: Steel strain distribution along the length of the beam (x-M-0)

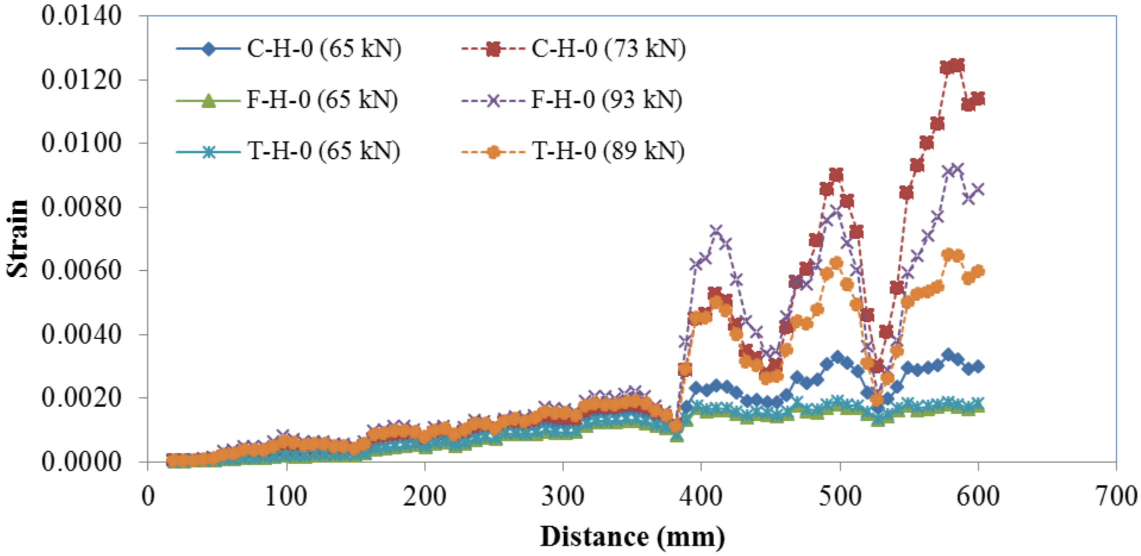

Figure C.3: Steel strain distribution along the length of the beam (x-H-0)

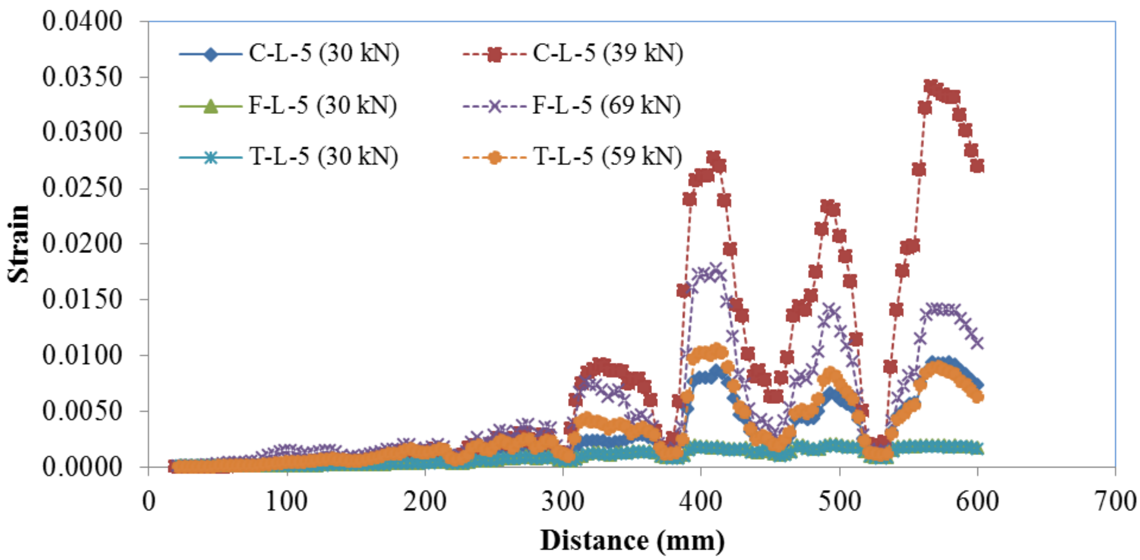

Figure C.4: Steel strain distribution along the length of the beam (x-L-5)

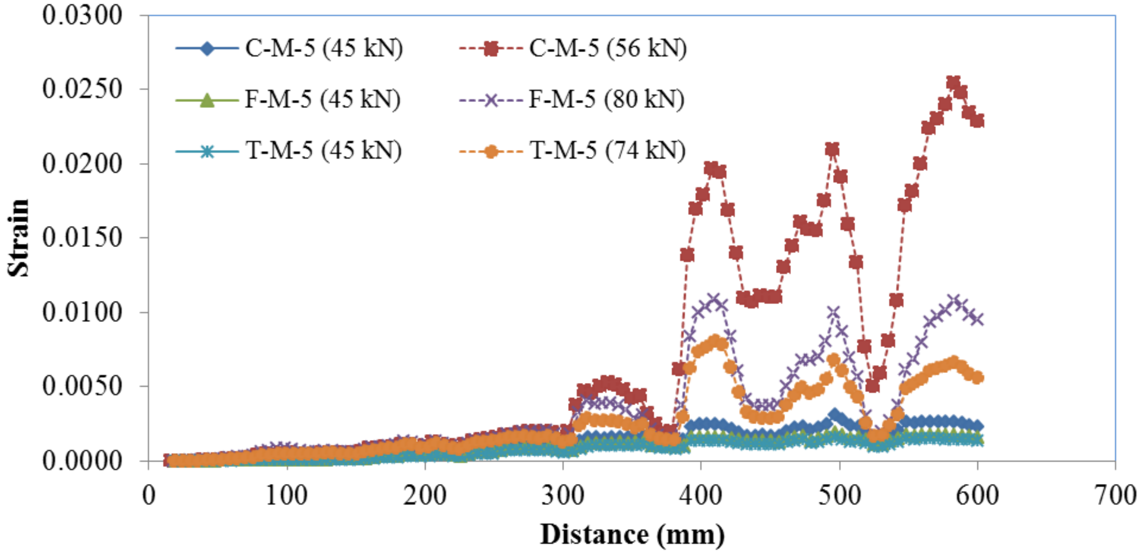

Figure C.5: Steel strain distribution along the length of the beam (x-M-5)

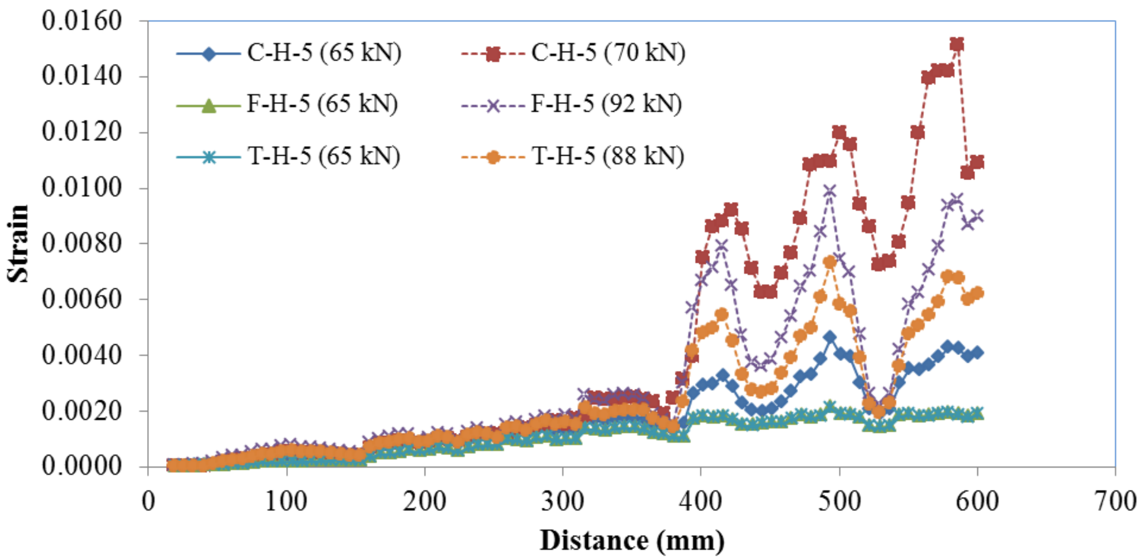

Figure C.6: Steel strain distribution along the length of the beam (x-H-5)

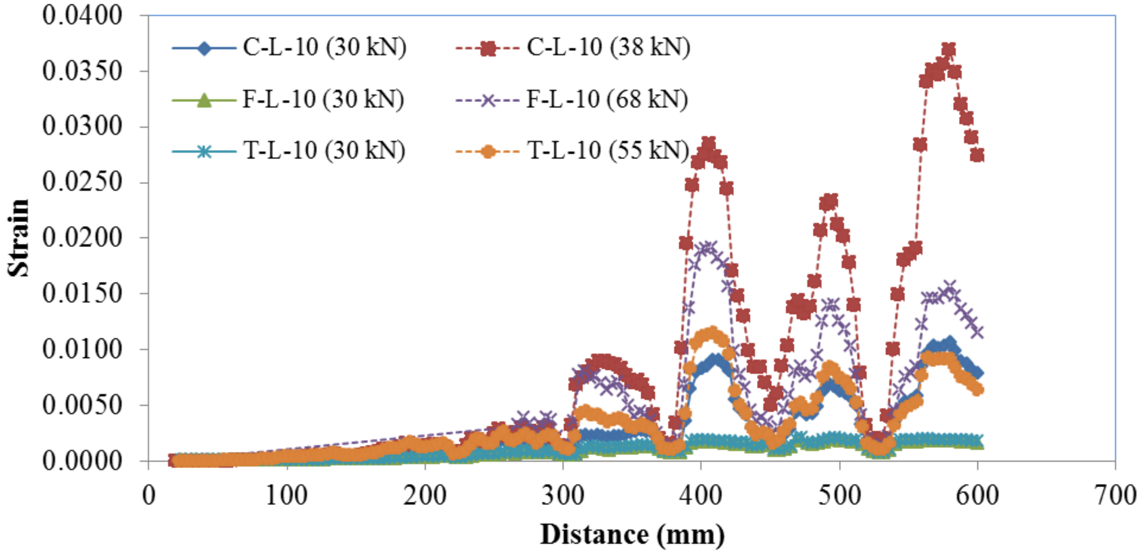

Figure C.7: Steel strain distribution along the length of the beam (x-L-10)

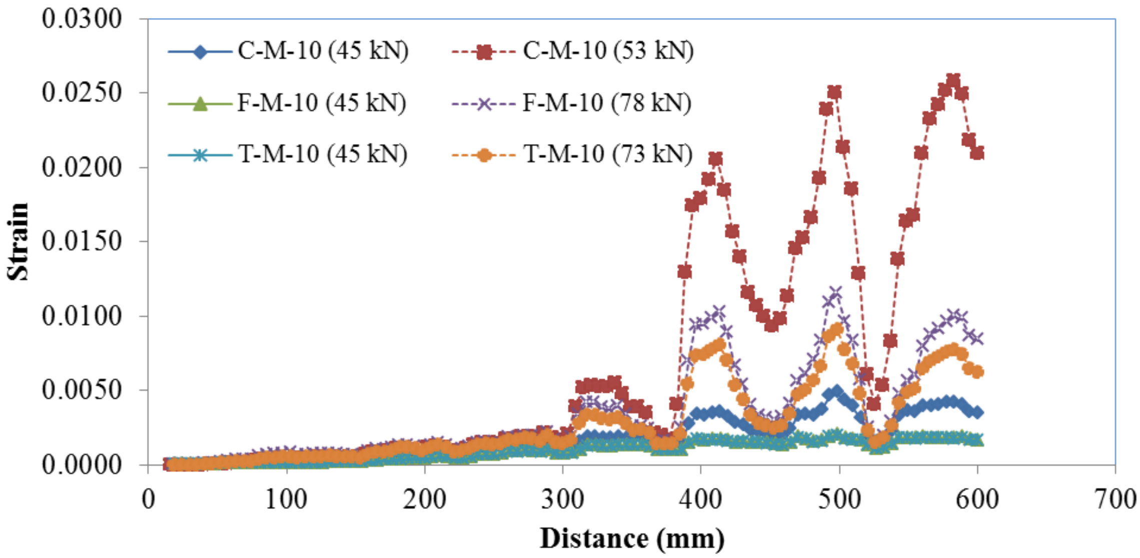

Figure C.8: Steel strain distribution along the length of the beam (x-M-10)

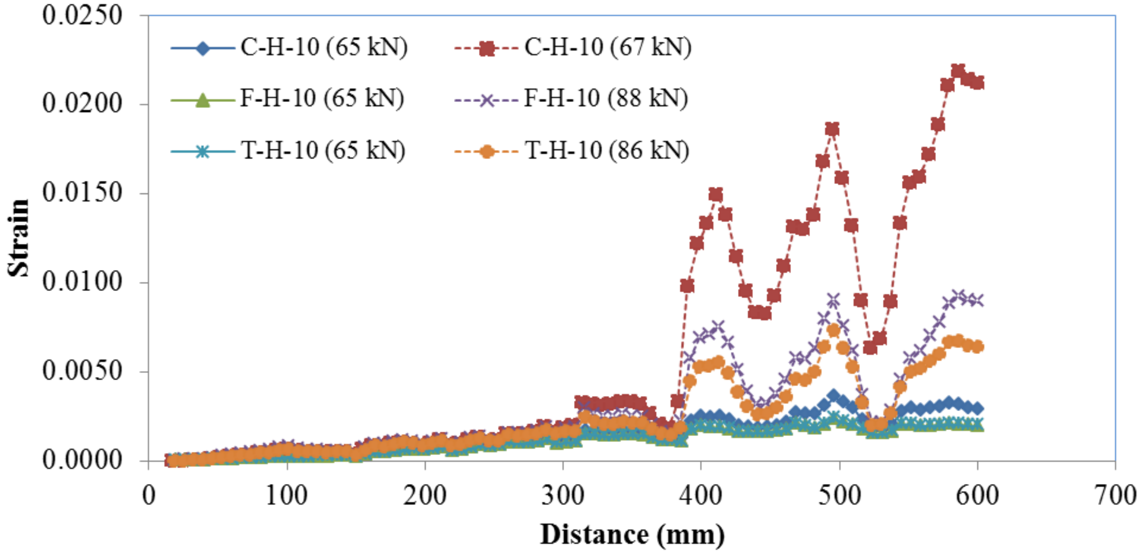

Figure C.9: Steel strain distribution along the length of the beam (x-H-10)

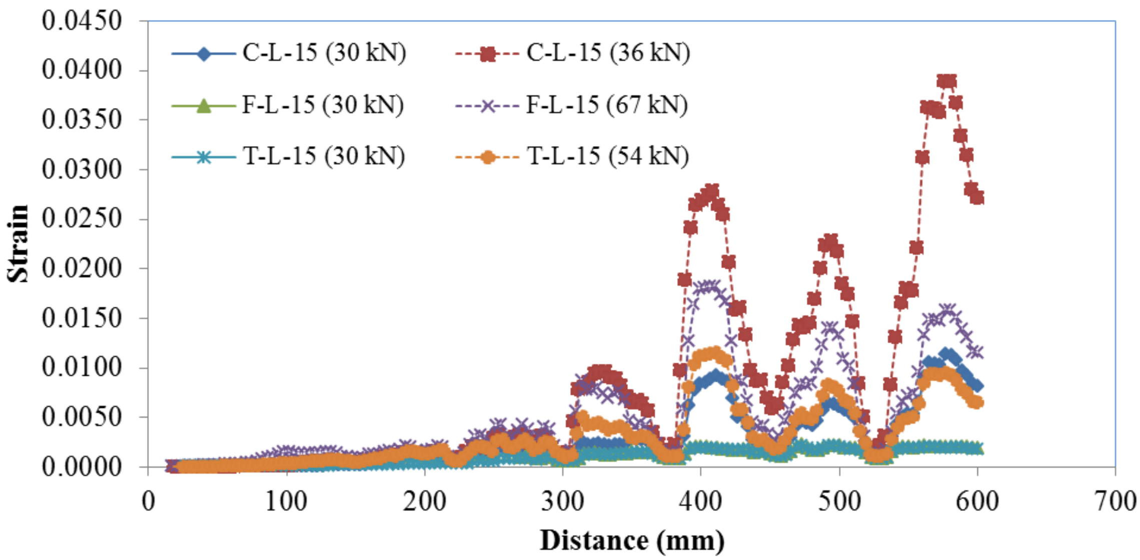

Figure C.10: Steel strain distribution along the length of the beam (x-L-15)

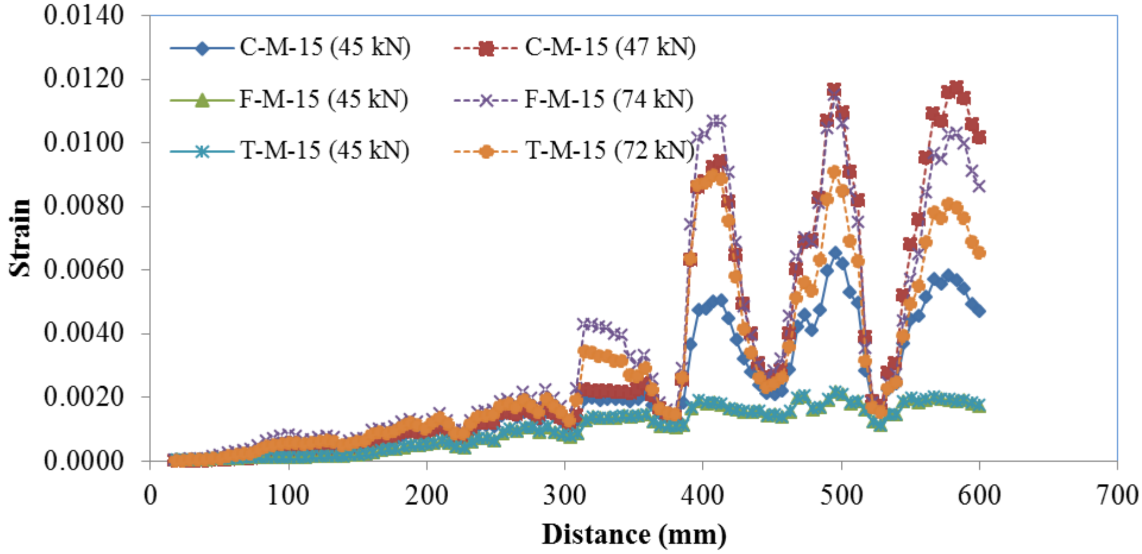

Figure C.11: Steel strain distribution along the length of the beam (x-M-15)

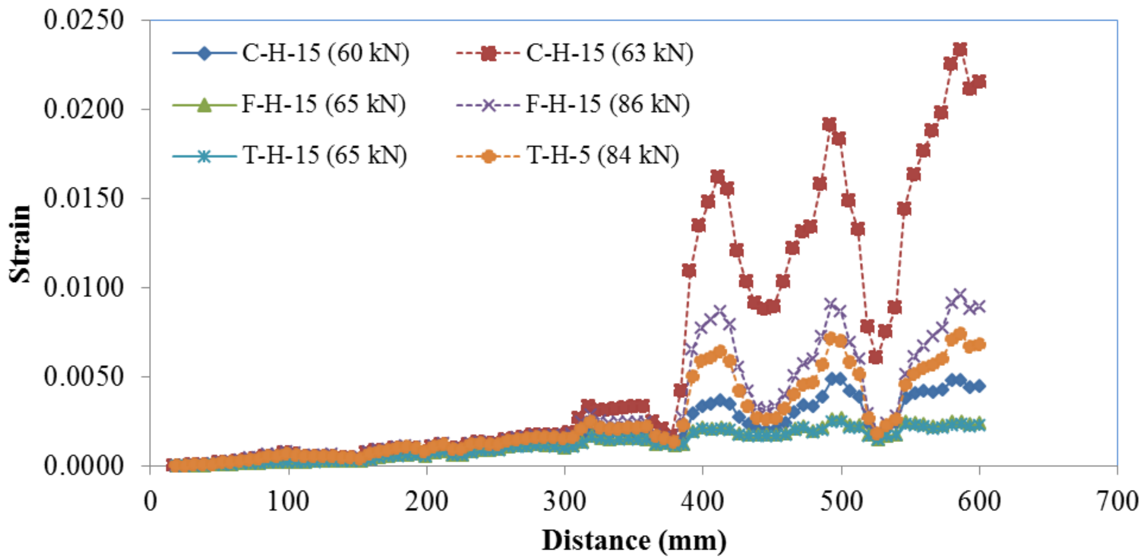

Figure C.12: Steel strain distribution along the length of the beam (x-H-15)

APPENDIX D: FRP/TRM STRAIN DISTRIBUTION

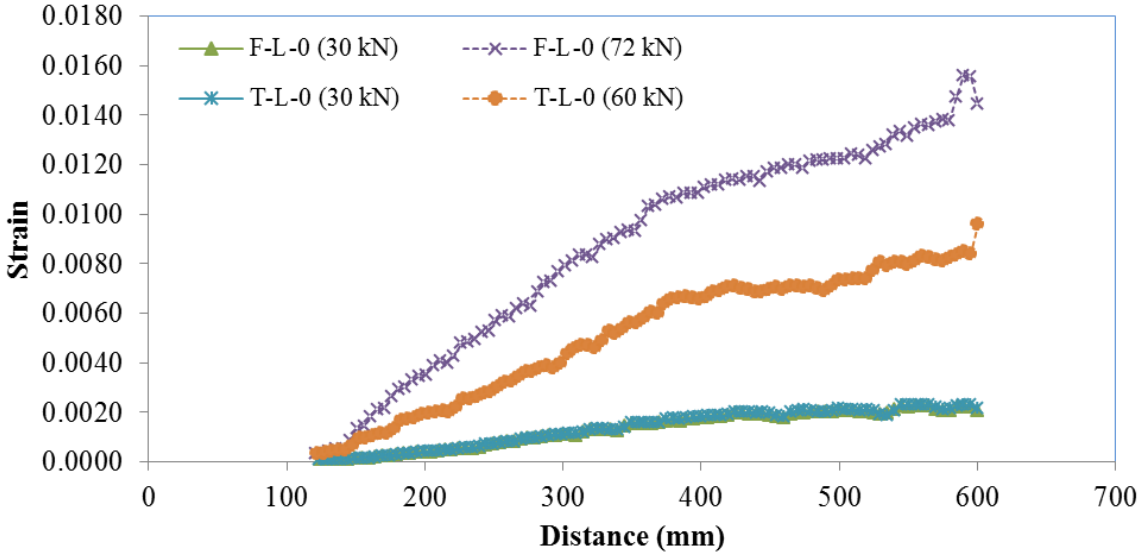

Figure D.1: FRP/TRM strain distribution along the length of the beam (x-L-0)

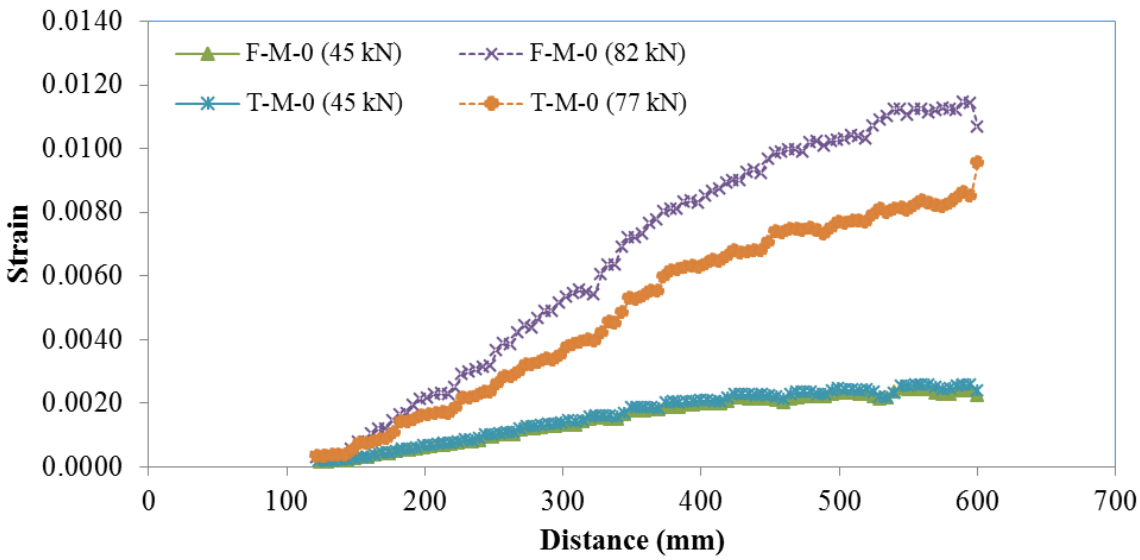

Figure D.2: FRP/TRM strain distribution along the length of the beam (x-M-0)

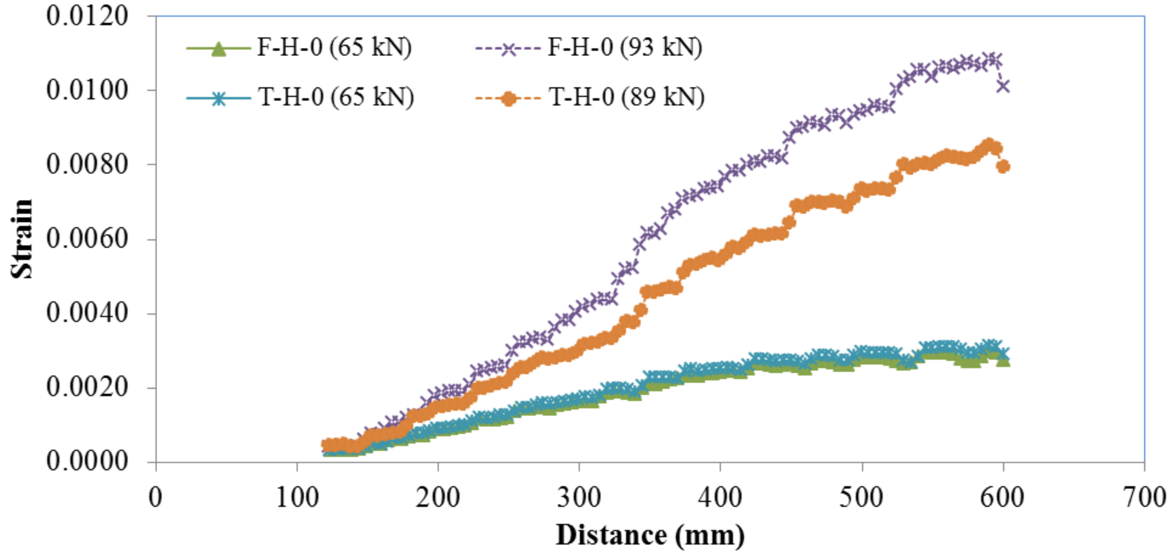

Figure D.3: FRP/TRM strain distribution along the length of the beam (x-H-0)

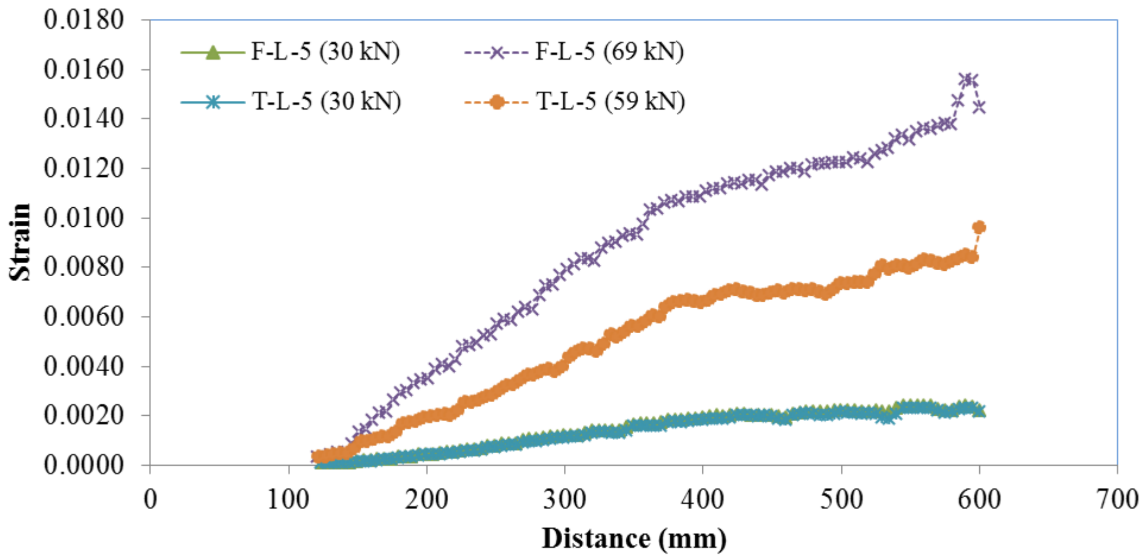

Figure D.4: FRP/TRM strain distribution along the length of the beam (x-L-5)

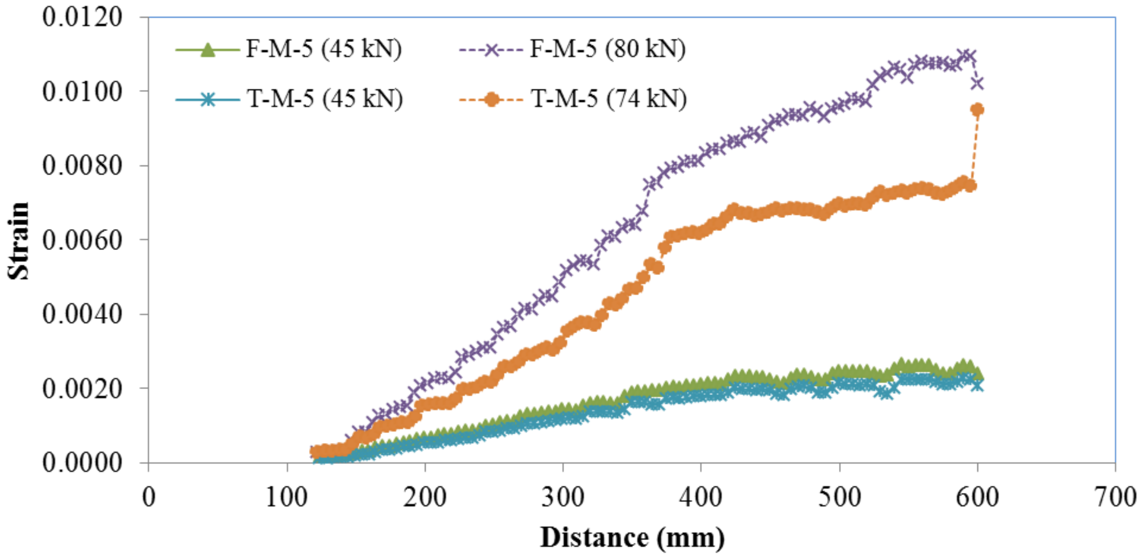

Figure D.5: FRP/TRM strain distribution along the length of the beam (x-M-5)

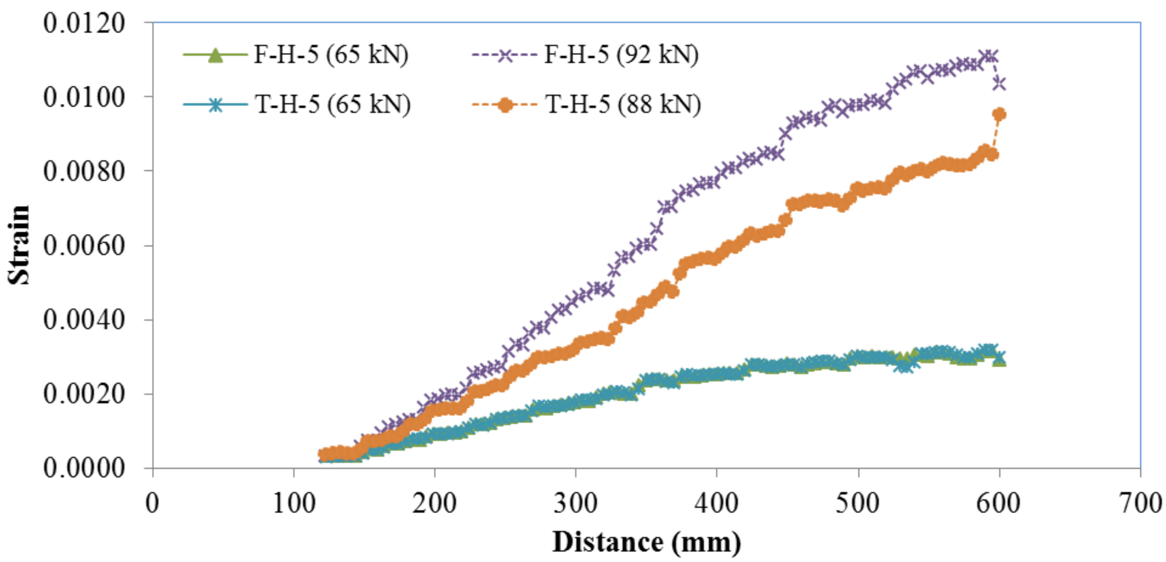

Figure D.6: FRP/TRM strain distribution along the length of the beam (x-H-5)

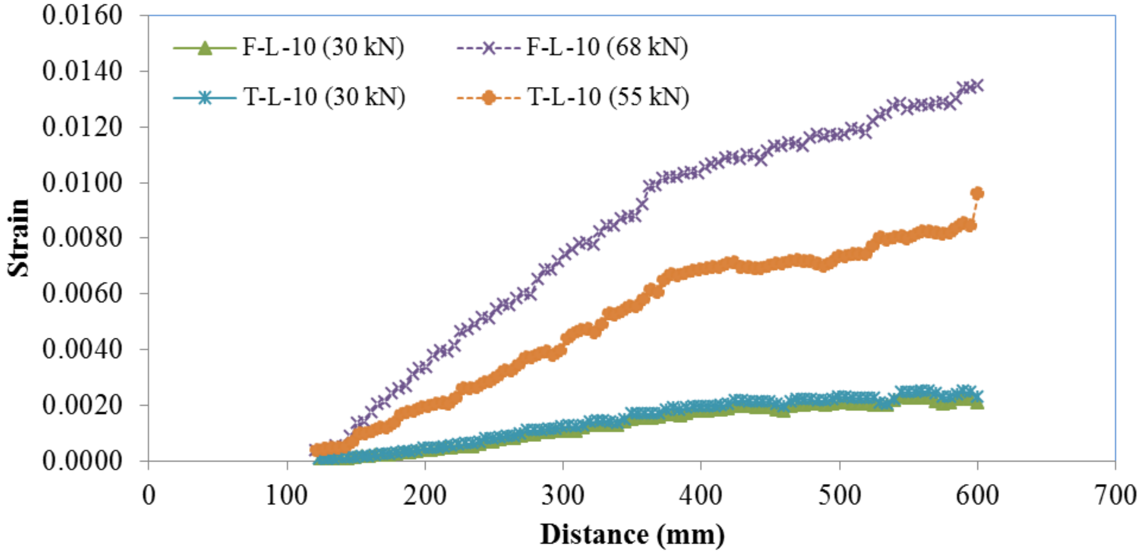

Figure D.7: FRP/TRM strain distribution along the length of the beam (x-L-10)

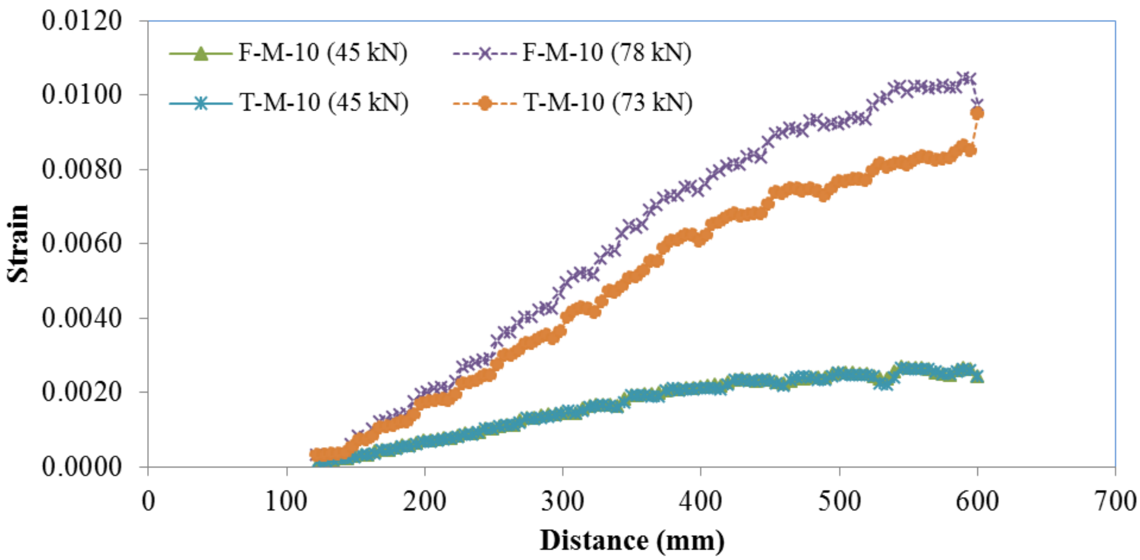

Figure D.8: FRP/TRM strain distribution along the length of the beam (x-M-10)

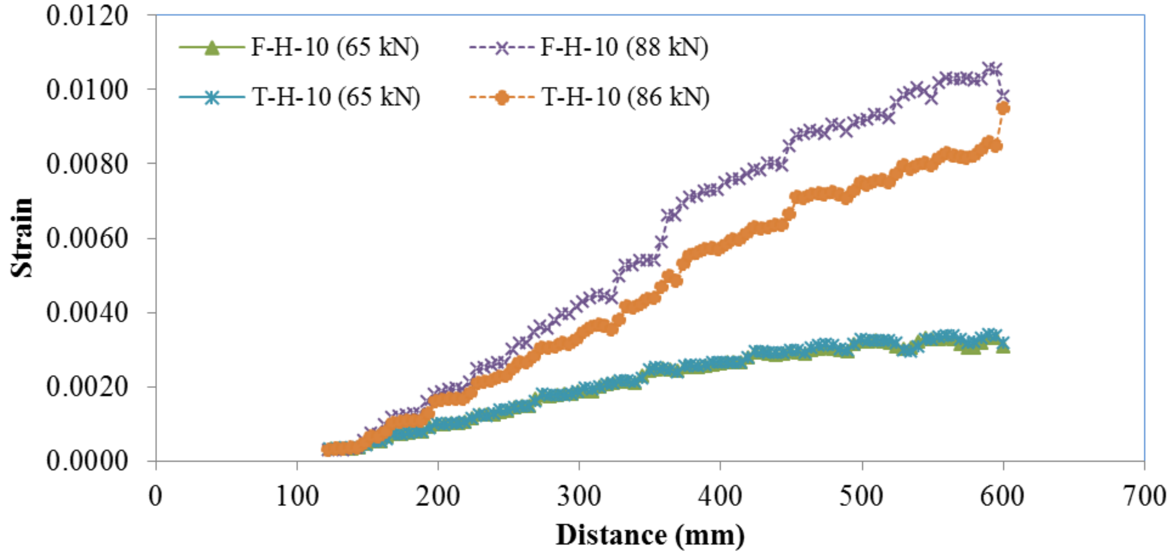

Figure D.9: FRP/TRM strain distribution along the length of the beam (x-H-10)

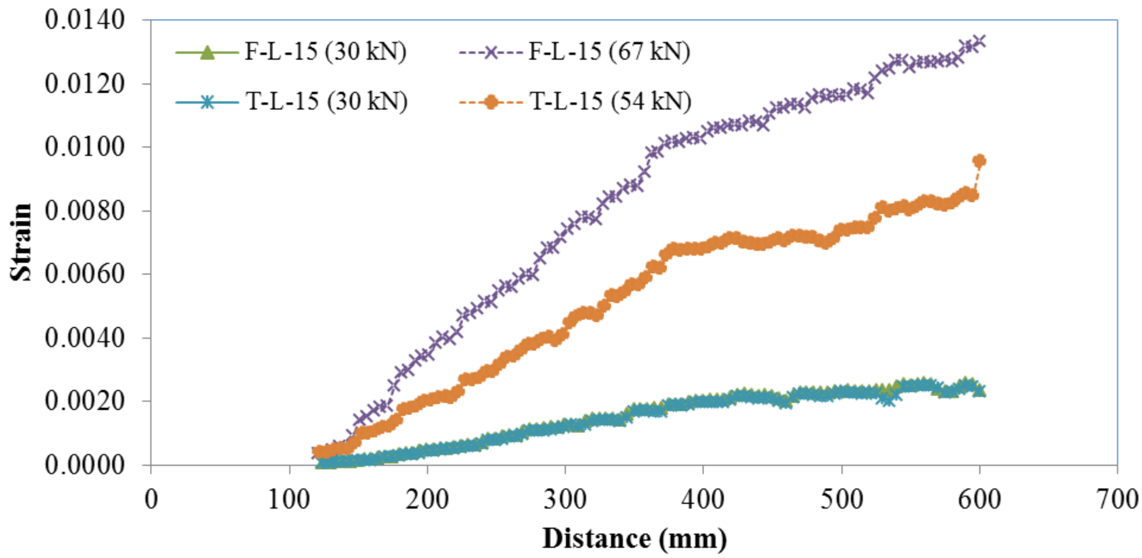

Figure D.10: FRP/TRM strain distribution along the length of the beam (x-L-15)

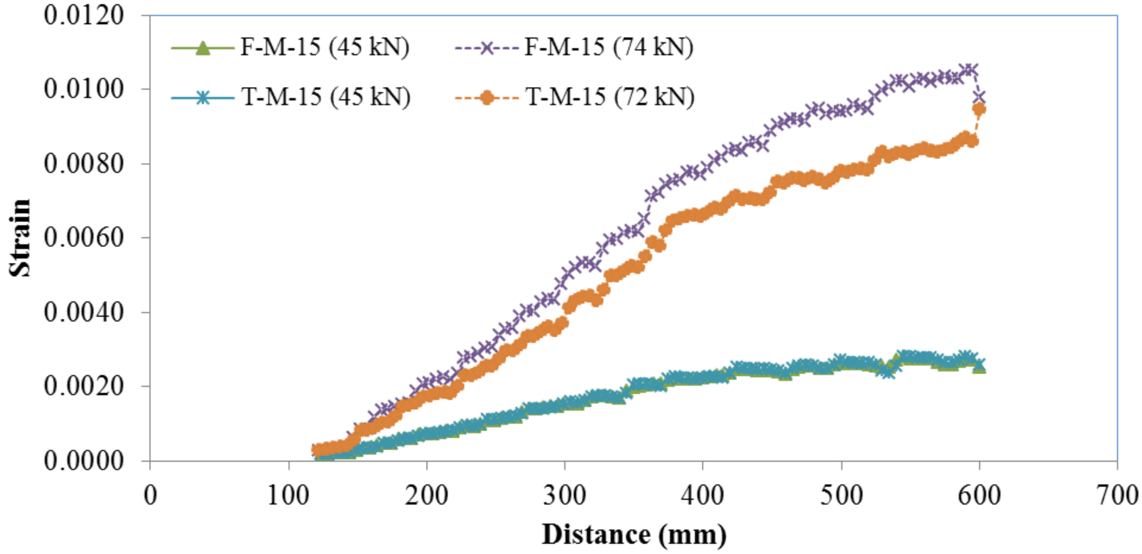

Figure D.11: FRP/TRM strain distribution along the length of the beam (x-M-15)

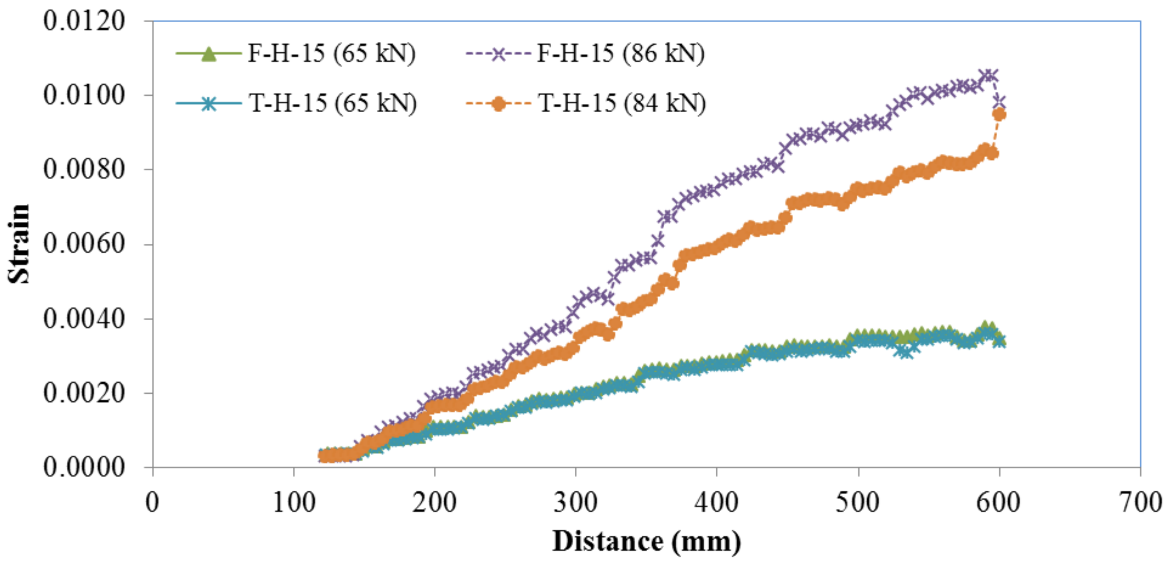

Figure D.12: FRP/TRM strain distribution along the length of the beam (x-H-15)

APPENDIX E: LOAD-DISPLACEMENT BEHAVIOUR FOR THE BEAMS

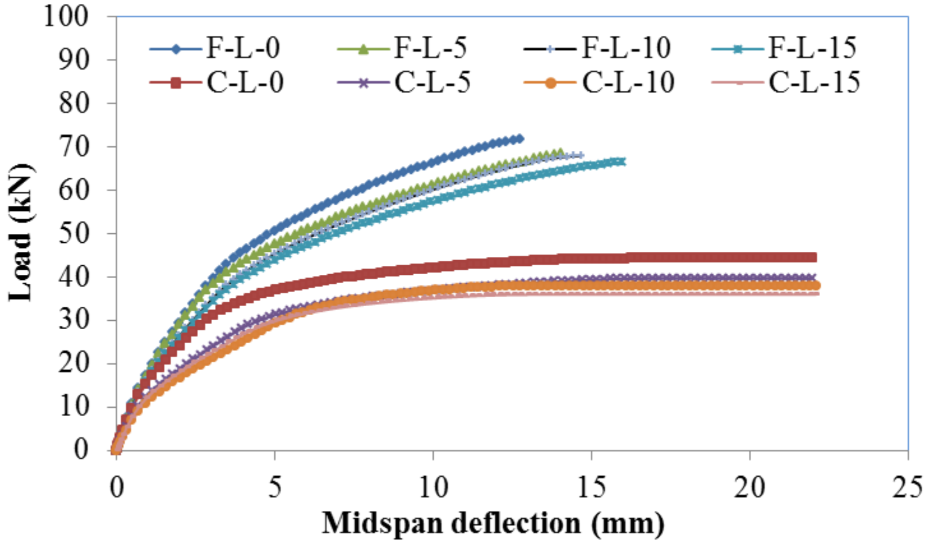

Figure E.1: F-L-x over C-L-x

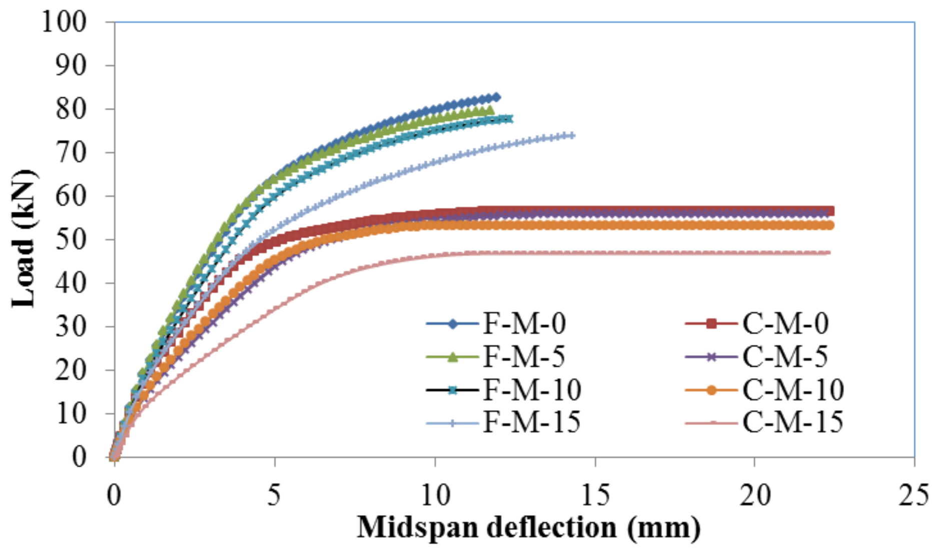

Figure E.2: F-M-x over C-M-x

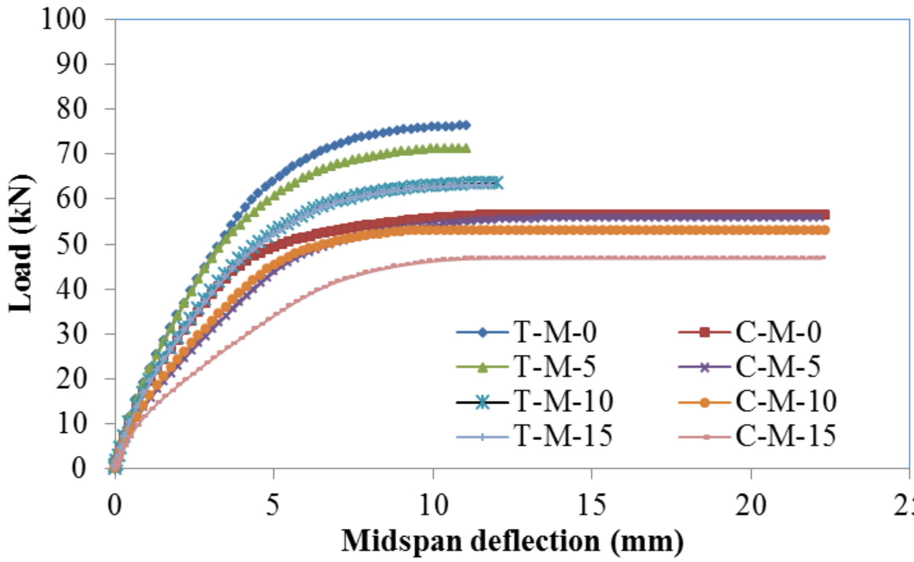

Figure E.3: T-M-x over C-M-x

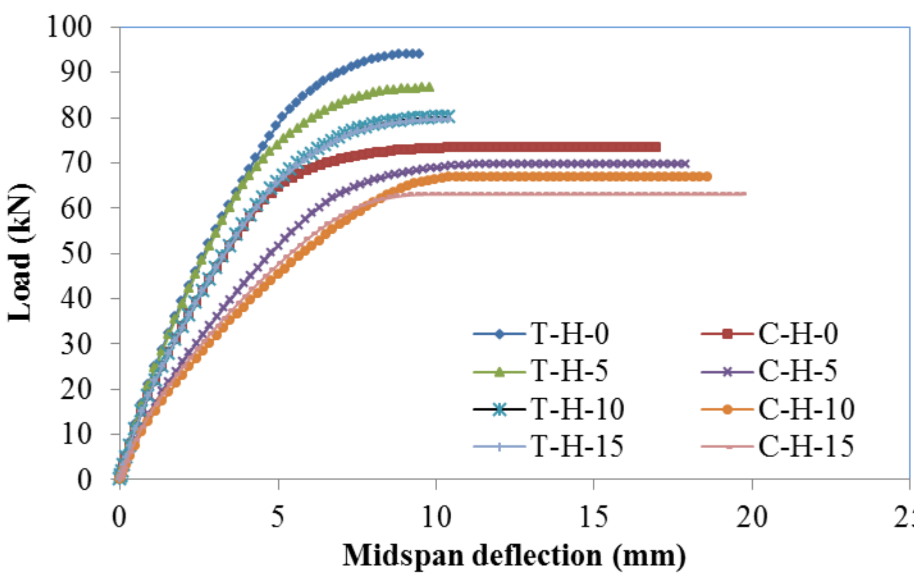

Figure E.4: T-H-x over C-H-x

APPENDIX F: EFFECT OF STRENTHENING SYSTEM ON CAPACITY

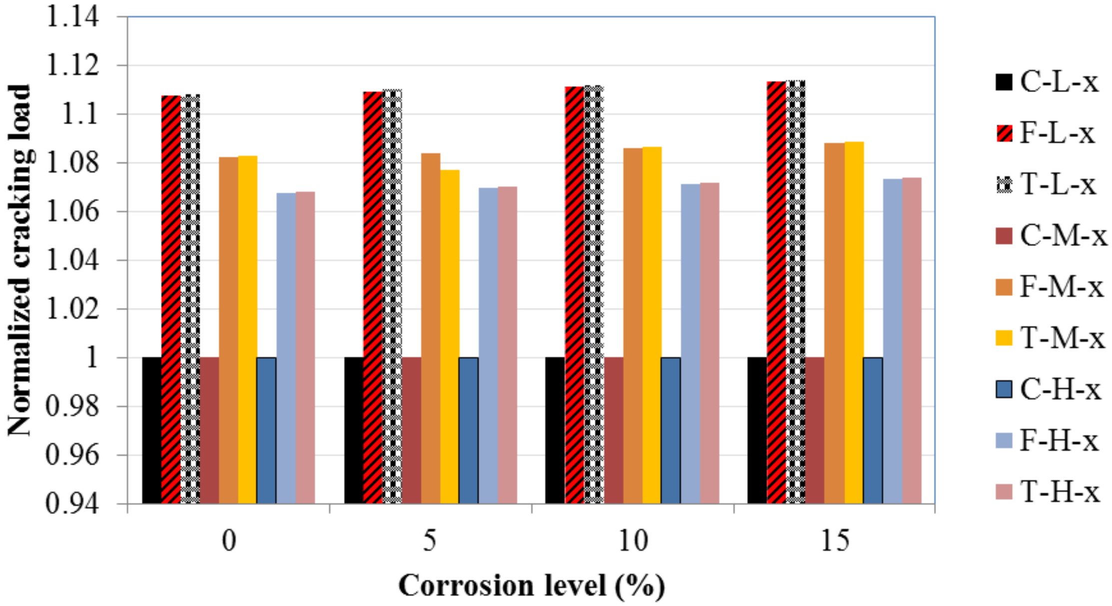

Figure F.1: The effect of strengthening system in cracking load

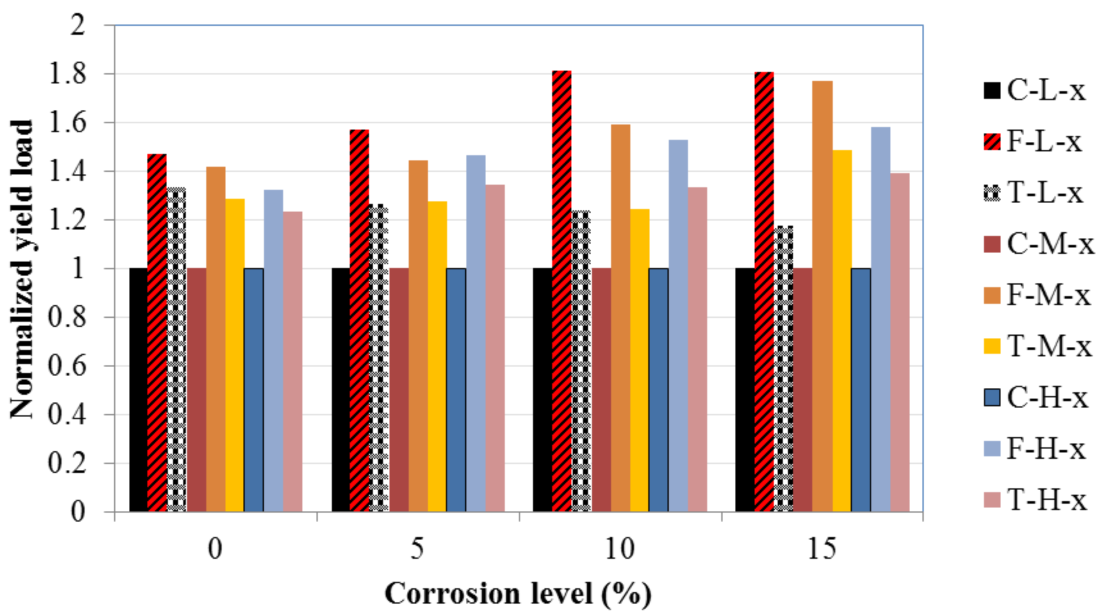

Figure F.2: The effect of strengthening system in yield load

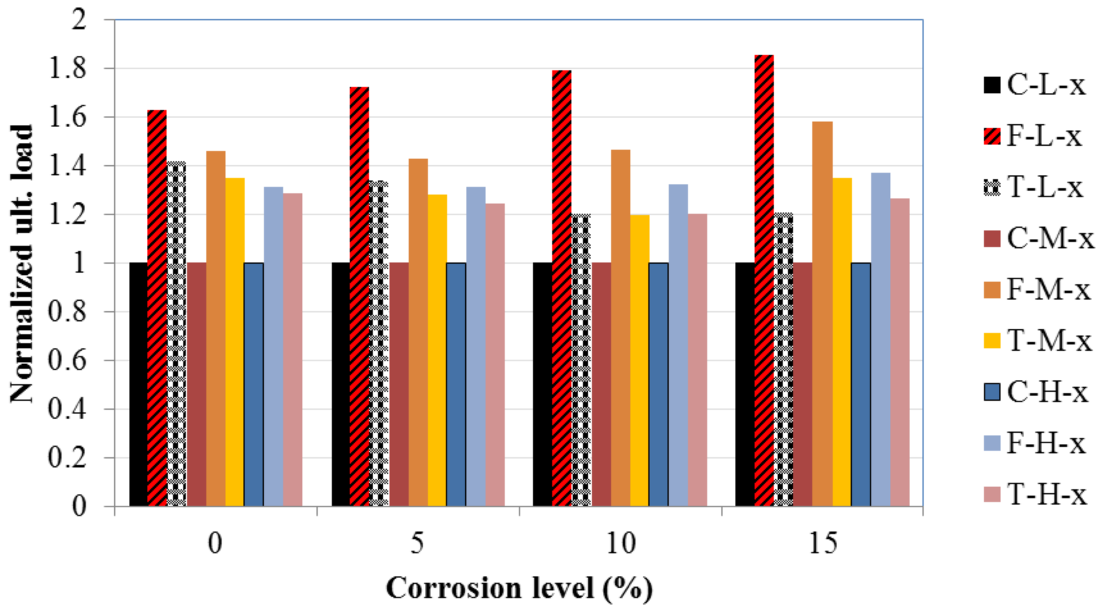

Figure F.3: The effect of strengthening system in ultimate load

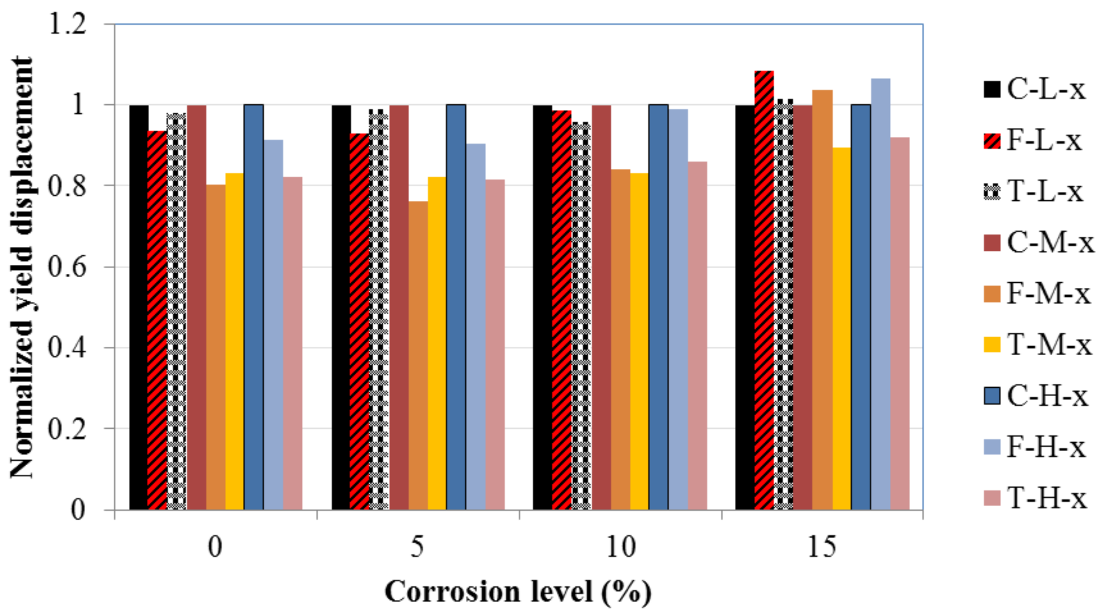

Figure F.4: The effect of strengthening system in yield displacement

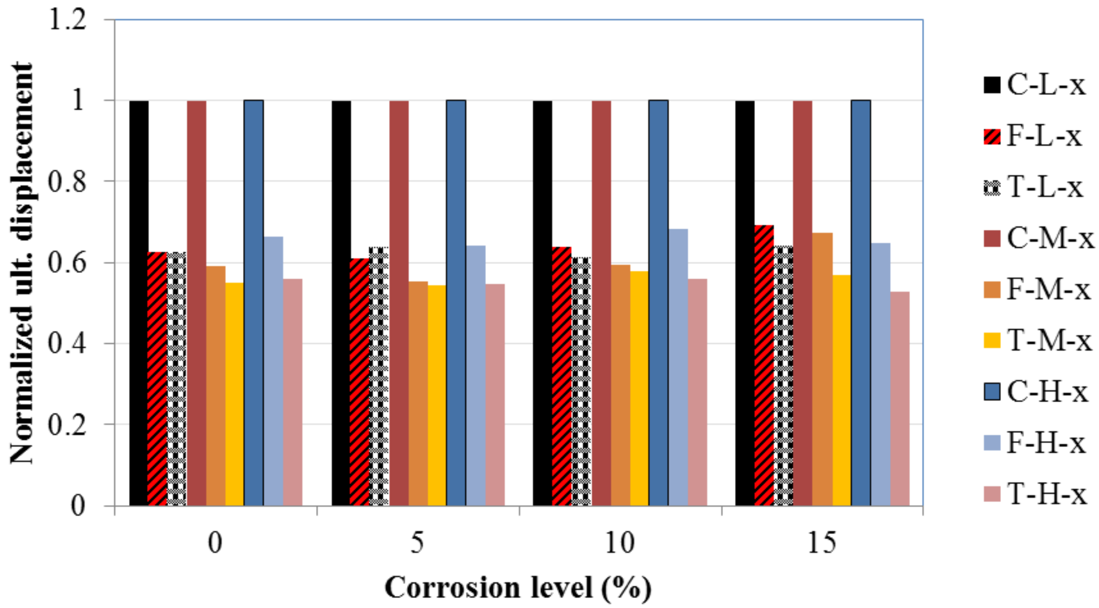

Figure F.5: The effect of strengthening system in ultimate displacement

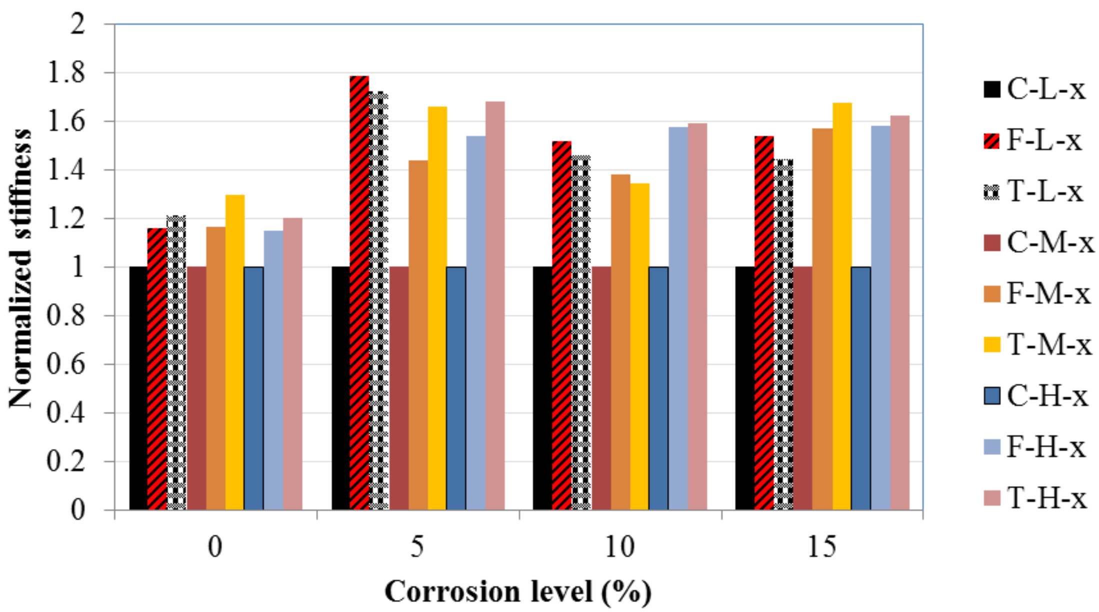

Figure F.6: The effect of strengthening system in stiffness

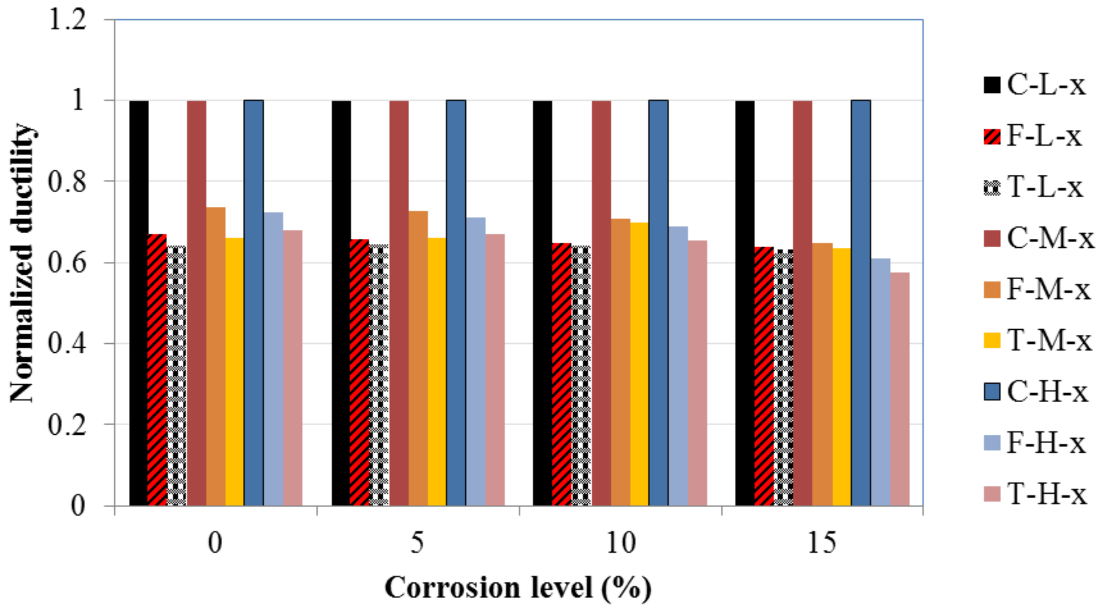

Figure F.7: The effect of strengthening system in ductility